DEVELOPMENT OF GLANCING ANGLE IMAGING METHODOLOGY (GAIM) FOR DETECTION OF PROTRUSION AND BOWING OF PFBR FUEL SUB-ASSEMBLIES

By

G.M.S.K. CHAITANYA

(PHYS 02 2012 04 014)

Indira Gandhi Centre for Atomic Research, Kalpakkam

A thesis submitted to the

Board of Studies in Physical Sciences

In partial fulfillment of requirements

for the Degree of

DOCTOR OF PHILOSOPHY

of

HOMI BHABHA NATIONAL INSTITUTE

August, 2019

Homi Bhabha National Institute[1]

Recommendations of the Viva Voce Committee

As members of the Viva Voce Committee, we certify that we have read the dissertation prepared by **G.M.S.K. Chaitanya** entitled **"Development of glancing angle imaging methodology (GAIM) for detection of protrusion and bowing of PFBR fuel sub-assemblies"** and recommend that it may be accepted as fulfilling the thesis requirement for the award of Degree of Doctor of Philosophy.

G. Amarendra June 21, 2021

Chairman - Dr. G. Amarendra Date:

Guide / Convener - Dr. Anish Kumar Date: 21/6/2021

Examiner - Dr. Joseph Moysan Date: 24/06/21

Member 1- Dr. B. Purna Chandra Rao Date: 21/6/2021

Member 2- Dr. V.S. Srinivasan Date: 21/6/2021

V.S. Srinivasan

Final approval and acceptance of this thesis is contingent upon the candidate's submission of the final copies of the thesis to HBNI.

I/We hereby certify that I/we have read this thesis prepared under my/our direction and recommend that it may be accepted as fulfilling the thesis requirement.

Date:

Place:

Guide

STATEMENT BY AUTHOR

This dissertation has been submitted in partial fulfillment of requirements for an advanced degree at Homi Bhabha National Institute (HBNI) and is deposited in the Library to be made available to borrowers under rules of the HBNI.

Brief quotations from this dissertation are allowable without special permission, provided that accurate acknowledgement of source is made. Requests for permission for extended quotation from or reproduction of this manuscript in whole or in part may be granted by the Competent Authority of HBNI when in his or her judgment the proposed use of the material is in the interests of scholarship. In all other instances, however, permission must be obtained from the author.

Chaitanya

[G.M.S.K. Chaitanya]

DECLARATION

I, hereby declare that the investigation presented in the thesis has been carried out by me. The work is original and has not been submitted earlier as a whole or in part for a degree / diploma at this or any other Institution / University.

[G.M.S.K. Chaitanya]

List of Publications arising from the thesis

Journal

Published

1. Development of ultrasonic glancing angle imaging methodology for detection of subassembly protrusion in fast breeder reactors, **G.M.S.K. Chaitanya** and Anish Kumar, Nuclear Engineering and Design, 2017, Vol. 325, 184–191.
2. Detection of subassembly bowing in a fast breeder reactor using glancing angle ultrasonic imaging. **G.M.S.K. Chaitanya** and Anish Kumar, Annals of Nuclear Energy, 2021, Vol. 150, 107821.

Book chapters

1. Development of automated scanners for underwater and under-sodium ultrasonic imaging", **G.M.S.K.Chaitanya**, Govind Kumar Sharma, Anish Kumar, B. Purnachandra Rao. Communications in Computer and Information Science, 2016, Vol. 627, 109-117. Springer publications, DOI 10.1007/978-981-10-2845-8.

Conferences

1. Ultrasonic glancing angle imaging methodology for estimation of sub-assembly (SA) protrusion in fast breeder reactors. **G.M.S.K.Chaitanya** and Anish Kumar. Conference and Exhibition on Non-Destructive Evaluation (NDE 2017), 14-16 December 2017, Chennai.

2. Imaging of FBR fuel sub-assembly heads by superimposing the glancing angle imaging data obtained from different orientations. **G.M.S.K.Chaitanya** and Anish Kumar. Research Scholars Meet on Materials Science and Engineering of Nuclear Materials, May 7-9, 2018 IGCAR, Kalpakkam.

[G.M.S.K. Chaitanya]

Homi Bhabha National Institute[1]

Recommendations of the Viva Voce Committee

As members of the Viva Voce Committee, we certify that we have read the dissertation prepared by **G.M.S.K. Chaitanya** entitled **"Development of glancing angle imaging methodology (GAIM) for detection of protrusion and bowing of PFBR fuel sub-assemblies"** and recommend that it may be accepted as fulfilling the thesis requirement for the award of Degree of Doctor of Philosophy.

G. Amarendra — June 21, 2021

Chairman - Dr. G. Amarendra — Date:

Guide / Convener - Dr. Anish Kumar — Date: 21/6/2021

Examiner - Dr. Joseph Moysan — Date: 24/06/21

Member 1- Dr. B. Purna Chandra Rao — Date: 21/6/2021

Member 2- Dr. V.S. Srinivasan — Date: 21/6/2021

V.S. Srinivasan

Final approval and acceptance of this thesis is contingent upon the candidate's submission of the final copies of the thesis to HBNI.

I/We hereby certify that I/we have read this thesis prepared under my/our direction and recommend that it may be accepted as fulfilling the thesis requirement.

Date:

Place:

Guide

STATEMENT BY AUTHOR

This dissertation has been submitted in partial fulfillment of requirements for an advanced degree at Homi Bhabha National Institute (HBNI) and is deposited in the Library to be made available to borrowers under rules of the HBNI.

Brief quotations from this dissertation are allowable without special permission, provided that accurate acknowledgement of source is made. Requests for permission for extended quotation from or reproduction of this manuscript in whole or in part may be granted by the Competent Authority of HBNI when in his or her judgment the proposed use of the material is in the interests of scholarship. In all other instances, however, permission must be obtained from the author.

Chaitanya

[G.M.S.K. Chaitanya]

DECLARATION

I, hereby declare that the investigation presented in the thesis has been carried out by me. The work is original and has not been submitted earlier as a whole or in part for a degree / diploma at this or any other Institution / University.

[G.M.S.K. Chaitanya]

List of Publications arising from the thesis

Journal

Published

1. Development of ultrasonic glancing angle imaging methodology for detection of subassembly protrusion in fast breeder reactors, **G.M.S.K. Chaitanya** and Anish Kumar, Nuclear Engineering and Design, 2017, Vol. 325, 184–191.
2. Detection of subassembly bowing in a fast breeder reactor using glancing angle ultrasonic imaging. **G.M.S.K. Chaitanya** and Anish Kumar, Annals of Nuclear Energy, 2021, Vol. 150, 107821.

Book chapters

1. Development of automated scanners for underwater and under-sodium ultrasonic imaging", **G.M.S.K.Chaitanya**, Govind Kumar Sharma, Anish Kumar, B. Purnachandra Rao. Communications in Computer and Information Science, 2016, Vol. 627, 109-117. Springer publications, DOI 10.1007/978-981-10-2845-8.

Conferences

1. Ultrasonic glancing angle imaging methodology for estimation of sub-assembly (SA) protrusion in fast breeder reactors. **G.M.S.K.Chaitanya** and Anish Kumar. Conference and Exhibition on Non-Destructive Evaluation (NDE 2017), 14-16 December 2017, Chennai.

2. Imaging of FBR fuel sub-assembly heads by superimposing the glancing angle imaging data obtained from different orientations. **G.M.S.K.Chaitanya** and Anish Kumar. Research Scholars Meet on Materials Science and Engineering of Nuclear Materials, May 7-9, 2018 IGCAR, Kalpakkam.

Chaitanya

[G.M.S.K. Chaitanya]

Table of Contents

List of Figures

List of tables

List of Abbreviations and Symbols

AIN	Aluminum Nitride
ASTRID	Advanced Sodium Technological Reactor for Industrial Demonstration
BARC	Bhabha Atomic Research Centre
$Bi_4Ti_3O_{12}$	Bismuth Titanate
BWT	Bundle Wire Technology
CCPM	Core Cover Plate Mechanism
CCW	Counter clock wise
CEA	Commissariat à l'énergie atomique et aux énergies alternatives (The French Alternative Energies and Atomic Energy Commission)
CW	Clock wise
D	Diameter of the piezoelectric element
dB	Decibel
DFR	Dounreay Fast Reactor
DOLMEN	Double Latitude pour Maintenance En sodium (Na)
DVTs	Down Viewing Transducers
EBR-1	Experimental Breeder Reactor – 1
EBR-2	Experimental Breeder Reactor – 2
EMATs	Electro Magnetic Acoustic Transducers
ETE	Eight-Twenty four-Eight (8-24-8)
f	Frequency of the ultrasonic transducer
FBRs	Fast Breeder Reactors
FBTR	Fast Breeder Test Reactor
FFTF	Fast Flux Test Facility
FRTG	Fast Reactor Technology Group
FSAs	Fuel Sub-Assemblies
GAIM	Glancing Angle Imaging Methodology
ID	Inner Diameter
IGCAR	Indira Gandhi Centre for Atomic Research

IHX	Intermediate Heat Exchangers
IMARSOD	IMAgerie Rapide en SODium
IVTP	In-Vessel Transfer Port
JAEA	Japan Atomic Energy Agency
LabVIEW	Laboratory Virtual Instrument Engineering Workbench
LBE	Lead-Bismuth Eutectic
$LiNbO_3$	Lithum Niobate
LMFBR	Liquid Metal Fast Breeder Reactor
LRP	Large Rotating Plug
LSAS	Linked Sweep-Arm Scanner
MHz	Mega Hertz
MI	Mineral Insulated
MOX	Mixed Uranium-Plutonium Oxide
MS/s	Mega Samples per second
MYRRHA	Multi-purpose hYbrid Research Reactor for High-tech Applications
NI	National Instruments
OD	Outer Diameter
$PbNb_2O_6$	Lead Metaniobate
PCI	Peripheral Component Interconnect
PE	Pulse-Echo
PFBR	Prototype Fast Breeder Reactor
PFR	Prototype Fast Reactor
PNC	Power Reactor and Nuclear Fuel Development Corporation
PNNL	Pacific Northwest National Laboratory
PSA	Periphery Subassembly
RMS value	Root Mean Square value
RUSV	Rigid Under-sodium Viewer
SA	Sub-Assembly
SA head	Sub-Assembly head
SA#X	Sub-Assembly no. ‘X’; X = {1-19, C}; C-Central SA

SAFT	Synthetic Aperture Focusing Technique
SNR	Signal to Noise Ratio
SRP	Small Rotating Plug
SS	Stainless Steel
SSA	Shielding Sub-Assemblies
SVTs	Side Viewing Transducers
T_c	Curie temperature
TOF	Time of Flight
TOF_p	Time of Flight as a function of protrusion
TTTB	Twenty four- Twenty four- Twenty four (bowed SA)
TUSHT	High-Temperature Ultrasonic Transducers
TV – 5	Test Vessel – 5
UHAS	Under-sodium Honeycomb Arrangement Setup
UK	United Kingdom
UKAEA	United Kingdom Atomic Energy Authority
USA	United States of America
USUSS	Under Sodium Ultrasonic Scanner
USV	Under Sodium Viewing system
VENUS	Visualisation undEr Na by Ultrasounds
VISUS	ultrasonic sodium VISUalization Systems
ZTZ	Zero-Twenty four-Zero (0-24-0)
$\alpha/2$	-6dB beam divergence of the ultrasonic wave
θ	Polar angle
λ	Wavelength of ultrasonic wave
υ	Velocity of ultrasonic wave
φ	Azimuthal angle

Chapter 7. Summary and Future work

7.1 Summary

In the present thesis, for the first time, ultrasonic glancing angle imaging methodology (GAIM) is developed for detection of protrusion, bowing and for mapping of fuel subassembly (FSA) heads without actually going on top of each FSA in a pool type sodium cooled fast breeder reactor. The GAIM is demonstrated successfully through under water experimental studies.

The review of under-sodium ultrasonic scanner systems and the methodologies developed for imaging of the reactor internal components in various countries indicated the limitations of the present under-sodium ultrasonic scanners for detection of protrusion, bowing and for mapping of fuel FSAs. It is identified that in all the under-sodium scanner and associated methodologies, imaging of FSAs can only be performed by keeping the ultrasonic transducer(s) above the FSAs.

The main objective of the present thesis was to develop an inspection methodology to circumvent the above limitations. The salient results obtained in the thesis are listed below:

- ❖ GAIM was developed and demonstrated through under water experiments using 19 SA heads placed in the form of a honeycomb arrangement.
- ❖ The experimental parameters such as glancing angle and the transducer vertical height from the SA head top were systematically optimized using the A-scan signals obtained from the honeycomb arrangement at various heights and glancing angles.

- ❖ The optimized vertical height and glancing angle of the ultrasonic transducer were 40 mm and 5°, respectively for the given honeycomb arrangement. Glancing angle images of the honeycomb arrangement were acquired from the optimized position.
- ❖ A LabVIEW program was specifically developed for acquiring the sector scan images and for generation of glancing angle images.
- ❖ From the glancing angle image, it was identified that the diffracted signals from each SA head are obtained from 6 sharp edges on the outer geometry of SA head and from inner diameter (ID), when the beam is incident radially on the rear end ID.

Protrusion detection

- ❖ Enhanced echo amplitude corresponding to a protruded SA and masking of signals corresponding to SAs behind the protruded SA, were two signatures identified for qualitative estimation of protrusion.
- ❖ Multiple protrusion detection was identified using GAIM by giving random protrusion to SA heads in the honeycomb arrangement. In addition to this, the sensitivity of GAIM for this experimental setup was found to be 1 mm of protrusion
- ❖ Amplitude and time of flight (TOF) of the ultrasonic signal at different protrusion heights and for different orientations of a SA head viz, 0°, 10°, 20° and 30° were used for quantitative estimation of protrusion.
- ❖ A continuous increase in amplitude and decrease in TOF, trend was observed with the extent of protrusion for all the orientations of SA head. Theoretically calculated TOF values are in good agreement with the experimentally measured TOF values.

Bowing detection

- Unlike in the case of protrusion detection, bowing requires data to be acquired from two different probe locations.
- Bowing detection of a SA head was carried out from two different locations separated by an angle of 180°.
- Signatures identified for qualitative estimation of bowing are:
  i. enhanced echo amplitude corresponding to a bowed SA away from the transducer,
  ii. change in the TOF of bowed SA head and
  iii. masking of signals behind the bowed SA head when the SA head is bowed away from the transducer.
- Random SA head bowing detection in the honeycomb arrangement was carried out by giving 2° bowing (towards and away from the ultrasonic transducer) to a SA head in the honeycomb arrangement.
- Quantitative estimation of SA head bowing in the honeycomb arrangement was successfully demonstrated by comparing experimentally measured change in TOF of bowed SA head with the theoretically calculated TOF change. Experimentally and theoretically calculated TOF change are in good agreement.

Application of GAIM in sodium environment

- After successful development and demonstration of GAIM in water, GAIM was explored in sodium environment.
- Due to non-availability of hermetically sealed 2 MHz under-sodium transducer, a readily available 1 MHz transducer connected with a 10 m long Mineral Insulated (MI) cable was used to carry out under-sodium experiments.

- Response of ultrasonic transducers in water and sodium environment was compared.
- Ultrasonic signal strength of the 1 MHz transducer gradually improved up to 10 days of sodium exposure. The initial ringing got reduced with wetting of the transducer.
- However, it is observed that even after 10 days of sodium exposure, noise level in ultrasonic signals is higher in sodium as compared to that in water.
- A cross-correlation and time shift followed by subtraction processing was developed for removing the initial ringing of under-sodium ultrasonic signals.
- Θ-Z scanning of under-sodium honeycomb arrangement setup (UHAS) in different orientations was carried out using 1 MHz transducer after 10 days of sodium exposure.
- However, even after signal processing, diffracted signals could not be observed/resolved in any of the configurations due to poor signal to noise ratio in the ultrasonic signals obtained using 1 MHz probe in under-sodium environment. This is attributed to, inherent low SNR of 1 MHz probe with 10 m long MI cable, very weak diffracted signal from the SA heads, larger initial ringing of transducer due to higher ultrasonic velocity in sodium as compared to that in water and more electromagnetic noise pick-up near the sodium vessel due to other electrical appliances.

7.2 Future work

From the study undertaken in the thesis, it is observed that even though the GAIM could be successfully demonstrated in under water configuration for detection of protrusion and bowing, the diffracted signals could not be obtained in under-sodium condition. The GAIM utilizes the diffracted echoes, which are inherently of lower amplitude than the reflected echoes. Hence, it is required to improve the SNR of the ultrasonic signals to resolve the diffracted signals from the SA heads in the sodium environment. To resolve/observe the signals from the SA heads, the following are proposed as directions for future works:

- A high voltage tone burst pulser/receiver may be used to improve the SNR.
- A probe with better sensitivity and low ringing should be explored. High frequency (2-5 MHz) under-sodium ultrasonic transduces may be used to reduce the initial ringing.
- As limited number of scenarios can be validated experimentally, semi-analytical simulations using CIVA may be useful to generate larger configurations.
- De-convolution algorithm may be explored to further enhance diffracted signals from the SA heads.
- Development of automated image analysis algorithm as part of inverse problem for deciphering the protrusion/bowing from experimental data may be useful for the operator.
- The possibility of using a phased array ultrasonic probes for GAIM may be explored. Application of a phased array probe will lead to improved sensitivity due to focusing of beam at the desired location and also the physical transducer sweep can be replaced with an electronic sweep.

Chapter 7. Summary and Future work

7.1 Summary

In the present thesis, for the first time, ultrasonic glancing angle imaging methodology (GAIM) is developed for detection of protrusion, bowing and for mapping of fuel subassembly (FSA) heads without actually going on top of each FSA in a pool type sodium cooled fast breeder reactor. The GAIM is demonstrated successfully through under water experimental studies.

The review of under-sodium ultrasonic scanner systems and the methodologies developed for imaging of the reactor internal components in various countries indicated the limitations of the present under-sodium ultrasonic scanners for detection of protrusion, bowing and for mapping of fuel FSAs. It is identified that in all the under-sodium scanner and associated methodologies, imaging of FSAs can only be performed by keeping the ultrasonic transducer(s) above the FSAs.

The main objective of the present thesis was to develop an inspection methodology to circumvent the above limitations. The salient results obtained in the thesis are listed below:

- ❖ GAIM was developed and demonstrated through under water experiments using 19 SA heads placed in the form of a honeycomb arrangement.
- ❖ The experimental parameters such as glancing angle and the transducer vertical height from the SA head top were systematically optimized using the A-scan signals obtained from the honeycomb arrangement at various heights and glancing angles.

- The optimized vertical height and glancing angle of the ultrasonic transducer were 40 mm and 5°, respectively for the given honeycomb arrangement. Glancing angle images of the honeycomb arrangement were acquired from the optimized position.
- A LabVIEW program was specifically developed for acquiring the sector scan images and for generation of glancing angle images.
- From the glancing angle image, it was identified that the diffracted signals from each SA head are obtained from 6 sharp edges on the outer geometry of SA head and from inner diameter (ID), when the beam is incident radially on the rear end ID.

Protrusion detection

- Enhanced echo amplitude corresponding to a protruded SA and masking of signals corresponding to SAs behind the protruded SA, were two signatures identified for qualitative estimation of protrusion.
- Multiple protrusion detection was identified using GAIM by giving random protrusion to SA heads in the honeycomb arrangement. In addition to this, the sensitivity of GAIM for this experimental setup was found to be 1 mm of protrusion
- Amplitude and time of flight (TOF) of the ultrasonic signal at different protrusion heights and for different orientations of a SA head viz, 0°, 10°, 20° and 30° were used for quantitative estimation of protrusion.
- A continuous increase in amplitude and decrease in TOF, trend was observed with the extent of protrusion for all the orientations of SA head. Theoretically calculated TOF values are in good agreement with the experimentally measured TOF values.

Bowing detection

- Unlike in the case of protrusion detection, bowing requires data to be acquired from two different probe locations.
- Bowing detection of a SA head was carried out from two different locations separated by an angle of 180°.
- Signatures identified for qualitative estimation of bowing are:
  - i. enhanced echo amplitude corresponding to a bowed SA away from the transducer,
  - ii. change in the TOF of bowed SA head and
  - iii. masking of signals behind the bowed SA head when the SA head is bowed away from the transducer.
- Random SA head bowing detection in the honeycomb arrangement was carried out by giving 2° bowing (towards and away from the ultrasonic transducer) to a SA head in the honeycomb arrangement.
- Quantitative estimation of SA head bowing in the honeycomb arrangement was successfully demonstrated by comparing experimentally measured change in TOF of bowed SA head with the theoretically calculated TOF change. Experimentally and theoretically calculated TOF change are in good agreement.

Application of GAIM in sodium environment

- After successful development and demonstration of GAIM in water, GAIM was explored in sodium environment.
- Due to non-availability of hermetically sealed 2 MHz under-sodium transducer, a readily available 1 MHz transducer connected with a 10 m long Mineral Insulated (MI) cable was used to carry out under-sodium experiments.

- Response of ultrasonic transducers in water and sodium environment was compared.
- Ultrasonic signal strength of the 1 MHz transducer gradually improved up to 10 days of sodium exposure. The initial ringing got reduced with wetting of the transducer.
- However, it is observed that even after 10 days of sodium exposure, noise level in ultrasonic signals is higher in sodium as compared to that in water.
- A cross-correlation and time shift followed by subtraction processing was developed for removing the initial ringing of under-sodium ultrasonic signals.
- Θ-Z scanning of under-sodium honeycomb arrangement setup (UHAS) in different orientations was carried out using 1 MHz transducer after 10 days of sodium exposure.
- However, even after signal processing, diffracted signals could not be observed/resolved in any of the configurations due to poor signal to noise ratio in the ultrasonic signals obtained using 1 MHz probe in under-sodium environment. This is attributed to, inherent low SNR of 1 MHz probe with 10 m long MI cable, very weak diffracted signal from the SA heads, larger initial ringing of transducer due to higher ultrasonic velocity in sodium as compared to that in water and more electromagnetic noise pick-up near the sodium vessel due to other electrical appliances.

7.2 Future work

From the study undertaken in the thesis, it is observed that even though the GAIM could be successfully demonstrated in under water configuration for detection of protrusion and bowing, the diffracted signals could not be obtained in under-sodium condition. The GAIM utilizes the diffracted echoes, which are inherently of lower amplitude than the reflected echoes. Hence, it is required to improve the SNR of the ultrasonic signals to resolve the diffracted signals from the SA heads in the sodium environment. To resolve/observe the signals from the SA heads, the following are proposed as directions for future works:

- A high voltage tone burst pulser/receiver may be used to improve the SNR.
- A probe with better sensitivity and low ringing should be explored. High frequency (2-5 MHz) under-sodium ultrasonic transduces may be used to reduce the initial ringing.
- As limited number of scenarios can be validated experimentally, semi-analytical simulations using CIVA may be useful to generate larger configurations.
- De-convolution algorithm may be explored to further enhance diffracted signals from the SA heads.
- Development of automated image analysis algorithm as part of inverse problem for deciphering the protrusion/bowing from experimental data may be useful for the operator.
- The possibility of using a phased array ultrasonic probes for GAIM may be explored. Application of a phased array probe will lead to improved sensitivity due to focusing of beam at the desired location and also the physical transducer sweep can be replaced with an electronic sweep.

Chapter 1. Introduction

1.1 Background context

Many countries like Belgium, France, Germany, India, Japan, UK and USA have built and operated Fast Breeder Reactors (FBRs). In India, two FBRs namely Fast Breeder Test Reactor (FBTR) and Prototype Fast Breeder Reactor (PFBR) exist as part of "India's three-stage nuclear programme." [1]. Figure 1.1 shows the pictorial representation of India's three-stage nuclear power programme. The program is based on optimum utilization of modest Uranium and abundant Thorium resources available in India [1].

The natural Uranium has only 0.7% of U-235 and 99.3% U-238. Among these two isotopes, U-235 is fissile material. In the first stage of nuclear program, natural Uranium is used as fuel, in which fertile isotope U-238 is converted to Pu-239 through neutron capture and beta radiation. In the second stage, Pu-239 obtained from first stage is used as fuel. U-238 and Th-232 are used as blanket materials around Pu-239 fuel core. U-238 will undergo nuclear transmutation to produce fresh Pu-239 and Th-232 will be converted to U-233 through neutron capture reactions. In the third stage, U-233 obtained in second stage is used as fuel. In addition to this, Th-232 which is used as blanket around U-233 fuel core will generate more U-233 by undergoing neutron capture. The first, second and third stage reactors are called, Pressurised Heavy Water Reactors (PHWRs), Fast Breeder Reactor (FBRs) and Breeder Reactors (BRs) [1].

In the stage 1 comprising of PHWR reactors, 12 GWe, 30y represents the estimated amount of nuclear power output that can be generated using the Uranium resources available in India for a period of 30 Yrs. Similarly, the figures in satge 2 and stage 3 represent the estimated power and duration of nuclear energy generation with the available Uranium and Thorium resources in India through the three stage nuclear program [2].

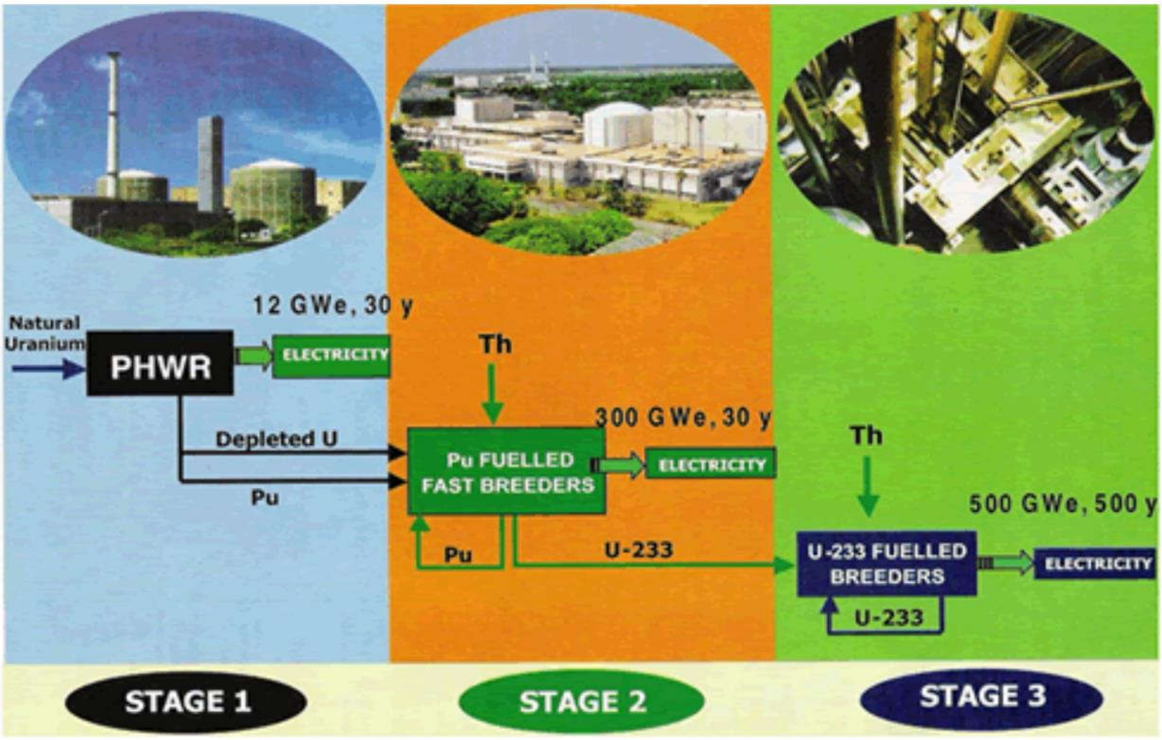

Figure 1.1 India's three-stage nuclear power programme [1]

FBRs are of two types: one is loop-type and the other one is pool-type. FBTR is a loop-type reactor and PFBR is a pool-type rector. PFBR is presently under advanced stage of commissioning at Kalpakkam, Tamil Nadu, India. In a pool-type reactor, all its internals including core and primary sodium circuit are immersed in liquid sodium. The performance of the core structural materials (subassemblies) decides the successful operation and operating cost of a sodium cooled FBR. In PFBR, the temperature of nuclear core during operation will be around 550°C and the maximum neutron flux level in the core will be ~8×10^{15} n.cm^{-2}s^{-1}. Due to high temperature and prolonged irradiation, growth and in turn protrusion of hexagonal shaped Fuel Sub-Assemblies (FSAs) beyond the general level is expected.

In addition to this, due to intense neutron flux gradient in the core, FSAs will undergo differential elongation which leads to bending or bowing of FSAs. Before any fuel handling campaign, it is mandatory to ensure that there is no protrusion and bowing of any Sub-Assembly (SA) in the reactor core beyond a permissible level. Since liquid sodium is opaque, it is not possible to use optical techniques to detect protrusion/bowing and for imaging of FSAs in the reactor. Ultrasonics is the most promising method for protrusion, bowing detection and for mapping of FSAs.

Many countries have developed under-sodium ultrasonic scanners and imaging methodologies for identifying reactor internals. The details of under-sodium scanner systems and the methodologies developed by different countries are discussed in Chapter – 2. Most of the countries developed complex robotic arm based under-sodium ultrasonic scanners. However, due to rotational constraints of rotating plugs, on which scanners are mounted, mapping of complete core is often not possible.

As an alternative to complex robotic arm scanners, this thesis deals with development of a new methodology namely ultrasonic Glancing Angle Imaging Methodology (GAIM), for detection of SA protrusion and bowing in the core. In this thesis, a systematic development of the methodology, experimental parameter optimization, SA protrusion and bowing identifications, qualitative and quantitative estimation of SA protrusion and bowing, mapping of SA honeycomb arrangement and identification of multiple protrusion in the honeycomb arrangement are presented. One of the main advantages of this methodology is, mapping of FSAs can be performed without actually going on to the top of each FSA. In addition to this, feasibility of applying GAIM in sodium environment is also studied. A LabVIEW program was specifically developed for acquiring the sector scan images and for generation of glancing angle images. Cross correlation and time shift followed by subtraction processing was used to improve the SNR of under sodium signals.

1.2 Outline of the thesis

The thesis is organized into seven chapters and the contents of each chapter are summarized below:

Chapter 1 discusses background context for the work carried out in this thesis. This chapter discusses briefly about FBRs. The reactor conditions during operation, consequences of these conditions (like protrusion and bowing) on FSA and requirement of under-sodium ultrasonic imaging are mentioned.

Chapter 2 presents literature review of various under-sodium ultrasonic scanners and associated methodologies developed by different countries for protrusion, bowing detection and for scanning of reactor internals. Under sodium scanners and methodologies developed by India for detection of protrusion and mapping of FSAs in PFBR are discussed in detail. The limitations of under sodium scanners and development of GAIM as an alternative to complex robotic scanner is presented. Literature review about application of glancing angle study in ultrasonic thermometry to monitor the temperature of sodium flow at the outlet of reactor core in FBRs are also discussed in this chapter. At the end, motivation and objectives of the present thesis arrived in view of the literature review are listed.

Chapter 3 presents the underwater experimental setup used for developing of GAIM. This section also describes the following experimental setups:

- optimization of parameters for developing GAIM,

- identification of diffracted echoes from the SA top using a rotatable table
- qualitative and quantitative estimation of protrusion and bowing,
- superposition of glancing angle data from two orientations for better visualization of honeycomb arrangement and
- minimum and multiple protrusion detection in a honeycomb arrangement

Experimental setup used for application of GAIM in sodium environment is discussed. Details about sodium test vessel, fabrication of under-sodium honeycomb arrangement setup (UHAS) and imaging of UHAS in different orientations in the sodium environment are also discussed in this chapter.

Chapter 4 discusses optimization of experimental parameters for mapping of honeycomb arrangement using GAIM. Identification of diffracted echoes from the SA head are presented. Qualitative and quantitative estimation of SA protrusion is presented. Signatures used for qualitative estimation of protrusion are listed. Parameters used for quantitative estimation of protrusion are also discussed. Random and multiple SA protrusion detection in the honeycomb arrangement is mentioned. Sensitivity of GAIM for the given honeycomb arrangement is determined.

Chapter 5 describes the detection of SA head bowing using GAIM. Parameters that can be used for qualitative and quantitative estimation of bowing are discussed. Superimposition of glancing angle images acquired from two different orientations for better visualization of the honeycomb arrangement are presented. Random SA bowing detection using the GAIM in the honeycomb arrangement is discussed. At the end of the chapter, influence of various experimental parameters on detection of protrusion and bowing using GAIM are mentioned.

Chapter 6 deals with experimental trials performed to study the feasibility of applying GAIM in under-sodium environment. The characteristics of signals acquired in sodium is compared with those obtained in water. The effect of wetting on the initial ringing of the under-sodium ultrasonic transducer is shown. Signal processing developed to improve the signal to noise ration (SNR) of under sodium ultrasonic signals is explained.

Chapter 7 summarizes the major results obtained, conclusions drawn and the scope for future work.

Chapter 2. Literature survey

2.1 Chapter overview

This chapter presents information about Prototype Fast Breeder Reactor (PFBR) and the design of Fuel Sub-Assemblies (FSA) used in PFBR. Conditions attributed to protrusion, bowing and need for detection of FSA protrusion and mapping of reactor core are discussed. Literature review of under-sodium ultrasonic scanner systems and associated methodologies developed by various countries for imaging of reactor internals, especially for detection of protrusion and bowing are presented. Limitations of existing under-sodium ultrasonic scanning systems and motivation for development of ultrasonic glancing angle imaging methodology (GAIM) are discussed in detail. The application of GAIM for ultrasonic thermometry to monitor the temperature of sodium flow at the outlet of reactor core in FBRs is also presented followed by objectives of present study.

2.2 About Prototype Fast Breeder Reactor (PFBR)

Prototype Fast Breeder Reactor (PFBR) is a sodium cooled reactor with an electrical power output of 500 MWe. It is at an advanced stage of commissioning at Kalpakkam, Tamil Nadu, India [3]. The main components of reactor include, main vessel, safety vessel, fuel sub-assemblies, primary sodium circuits and intermediate heat exchangers (IHXs). Figure 2.1 shows the cross-sectional view of PFBR. The prime material of construction is SS 316 and sodium is used as coolant, which provides efficient heat transfer from reactor core to steam generator [4]. In general liquid metal coolants like mercury, molten salt, sodium and lead-bismuth eutectic (LBE) are used in FBRs, among these liquid metals, most of the countries use liquid sodium as coolant in FBRs due to following reasons [5 – 6]:

- it has a high thermal conductivity varying from 85.8 W/m-K at 100°C to 63.9 W/m-K at 550°C.
- it also has a reasonably higher specific heat when compared to other metal coolants (~1340 J/kg-K).
- its melting and boiling temperatures are 97.8°C and 882°C, respectively and
- in addition to this, sodium has other advantages such as low neutron absorption cross section, low activation, high corrosion resistance of stainless steel in sodium and low moderation for fast neutrons.

In PFBR, main vessel is filled with 1150 t of liquid sodium and is blanketed by argon gas at the top. Reactor internals such as inner vessel, IHX, primary sodium pumps and SAs are immersed in liquid sodium. Mixed uranium-plutonium oxide (MOX) mixture is used as fuel in PFBR. This fuel is made in the form of pellets and placed in fuel pins [7]. D9 material is used for FSA because of its resistance to irradiation swelling. The details of the chemical composition of structural materials used in PFBR are given by Mannan et al. [8]. Figure 2.2 shows the hexagonal shaped FSA filled with 217 fuel pins. Total length of each FSA is 4 m. Top of each FSA has a hexagonal head of height 150 mm (highlighted with red box in Fig. 2.2). The internal diameter (ID) of FSA head is circular in shape with a diameter and thickness of 110 mm and 4 mm, respectively (highlighted with green box in Fig. 2.2).

Figure 2.3 show the arrangement of different types of subassemblies viz. (namely), control, blanket, reflector, shielding, storage subassemblies arranged from center to periphery of PFBR core. In PFBR, 181 FSAs are there in the center of reactor core. Each FSA consists of top and bottom blanket (Depleted UO_2) adjacent to MOX fuel pellets. In PFBR, the temperature of the nuclear core during operation will be ~550°C and the neutron flux levels will be in the order of ~ 8×10^{15} $n.cm^{-2}.s^{-1}$. High operational temperature and the intense neutron flux will result in issues like void swelling, irradiation creep and irradiation growth in the nuclear Fuel Subassemblies (FSAs), core structural materials and other reactor components [8 – 11].

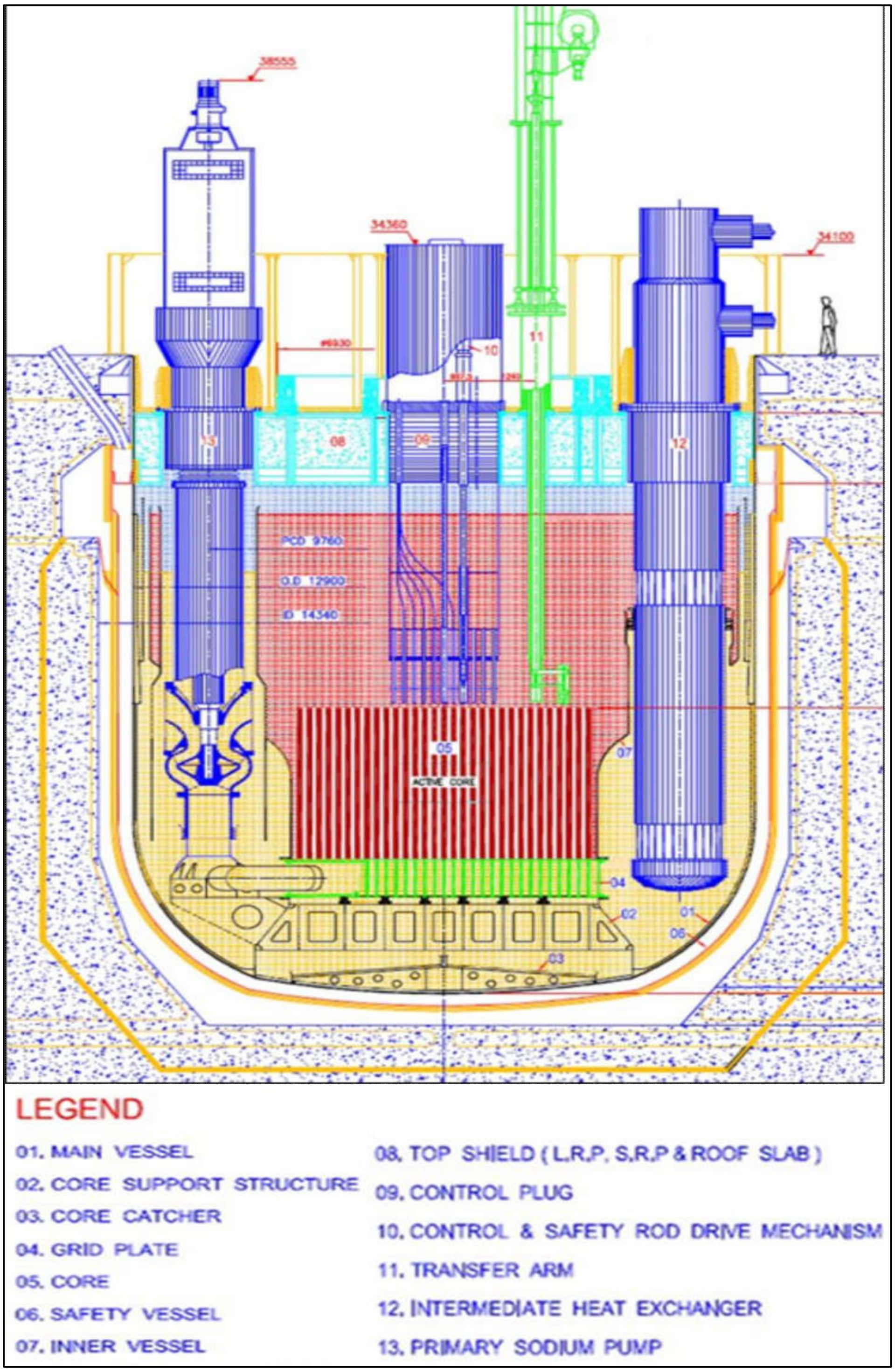

Figure 2.1 Cross-sectional view of PFBR [3]

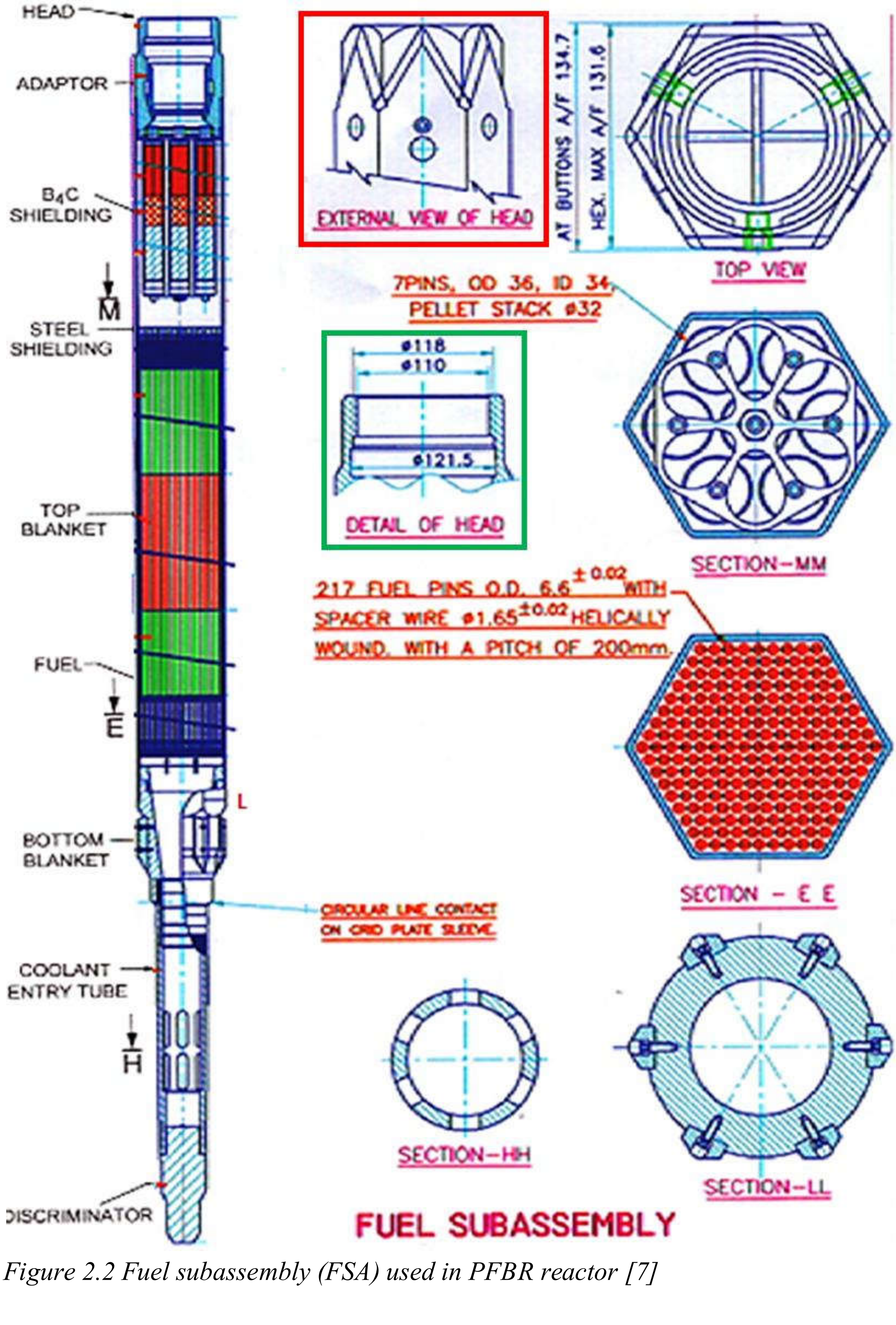

Figure 2.2 Fuel subassembly (FSA) used in PFBR reactor [7]

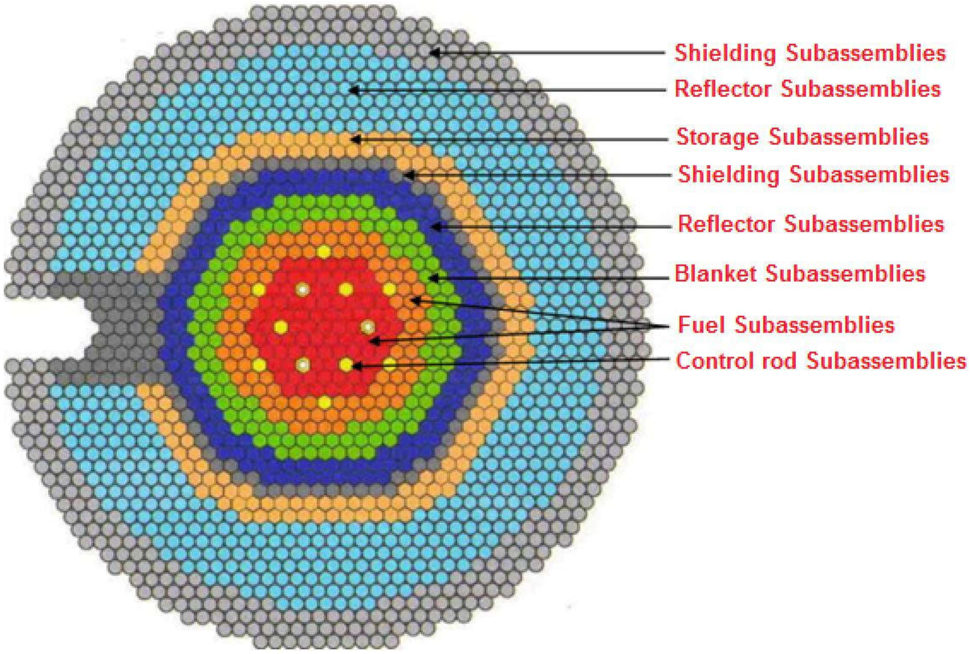

Figure 2.3 Arrangement of different subassemblies in PFBR [9]

Due to high temperature and irradiation, there is a possibility of FSAs growth. When growth exceeds permissible level, then it is called FSA "protrusion" [12]. Before any fuel handling operation, it is mandatory to ensure that none of the FSAs are protruded beyond the allowable limits. In addition to this, due to high neutron flux and temperature gradients, differential swelling of FSAs may occur. Because of neutron flux gradient, SAs in the periphery tend to bow outwards more, when compared to central FSAs. This is known as "flowering" of FSAs [13]. Bowing of FSA is proportional to neutron flux gradient. Excessive bowing will make fuel handling difficult to lift the spent FSAs from core. So, identifying the extent of protrusion and bowing are essential before all fuel handling campaigns. As liquid sodium is opaque, it is not possible to use conventional visual inspection methods to identify reactor internals. Hence, ultrasonic is the most suitable method for detection of core structural materials and reactor components in liquid sodium environment [14]. During PFBR shutdown, temperature of liquid sodium will be ~180°C. The neutron flux, gamma levels, sodium flow velocity and pressure will be around 120 $n.cm^{-2}.s^{-1}$, 1.2×10^3 Sv/h, 0.91 m/s and 500 mbar, respectively. It is reported that the maximum tilt of FSA that may undergo from its mid length in PFBR is around 2° causing a lateral displacement of ~30 mm from its actual position [15 – 16].

Ultrasonic inspection will be performed in PFBR using under-sodium ultrasonic scanner (USUSS) as detailed in Section 2.4.7.2. Only after getting clearance of no protrusion beyond the permissible limit using USUSS through Large Rotating Plug (LRP) and Small Rotating Plug (SRP) rotation, fuel handling is carried out during reactor shutdown. USUSS is placed in In-Vessel Transfer Port (IVTP) access opening in LRP for initial screening of any FSA protrusion and then in observation port of SRP for detailed analysis, if required. In addition to protrusion detection, mapping of FSAs heads is also performed by USUSS mounted on observation port by rotating LRP and SRP in tandem over the core of PFBR. However, due to rotational constraints of rotating plugs, on which scanner is mounted, mapping of complete core is often not possible [17 – 18].

To carry out imaging of core structural materials and reactor components, many countries have developed complex robotic arm-based scanners. Using these scanners, under-sodium ultrasonic viewing/imaging methodologies are developed [14, 19 – 20].

2.3 Types of probes and scanning configurations used for ultrasonic imaging

In the present section details about important/generic parameters like, temperature of liquid sodium, wetting of ultrasonic transducer in liquid sodium which effects the under sodium imaging are discussed.

In addition to this, a review of types of transducers used (single, phased array, guided wave…), configuration of transducer (s) arrangement (single element, multiple single element, circular …), scanning mechanism (raster scan, theta-Z scan …), under sodium scanners and associated scanning methodologies developed in various countries.

2.3.1 Wetting of ultrasonic transducer

A good acoustic coupling between the ultrasonic transducer face plate and the liquid through which ultrasonic waves are to be propagated is important to get better signal to noise ratio (SNR). This acoustic coupling between the transducer face and liquid is called wetting. It is defined as the ability of a liquid to spread on a solid surface (here it is transducer face plate). It is measured by the contact angle (θ_y), which depends on the interfacial energies between solid-liquid (γ_{SL}), liquid-vapour (γ_{LV}) and solid-vapour (γ_{SV}) surfaces. Contact angle is defined by the Young equation given below [21].

$$Cos(\theta_y) = \frac{\gamma_{SV} - \gamma_{SL}}{\gamma_{LV}} \tag{1}$$

Pictorial representation of the wetting and non-wetting system on a homogenous solid material is shown in Fig. A1. From the figure it can be observed that for good wetting system the contact angle is acute (Fig. 2.4a), whereas for the no-wetting system the contact angle ($\boldsymbol{\theta_y}$) is obtuse (Fig. 2.4b) [21].

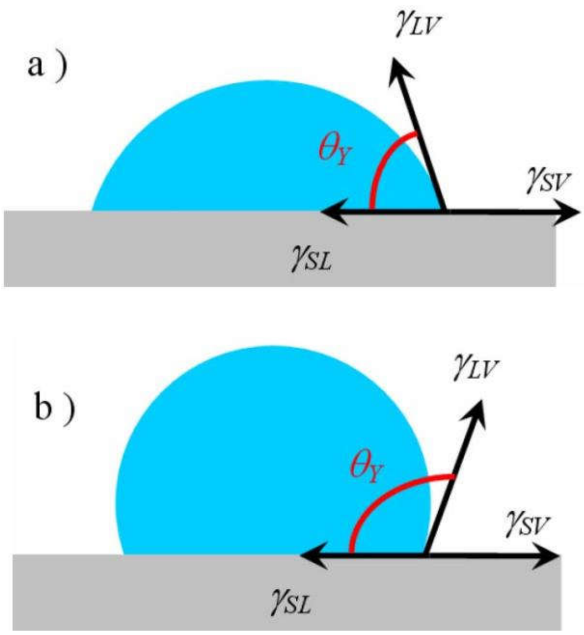

Figure 2.4(a) Wetting and (b) non-wetting of a liquid drop on the solid surface

Many factors like, roughness, temperature and formation of chromium oxide layer on the transducer face plate affects the wetting of stainless steel (SS) in liquid sodium below 300°C. It is reported that after 300°C of sodium temperature the wetting process is faster [22]. In addition to this, when there is roughness on the surface, then gas pockets are formed in the cavities due to which poor acoustic coupling is observed [23].

Paumel, et al. confirmed that the acoustic coupling is poor between sodium and stainless steel at 180°C due to the presence of gas pockets in the roughness cavities of the transducer face plate. They also established that, as the temperature of the sodium increases better acoustic coupling is achieved due to the dissolution of gas pockets and oxide layers at higher temperature [21].

Typical wetting angle values for a liquid sodium and stainless steel system is 105° – 100° for a temperature range of 100°C to 400° C of liquid sodium [24]. Whereas, for the water and stainless steel system at room temperature (25°C) the wetting angle is 0. That is the reason why, the acoustic coupling is obtained much faster in water-stainless steel system than in water.

2.3.2 Types of probes

Different types of ultrasonic probes were used for developing under-sodium ultrasonic imaging of reactor components. They are:

(i) single element ultrasonic transducer [25],

(ii) multiple single element ultrasonic transducers,

(iii) phased array ultrasonic transducer [26],

(iv) waveguide based ultrasonic transducers [27-28] and

(v) Electro Magnetic Acoustic Transducers (EMATs) [29-31]

In case of i – iii, piezoelectric crystal will be in direct contact with the medium in which ultrasonic waves are to be propagated.

In the case of (iv) a waveguide is used for sending the ultrasonic waves into the liquid metal for imaging of the reactor components. The ultrasonic transducer is not in contact with high temperature liquid metal, only waveguide is in contact with liquid metal [28]. In all other cases, transducer is in direct contact with high temperature liquid metal directly during imaging of reactor internals.

In case of (v), Lorentz force principle is applied in EMATs for generation and detection of ultrasonic waves in liquid sodium. In all other cases, ultrasonic wave is generated in the transducer and wetting of the transducer/waveguide surface affects the signal amplitude. In addition to this, Sheen et al., [32] developed phased array-based waveguide sensor for under-sodium viewing.

2.3.3 Scanning configurations

There are three most commonly used scanning configurations for identification of reactor internals. Based on the availability of space and movement constraint in reactor, any one of the three configurations are used in general. They are, summarized in Fig 2.5. For imaging multiple ultrasonic transducers and phased array based transducers are often used for fast scanning or redundancy, based on the requirement and availability of space in the reactor.

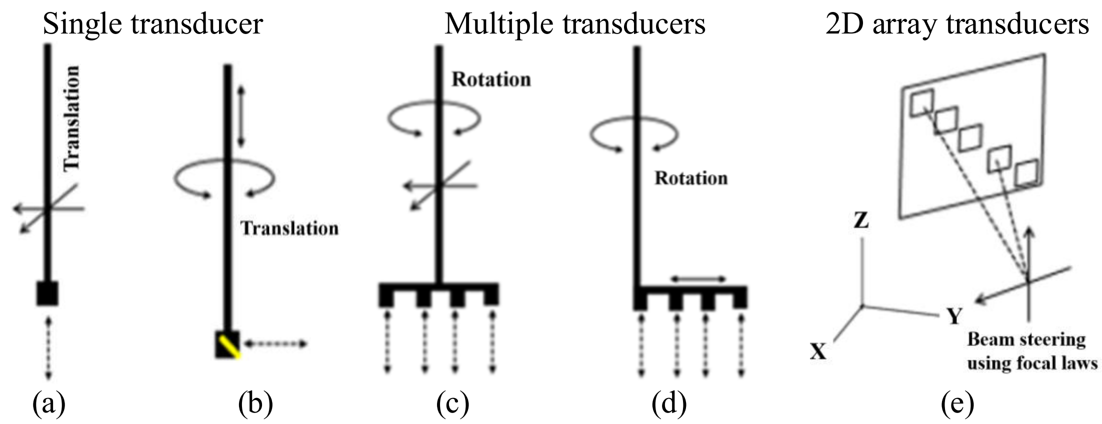

Figure 2.5 Different scanning configurations used in ultrasonic imaging [33]

In configuration shown in Figure. 2.5 a, ultrasonic beam propagates along Z-axis and probe moves along x and y axes. This is called as B-scan (translation of probe either in x-axis or y-axis) or C-scan (translation of probe both in x and y directions) imaging configuration.

In configuration shown in Figure 2.5 b, ultrasonic beam propagates along y-axis. The ultrasonic transducer is translated along z-axis and it can be rotated around central axis. This is called theta-Z imaging configuration or sector imaging configuration.

In configuration shown in Figure 2.5 c, scanning is carried out with multiple transducers and ultrasonic beam propagates along Z-axis. Here, ultrasonic transducers have three degrees of movement viz., x, y and theta. Using this configuration larger area can be covered than the single transducer case, as shown in Fig 2.5 a.

In configuration shown in Figure 2.5 d, scanning is carried out with multiple transducers and ultrasonic beam propagates along Z-axis. Here, transducer head, which is fixed to rotating axis translates along y-axis and have theta scanning along vertical rotating axis. There is no X-axis movement.

In configuration shown in Figure 2.5 e, small piezoelectric crystals are arranged to form a 2D matrix array. In this case, piezoelectric crystals are excited electronically and by applying different focusing laws, beam steering and focusing of ultrasonic beam at different depths are achieved. This is called the phased array ultrasonic imaging methodology.

Most of the under-sodium scanners use one of these scanning configurations for viewing/imaging the internals of the reactor [33]. In the next section, literature review of under-sodium scanners and corresponding imaging methodologies developed by different countries for imaging of FSAs and reactor components are discussed. In addition to this, the limitations of these methodologies and the motivation for the present work are presented.

2.4 Under-sodium scanners and associated imaging methodologies developed in different countries

Many countries have developed under-sodium scanner and imaging methodologies for visualizing reactor internals. In this section, developmental activities in different countries towards under-sodium imaging are discussed.

2.4.1 United States of America (USA)

The United States of America (USA) built many FBRs. Clementine was the world's first experimental fast-neutron reactor. The construction started in 1946 and it was commissioned in 1952. Later in 1964, Experimental Breeder Reactor – 1 (EBR-1) was commissioned and subsequently, EBR-2 was commissioned in 1994. During the year 1972, a prototype fast breeder reactor Fermi – 1 was commissioned. Later in 1980, a 400 MW thermal, liquid sodium cooled reactor named Fast Flux Test Facility (FFTF) reached criticality. In the below sections the under-sodium ultrasonic scanning systems developed for imaging these reactor internals are briefed.

2.4.1.1 Imaging using multiple single element ultrasonic probes

L. J. Bond, et al., [34] in 2012, developed an under-sodium ultrasonic scanner for reactor surveillance of Fast Flux Test Facility (FFTF) in USA. They developed azimuthal scanner with an array of ultrasonic transducers connected to a sweep arm as shown in the Figure 2.66. Eight focused piezoelectric transducers were used to carry out under-sodium experiments at sodium temperature range of 187°C – 217°C. All 8 transducers made up of PZT 5A material with a diameter of 3/8th of an inch. All 8 were focused transducers with a central frequency of 3 MHz. Using angular rotation, scanning of SA heads was carried out simultaneously using all transducers placed radially in a row. Figure 2.77 a and b show the actual image of the core mock-up at Fast Flux Test Facility (FFTF) and the corresponding under-sodium image obtained using 8 transducers, respectively. Figure 2.7 a shows the uniformly spaced circular and top SA mock-ups used for this study. From Fig. 2.7 b, ultrasonic images of flat plate and circular SA tops of the mock-up facility are clearly seen.

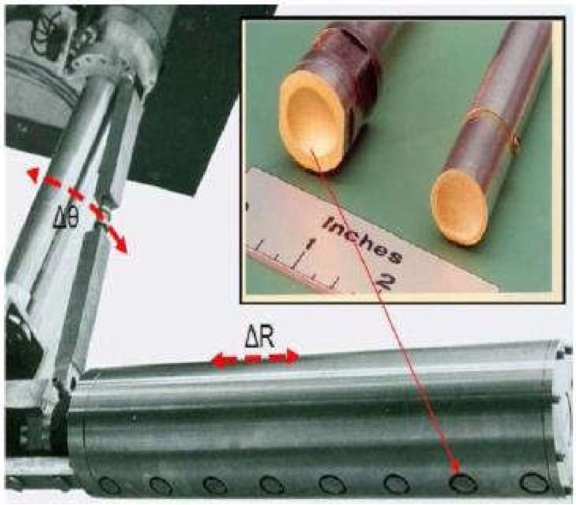

Figure 2.6 Sweep arm scanner head with 8 transducers [34]

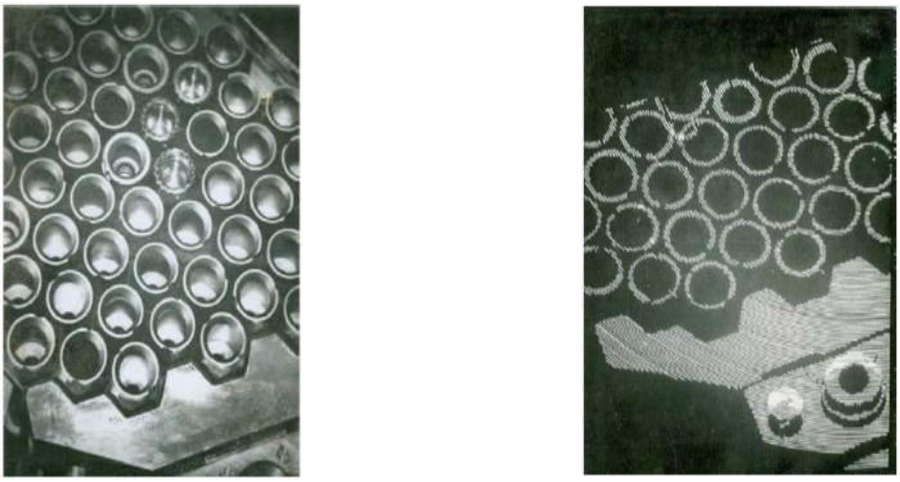

(a) (b)

Figure 2.7 (a) Core mock-up and (b) under-sodium image of core mock-up at FFTF [34]

2.4.1.2 <u>Imaging using phased array probe</u>

A linear array scanner was developed by Pacific Northwest National Laboratory (PNNL), USA for under-sodium imaging and in-service inspection of sodium cooled fast reactor at a temperature of 260°C [35]. The array consists of 12/24 Lead meta-niobate piezoelectric (K-81) elements with a central frequency of 2 MHz each. For quick wetting, a nickel alloy foil was used as the faceplate. Figure 2.88 shows the phased array probe developed by PNNL for under-sodium ultrasonic imaging. The acoustic response of 12 element array transducer obtained at a distance of 5 mm from the transducer faceplate is shown in Figure 2.9 [36]. From Fig. 2.8, spacing between few elements is clearly seen.

Figure 2.8 12 element phased array probe [36]

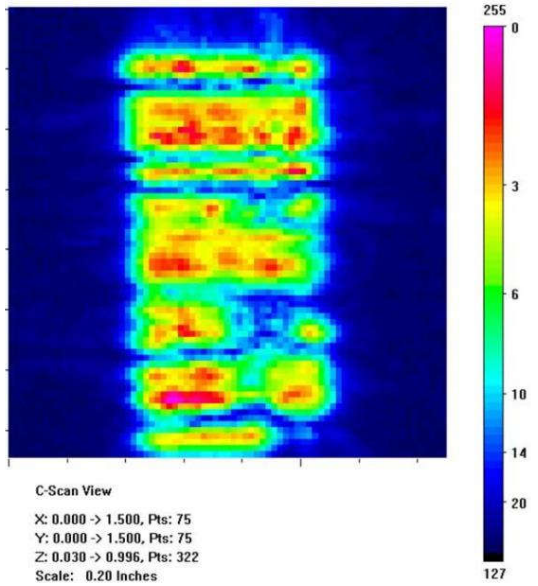

Figure 2.9 Near-field acoustic response of phased array probe [36]

2.4.1.3 <u>Imaging using waveguide probe</u>

When under-sodium imaging is carried out using a piezoelectric transducer, we must ensure that the operating temperature during inspection is less than its Curie temperature, to avoid a permanent damage to piezoelectric element. Operation at higher temperature, piezoelectric element with higher Curie temperatures (T_C) such as Lead Metaniobate ($PbNb_2O_6$) (T_C = 540°C), Lithum Niobate ($LiNbO_3$) (T_C = 1210°C), Modified Bismuth Titanate ($Bi_4Ti_3O_{12}$) (T_C = 600°C), Aluminum Nitride (AlN) (T_C = 110°C) should be used for inspection [37]. However, higher Curie temperature piezoelectric crystals are expensive. As an alternative to this, a waveguide can be used to send ultrasonic signals into liquid sodium using a low Curie temperature piezoelectric transducer.

A waveguide can be a plate or rod, through which ultrasonic waves are transmitted to the inspection point from the ultrasonic transducer. The main objective of a waveguide is to prevent transducer from coming in physical contact with high temperature sodium. Different types of waveguides were proposed in literature for improving Signal to Noise Ratio (SNR) and to reduce spurious signals. A waveguide can be a normal or spiral rod, Bundle Wire Technology (BWT) waveguide etc., which were used in a nuclear reactor for under-sodium imaging [25 – 28].

Argonne National Laboratory (ANL), USA developed a customized prototype waveguide of length 12″ with a bundle of thin rods covered with inner and outer tubes. This waveguide was a combination of bundled rod and spiralled sheet designs. This configuration was welded at the bottom with a gold plated focus lens (this lens have a focal length of 1" in air). A 5 MHz ultrasonic transducer for under-sodium C-scan imaging of a sample at a sodium temperature of 377°C was used for this study. Figure 2.1010 a and b show the schematic of experimental setup used for ultrasonic imaging and corresponding waveguide used for experiments, respectively [38].

Figure 2.111 (a-c) show the photograph of the sample, Time of Flight (TOF) and amplitude-based C-scan images obtained using waveguides, respectively. In Fig 2.11 a, the yellow square shows the scanned area on the sample. From Fig 2.11 b, it can be seen that TOF from flat surface of specimen is in green colour (less distance) than TOF from notches and "V" shaped grove in the scanned area of the sample. The same trend is observed in the amplitude based C-scan image also, high intensity (red colour) is observed from the flat surface of the sample than from the curved surfaces of the scanned area of the sample. In addition to this, low intensity reflection is observed from the two horizontal notches present in the scanning area.

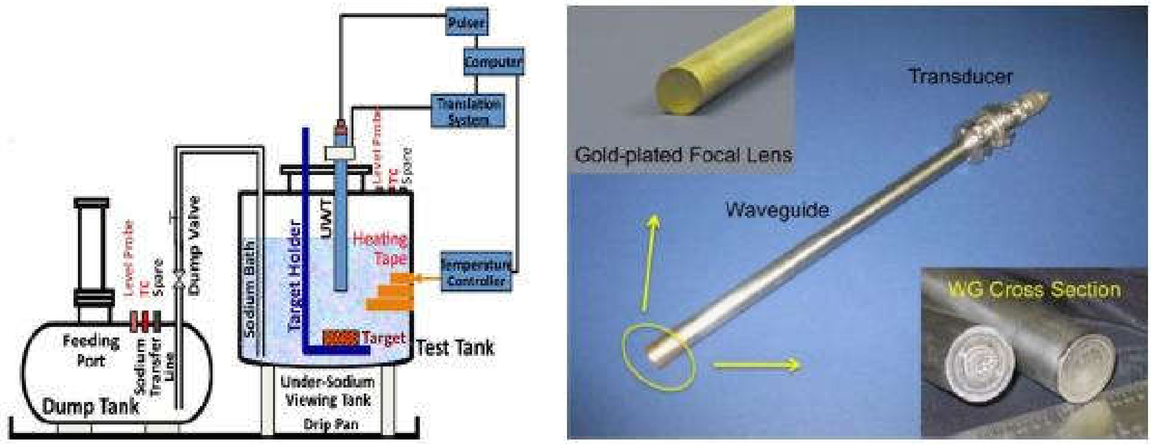

(a) (b)

Figure 2.10 (a) Schematic of under-sodium viewing facility and (b) waveguide used for under-sodium studies [38]

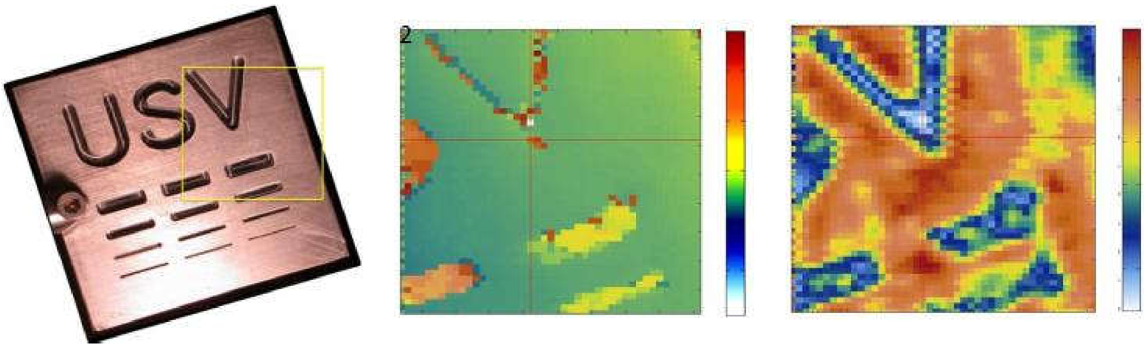

(a) (b) (c)

Figure 2.11 (a) Photograph, (b) time of flight and (c) amplitude based C-scan image of the sample used for under-sodium ultrasonic imaging using a wave guide [38]

2.4.2 United Kingdom (UK)

United Kingdom (UK) developed two fast breeder reactors namely, Dounreay Fast Reactor (DFR) and Prototype Fast Reactor (PFR). DFR and PFR went to criticality in 1959 and 1974, respectively. Both of them were owned and run by United Kingdom Atomic Energy Authority (UKAEA). The under-sodium ultrasonic scanning systems developed in these reactors are discussed briefly in the following sections.

2.4.2.1 *Imaging using multiple single element ultrasonic probes*

UK Atomic Energy Authority (UKAEA) and National Nuclear Corporation, UK had developed an under-sodium scanner used for inspection of fuel SA distortion in PFR core. The scanner was called as ultrasonic Rigid Under-sodium Viewer (RUSV). RUSV have a 11 m long tube with diameter of 25 cm which contains 12 transducers fixed at its bottom end. Out of the 12 transducers 8 Down/Vertical Viewing Transducers (DVTs) and 4 Side/Horizontal Viewing Transducers (SVTs) with central frequency of 5 MHz each. Figure 2.12 shows the schematic of RUSV. The scanner was inserted into the reactor through an opening in the rotating shield. The scanner was rotated using the combination of rotating shield movement and its own axis to scan core plenum area for protrusion detection of FSA. By rotating the scanner about its own axis, imaging of FSAs was carried out using DVTs fixed at the bottom of the scanner. The DVTs were excited in sequence and the amplitude and TOF of the echoes were recorded and stored along with encoder reading of the position of RUSV [39].

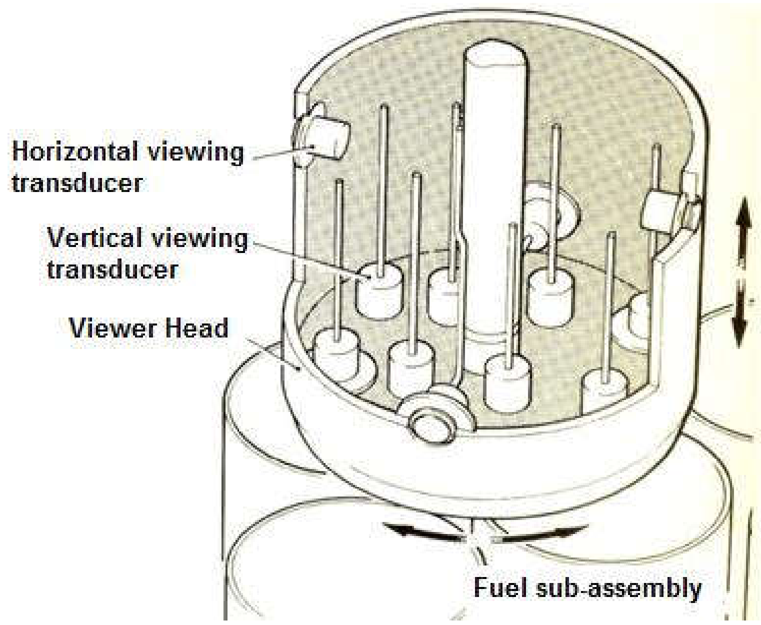

Figure 2.12 Ultrasonic Rigid Under-sodium Viewer (RUSV) developed by UKAEA for under-sodium inspection of PFR core [39]

Figure 2.133 a and b show the photograph of PFR core top before filling liquid sodium into the reactor and the schematic of each SA head of PFR core, respectively. It can be observed that SA head top were either circular or hexagonal in shape. The hexagonal SA heads were experimental subassemblies. Figures 2.13 c shows the TOF based under-sodium image of a section of PFR core. The color coding of the image represents distance of reflecting surface from transducer, each color covers a range of 25 mm from transducer. The green color represents the top ring of each SA head, blue color surface corresponds to orientation bar placed inside each SA head. In addition to this, red color surface corresponds to breeder plate at the bottom of each SA head. Different colors codes were given for easy identification of SA components.

In addition to TOF based image, amplitude-based image of PFR core was also obtained using RUSV as shown in the Fig. 2.13 d. For bowing measurements, visual fitting of pre drawn circle (whose diameter was same as diameter of the top ring of SA head) with under-sodium image was carried out to judge the condition of each SA head. If there was a miss match of ±1 mm between the pre drawn circle and SA top ring, then SA head was considered to be a bowed SA head. The TOF data was also used to measure the protrusion of 95% SA heads in PFR core with a precision of 0.25 mm [39 – 40].

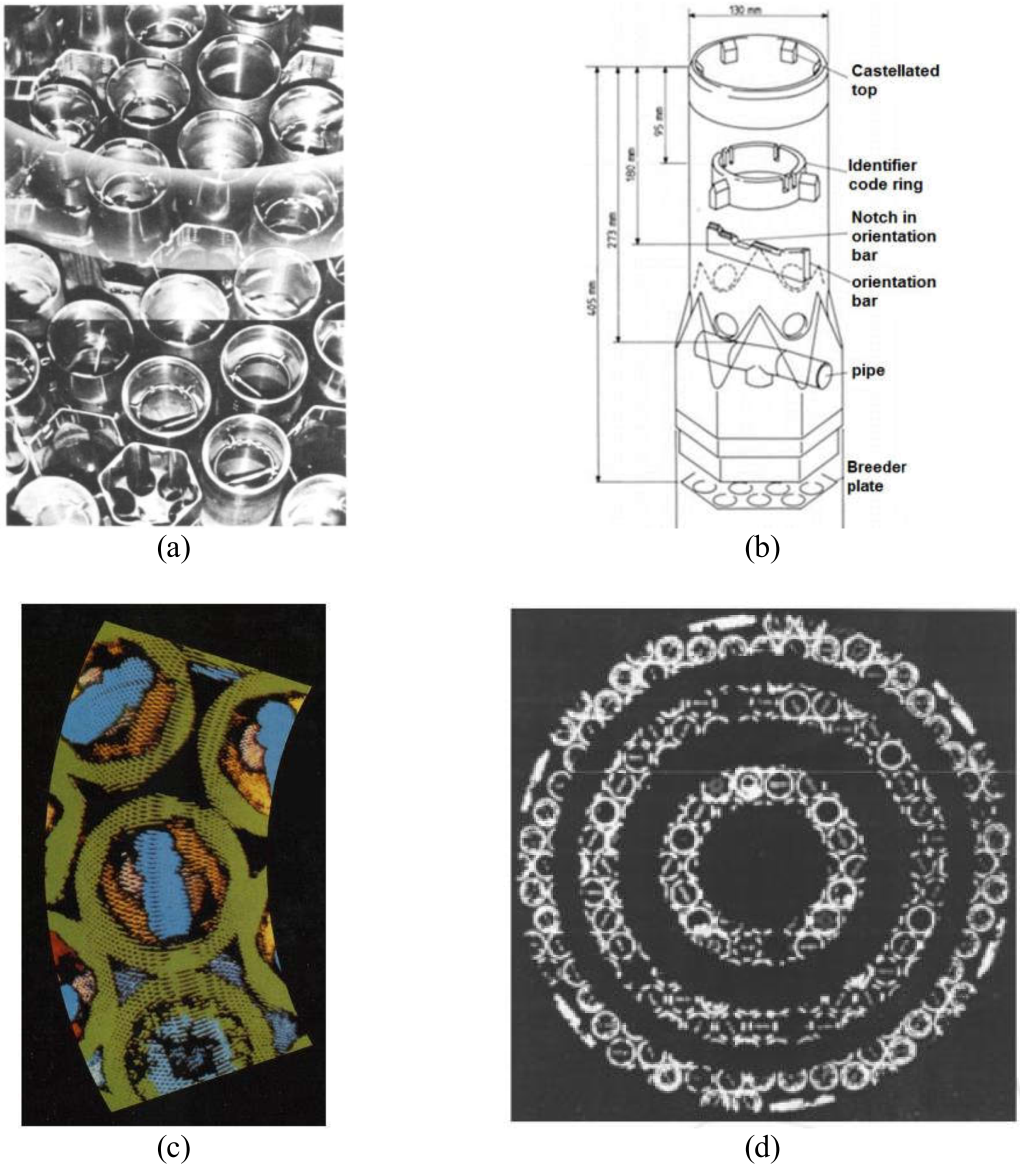

Figure 2.13 (a) Photograph of PFR core, (b) schematic of each SA head in PFR, (c) under-sodium image (TOF) of a sector of PFR and (d) Complete under-sodium image of PFR [39 – 40]

In addition to this, UKAEA also developed “Linked Sweep-Arm Scanner” (LSAS) for under-sodium imaging of reactor internals. Figure 2.144 a and b show the photograph and deployment sequence of LSAS into reactor, respectively. In LSAS an opening arm was lowered through a vertical tubular mast as shown in deployment sequence (step 1-5) in Fig. 2.14 b. Ultrasonic transducers were fixed to this lowered arm facing downwards at the bottom links. Figure 2.155 a and b show scanning of cylindrical FSAs’ tops carried out by LSAS in water and the corresponding image of the same, respectively. Each line in the image represents the reflected echo obtained from the top ring of the cylindrical SA head top. The scanning was performed using a 5 MHz DVT [41].

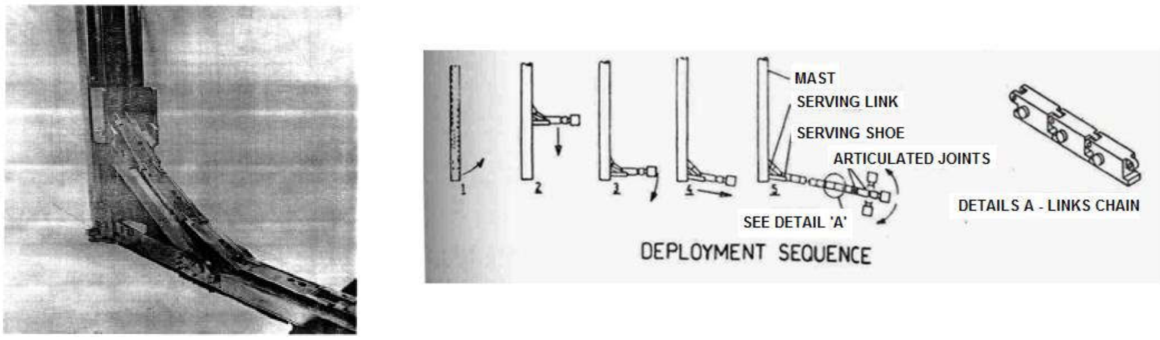

(a) (b)

Figure 2.14 (a) Actual picture and (b) deployment sequence of LSAS [41]

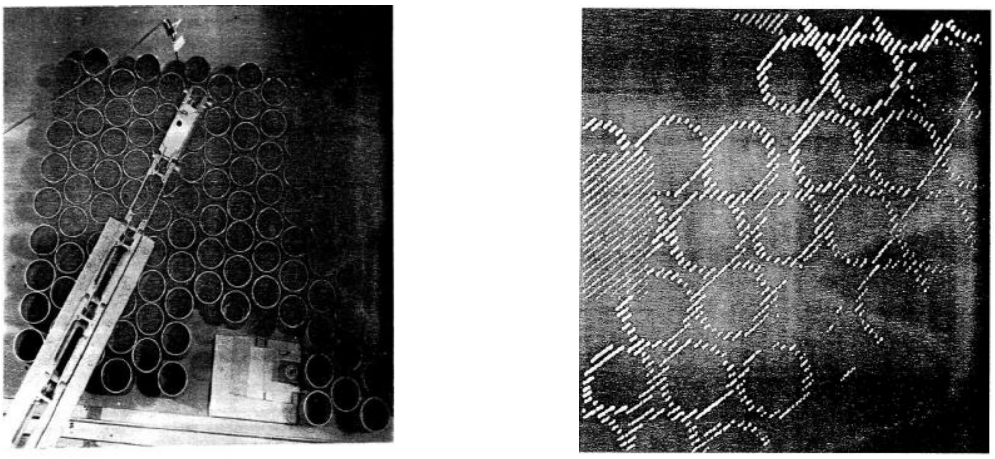

(a) (b)

Figure 2.15 (a) Scanning of cylindrical FSAs and (b) under water image of FSA heads using LSAS [41]

2.4.3 France

France has vast experience in FBR technology and in running nuclear reactors. Rapsodie, France's first experimental sodium-cooled reactor went critical in 1967. Later in the year 1973 and 1985, other two fast breeder reactors Phénix and Superphénix went critical, respectively. All three reactors are in the decommissioning process currently. In 2006, France started fourth generation of sodium-cooled fast breeder reactor called, Advanced Sodium Technological Reactor for Industrial Demonstration (ASTRID), in collaboration with other countries. The under-sodium ultrasonic scanning systems developed by France for imaging/scanning the internals of the reactors are discussed in brief.

2.4.3.1 Imaging using waveguide probe

In 1974, ultrasonic sodium VISUalization Systems, known as VISUS was developed for under-sodium scanning of FSA loading in Phénix [42]. It was a non-imaging system used for detection and location of obstacles which could hinder the movement of rotating plugs during fuel handling in Phénix. Figure 2.166 shows the positioning of the scanner system in the Phénix reactor. The ultrasonic transducer was fixed at the top of the scanner located above the roof slab and ultrasonic waves were sent into liquid sodium using the wave guide and angled mirrors. The scanner used NaK waveguide and 45° mirrors to direct its sound through plain diaphragms with a thickness and diameter of 2.9 mm and 45 mm, respectively. The scanner have two wave guides, one for transmitting ultrasonic waves and other for receiving reflected echoes from internals of reactor. Figure 2.177 shows the scanner mechanism of VISUS scanner and positioning of two wave guides in VISUS scanner [42]. The scanner performed theta-Z scanning of reactor core plenum area to identify any obstacles in exploration volume as shown in Fig. 2.17. The scanning angle was ± 135° on either side from rotating axis, in addition to this core plenum area of 200 mm was also scanned for identification of unwanted objects in the region of interest.

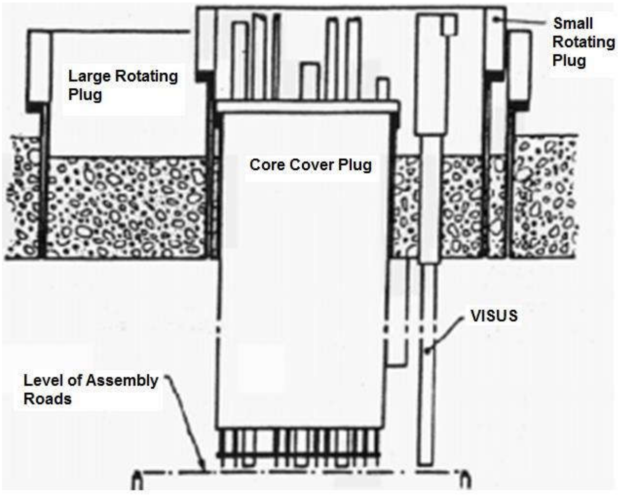

Figure 2.16 Location of VISUS scanner installed in Phénix [42]

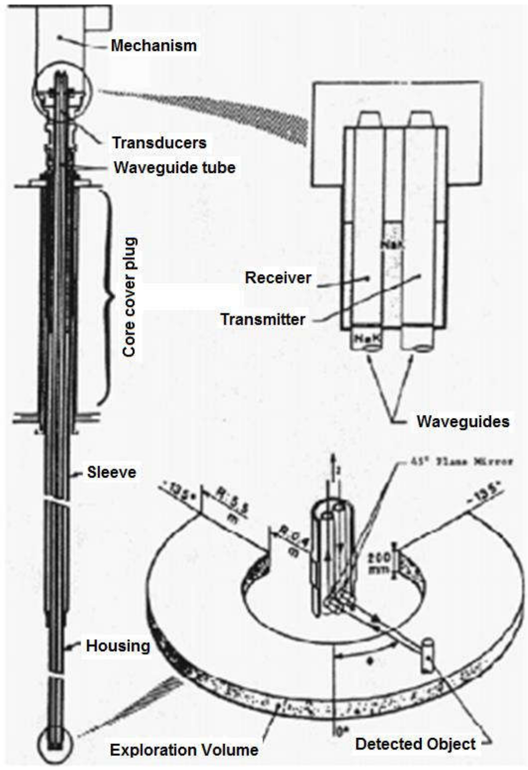

Figure 2.17 Scanning mechanism of VISUS scanner [42]

2.4.3.2 <u>Imaging using single element ultrasonic probe</u>

F. Baque et al., [43] reported single element high temperature ultrasonic transducers developed in France for under-sodium ultrasonic imaging namely, High-Temperature Ultrasonic Transducers (TUSHT). TUSHT transducer can work up to 600°C sodium temperature. Figures 2.18 a and b show different part present in TUSHT transducer and photograph of TUSHT transducer, respectively. The case diameter and central frequency of TUSTH transducer are 40 mm and 6.5 ± 0.4 MHz, respectively.

CEA developed scanning robot called VENUS (Visualisation undEr Na by Ultrasounds), for viewing under-sodium components and for identification of defects present in components. TUSHT transducer was fixed to VENUS robot and under-sodium scanning of mock-up sample was carried out at sodium temperature of 200°C [44].

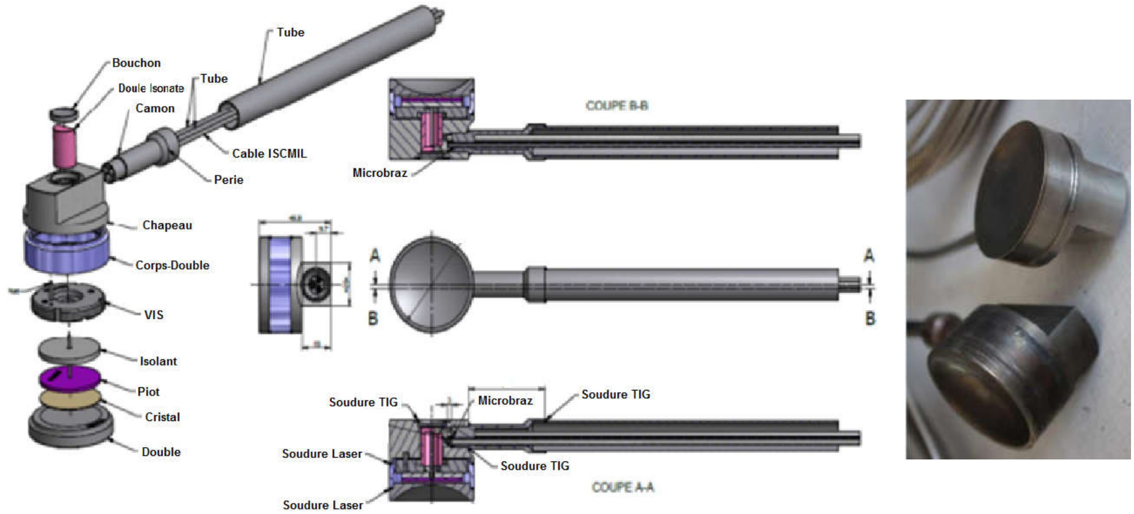

(a) (b)

Figure 2.18 (a) Different parts and (b) photograph of TUSHT transducer [43]

Figures 2.19 a and b show the photograph and schematic of VENUS robot respectively. VENUS scanner have 3 scanning axes namely, X, Y and Z. All 3 axes should work in tandem to perform a raster scan of a sample. The main advantage of VENUS scanner is that it can perform short distance (less than 200 mm) scanning, which can be useful for identifying lost part in a reactor. Under-sodium imaging trails were perform using the VENUS scanner in Double Latitude pour Maintenance En sodium (Na) (DOLMEN) sodium circuit present at CEA, Cadarache.

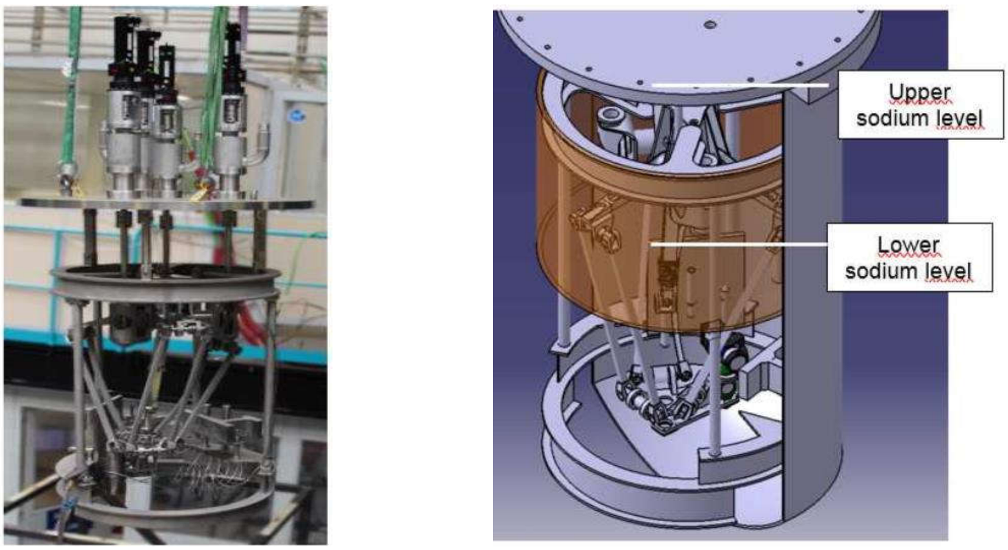

(a) (b)

Figure 2.19 (a) Photograph and (b) schematic of VENUS robot [44]

Raster scanning of mock-up sample was performed using VENUS robot and 3D reconstruction of mock-up was generated based on reflected ultrasonic intensities received from the mock-up sample. Figures 2.20 (a – c) show the photograph of mock-up sample, 3D reconstructed image superimposed on mock-up sample and (c) resolution of fine grooves and "cea" letters obtained from ultrasonic images generated using TUSHT transducer.

In Fig 2.20 a red square shows the area imaged on mock-up sample. The mock-up sample was made up of different geometries like, tube, triangle plate, different width grooves, and letters. The scanning of mock-up sample was carried out from close distance ranging from 150 – 200 mm. 3D re-constructed image shown in Fig. 2.20 b, it can be seen that different depths of the mock-up sample were represented by different colors. The tube like structure, which was close to transducer was represented by blue color, at the base plate which was far from the transducer has a red color representation. From ultrasonic signals shown in Fig 2.20 c, it can be observed that the thinnest groove which has a width of 500µ was also resolved/identified using TUSTH transducer due to the fact that scanning was performed at very close distance.

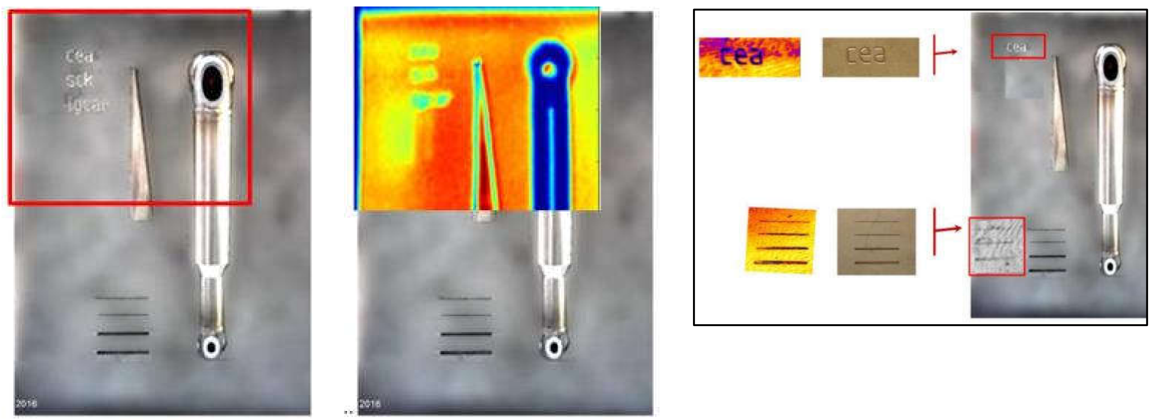

(a) (b) (c)

Figure 2.20 (a) Photograph, (b) 3D reconstruction and (c) resolution of fine grooves and "cea" letters of the mock-up sample [44]

2.4.3.3 Imaging using phased array probe

In addition to VISUS and VENUS scanners CEA developed, Ultrasonic phased array system was also developed for imaging of reactor internals in Superphénix reactor. The advanced IMAgerie Rapide en SODium (IMARSOD) system was developed using two linear arrays of 128 elements placed orthogonal to each other, one for transmitting and other for receiving ultrasonic signals. This system was developed for long distance scanning (greater 200 mm) of targets. Figure 2.10 a shows the schematic of ultrasonic beam focusing using IMARSOD scanner. The design of antenna was made in such a way that the focal zones of arrays form a vertical and horizontal lines. Focal point was identified by the intersection of vertical and horizontal lines. By applying different focal laws/delay laws to elements, beam steering and focusing of ultrasonic beam can be achieved. Under water experimental trails were performed to study performance of IMARSOD. The parameters to be used for two linear arrays were optimized using CIVA simulation and then under water trails were performed. Figure 2.21 b shows the CIVA model of the IMARSOD. Figures 2.21 c and d show the underwater experimental setup and underwater image of the target. From Fig 2.21 c it can be observed that, two orthogonal linear arrays were placed in front of a spherical target to be imaged. Different imaging methods like, C-scan, Full Matrix Capture and Total Focusing Methods showed good performance of IMARSOD system [44 – 45].

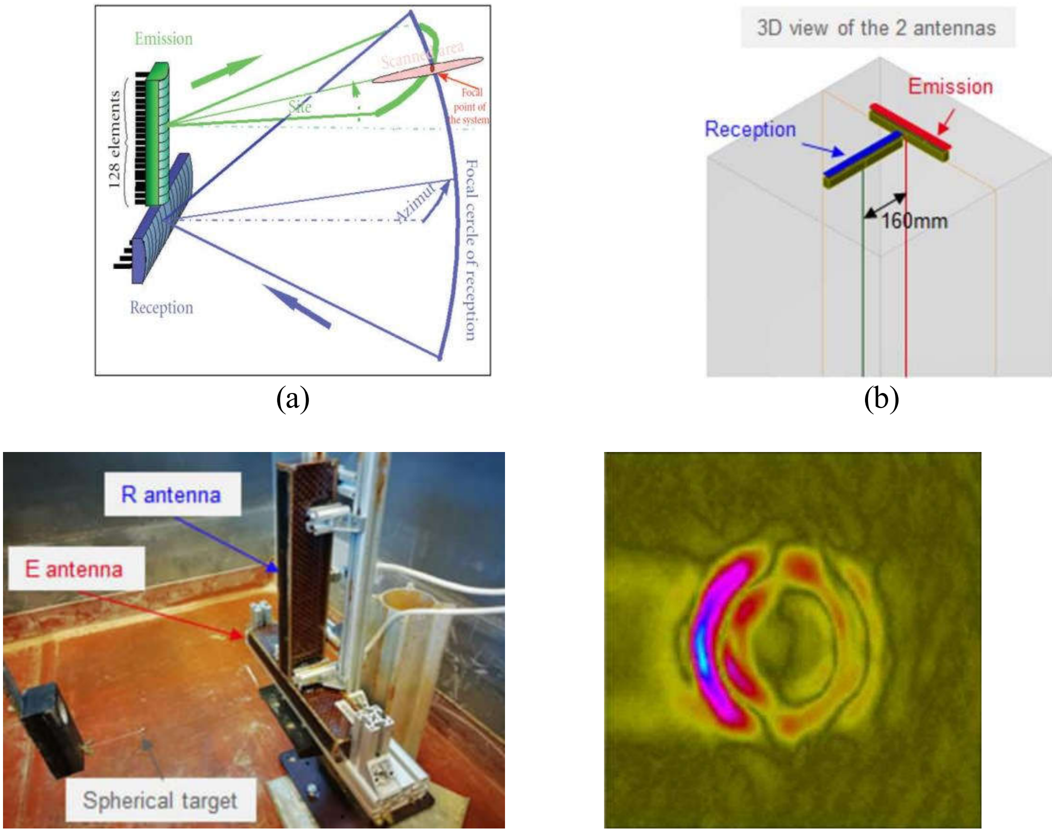

(a) (b)

(c) (d)

Figure 2.21 (a) Schematic, (b) CIVA model, (c) underwater experimental setup of ultrasonic phased array system and (d) underwater image of spherical target obtained using IMARSOD [44 – 45]

2.4.4 Japan

Japan Atomic Energy Agency (JAEA) started construction of experimental fast-breeder reactor "Joyo" in 1970. It is a Liquid Metal Fast Breeder Reactor (LMFBR), it attained criticality in 1977. Later in 1985, JAEA started construction of prototype FBR called "Monju", this reactor reached criticality in 1994. In the below sections, the under-sodium ultrasonic scanning systems developed in these reactors are discussed in brief.

2.4.4.1 Imaging using single element ultrasonic probe

In 1980, Toshiba (in association with Power Reactor and Nuclear Fuel Development Corporation (PNC)) developed a vertical Under-sodium Viewing System (USV) using high temperature transducer and suitable drive mechanism [20]. The USV was used as an instrumentation tool in Joyo reactor for visualizing reactor components. This was a vertical type scanner in which ultrasonic transducer was attached at the bottom end. The electronic system of this scanner could display the image. Figure 2.22 shows the USV scanner design. Two electrical motors were used for rotational movement of inner cylinders through electromagnetic couplers. Underwater imaging at room temperature and under-sodium imaging at 300°C was carried out on a customized sample using 5 MHz ultrasonic transducer. The transducer was made of Lithium Niobate ($LiNbO_3$) crystal. Due to space constraint and to avoid tension on the MI cable, a spiral trace scanning was carried out for imaging the sample in water and sodium.

Figure 2.23 shows the schematic of the customized sample used for imaging using USV. It can be observed from sample that different widths (same length of 15 mm) of acoustic reflectors varying from 3 mm to 14 mm were arranged in a circular pattern to evaluate the resolving power of scanner. Sufficient spacing was provided between the adjacent reflectors for better resolution of images. Figures 2.24 a and b, show the under-water image and under-sodium image of same sample, respectively. The sample was kept at a distance of 50 mm from ultrasonic transducer while scanning in water and in sodium at 300°C. It can be seen from Figs 2.24 a and b that images obtained in water and liquid sodium are similar to each.

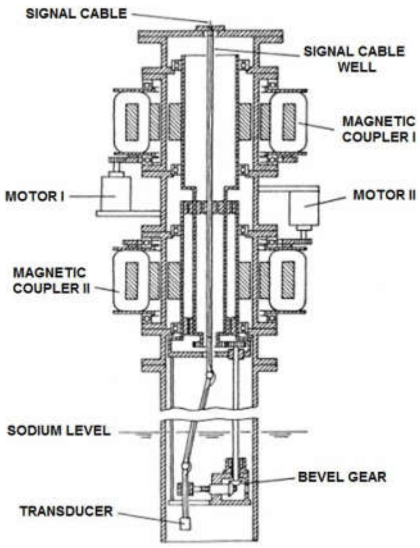

Figure 2.22 USV scanner design [20]

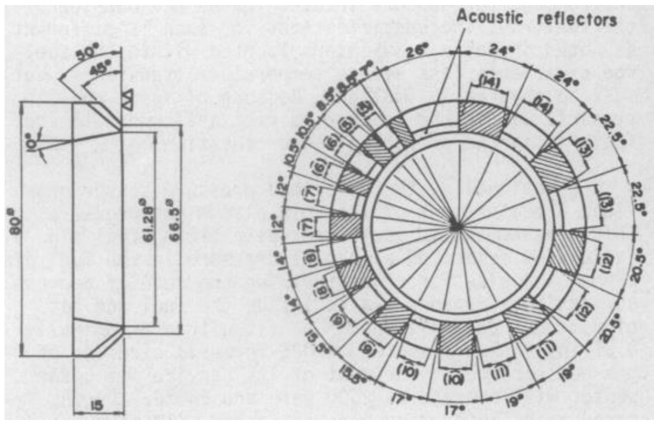

Figure 2.23 Schematic of the sample used for imaging in water and sodium using USV [20]

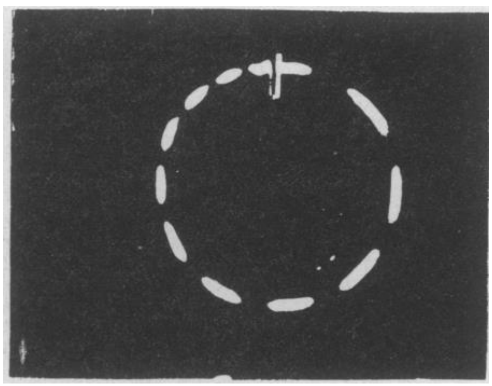

(a)

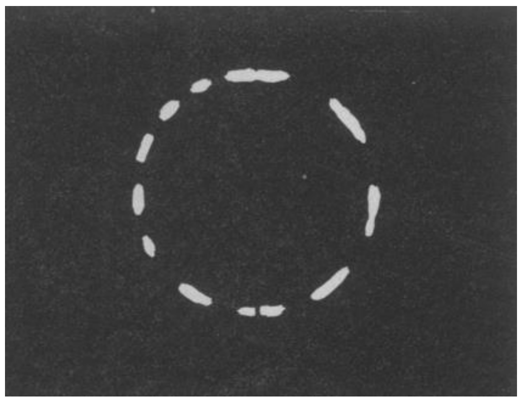

(b)

Figure 2.24 (a) Under water and (b) under-sodium image of the sample obtained using USV scanner [20]

2.4.4.2 <u>Imaging using phased array probe</u>

Toshiba Corporation and Japan Atomic Power Corporation developed a phased array based under-sodium imaging system for real time ultrasonic inspection and imaging of internals in Demonstration Fast Breeder Reactor (DFBR) in Japan. Figure 2.25 a and b show the schematic of phased array configuration of 36 X 36 elements transducer and its photograph, respectively. The individual piezoelectric elements were of size 2.5 mm × 2.5 mm, and each element was separated by 5 mm center – to – center distance. Synthetic Aperture Focusing Technique (SAFT) was used to synthesize the 3D images.

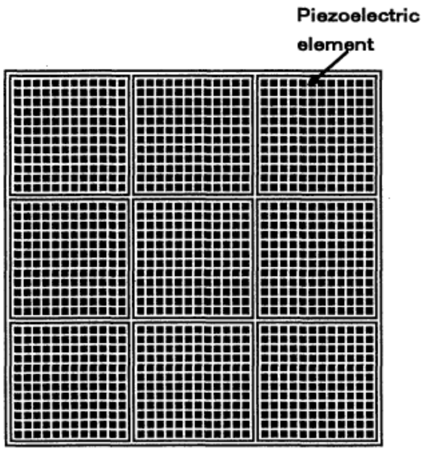

(a)

(b)

Figure 2.25 (a) Schematic of elements and (b) photo of phased array probe used for under-sodium imaging [20]

Figure 2.26 (a – c) show the sample used for under-sodium ultrasonic imaging and corresponding images obtained by imaging the sample at different distances of 400 mm and 1000 mm, respectively. The sample was a 110 mm X 110 mm square plate made up of stainless steel. Different diameter of concentric circles and different depths of circular cones were engraved on the sample for approximating the axial resolution. Sodium temperature was maintained at 200 ± 10°C during scanning. From under-sodium images, it is observed that circumferential resolution of 1.5 mm and 2 mm was achieved when scanning distance was 400 mm and 1 m, respectively. An axial resolution of 0.5 mm was achieved when scanning was performed from 400 mm and 1 m [20].

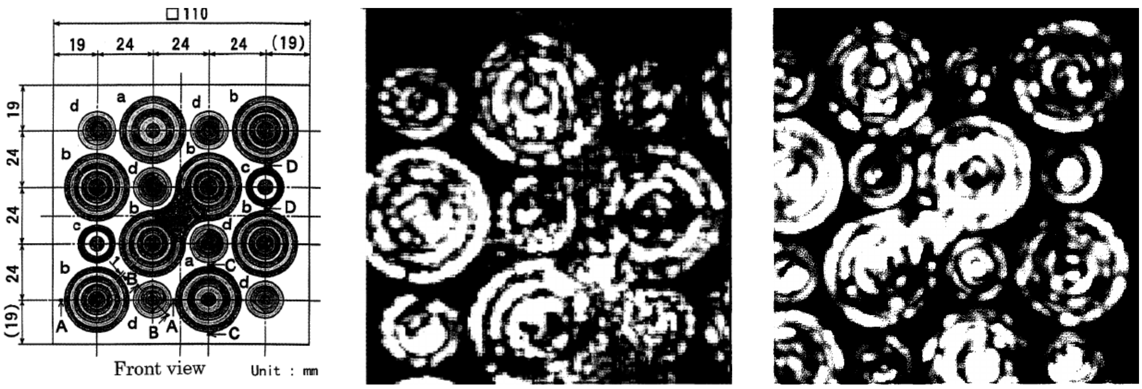

(a) (b) (c)

Figure 2.26 (a) Schematic of the sample used for under-sodium imaging, under-sodium image at a distance of (b) 400 mm and (c) 1000 mm [20]

2.4.5 Germany

The first fast breeder test reactor in Germany was KNK-II with 20 MW electric output. The construction of this reactor started in 1974 and reached criticality in 3 years. After successful operation, KNK-II was shut down in 1991. Later Germany started construction of SNR-300 proto type fast breeder reactor in 1973. However the reactor was stopped after completion of construction in 1985. The development of the under-sodium scanners and methodology used by Germany are presented in the below section.

2.4.5.1 Imaging using multiple single element probes

In 1984, Hans et al. 1984 [14] designed a scanner for German reactor SNR -300. It was an offset arm type scanner. The transducers attached to it could move in radial direction, as shown in the schematic Figure 2.27. It consisted of a lance (i.e., a metallic shaft) with ~ 2.5 m long offset arm assembled with a multi-head transducer assembly. Two servomotor drives were used for rotation of the arm and radial movement of transducer head. Figure 2.28 a and b show the schematic and photograph of scanner. Scanner was meant for scanning top of FSAs and for inspecting instrumentation plate (i.e., below control plug). With the combined motion of rotating arm and radial movement of transducer head, point by point scanning of core was carried out by sweeping the lance over the core in sodium at 230°C. Lithium Niobate ($LiNbO_3$) crystal with a frequency of 4 MHz was used for scanning reactor internals. The measurements were based on TOF calculations.

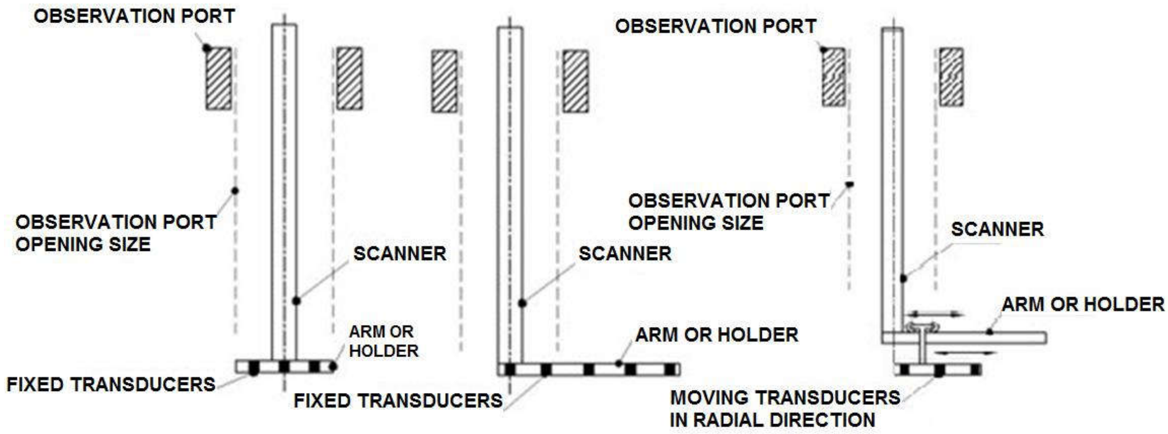

Figure 2.27 Schematic of rotational movement and radial movement of transducers fixed to lance [14]

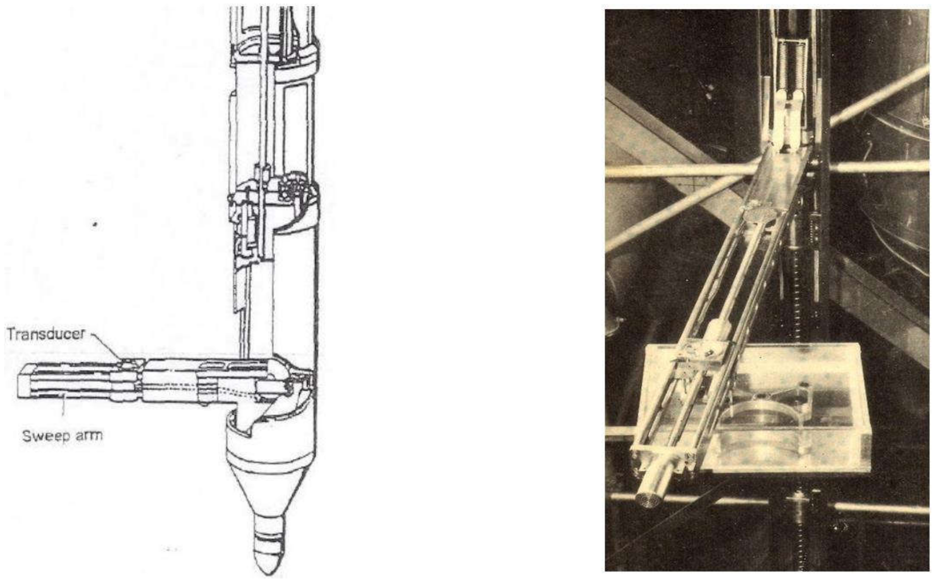

(a) (b)

Figure 2.28 (a) Schematic and (b) actual image of under-sodium scanner [14]

Wessels J, 1991 [46] developed a scanner for under-sodium viewing by arranging eight transducers in a circular manner for under-sodium inspection of German reactor. Figure 2.29 shows the arrangement of ultrasonic transducers in circular manner. The scanner used an arm-based handling device for imaging reactor core. The under-sodium imaging of a sample is shown in Figure 2.3030. The transducers have a central frequency of 4 MHz. Probes with different focusing distances varying from 40 mm to 130 mm were used for imaging of sample at sodium temperature of 230°C. In addition to this, un-focused 3 and 4 MHz probes were also used for imaging.

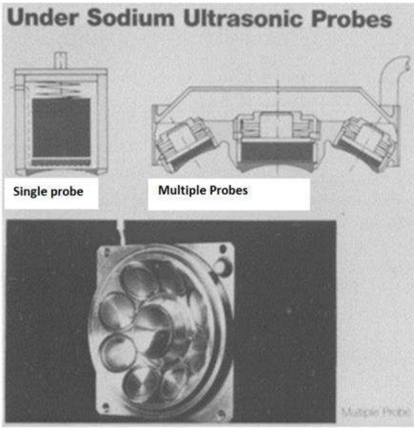

Figure 2.29 Circular headed ultrasonic scanner [46]

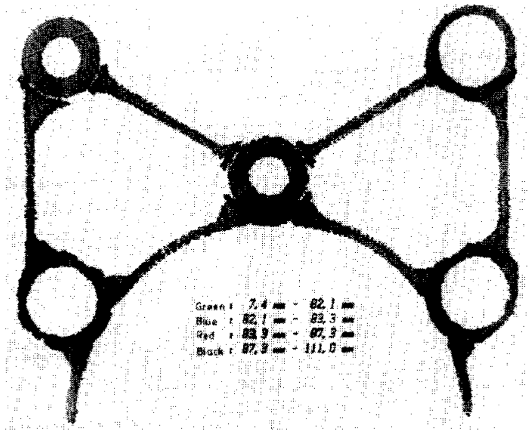

Figure 2.30 Under-sodium image of the sample at 230°C [46]

2.4.6 Belgium

A Belgium fast research reactor named, Multi-purpose hYbrid Research Reactor for High-tech Applications (MYRRHA) uses different FSA identification system. Each FSA top was fabricated with a unique combination of notches for identifying each FSA using ultrasonic transducers. Figure 2.31 shows sample FSA tops with unique notches for each FSA top for ease of identification. Direct/differential measurement technique was used for identification of notches and thus each FSA. To avoid any error in the notch identification Hamming code error correction was used. In addition to this, a linear system algorithm was used for identification of each notch in case of multiple transducer failure [47 – 49].

Figure 2.31 FSA mock-ups used in MYRRHA reactor [47]

2.4.7 India

In India, early development of under-sodium ultrasonic viewing system was reported by Swaminathan et al., [50] and later by Rajendran et al. [51] for Fast Breeder Test Reactor (FBTR) core scanning. The system deployed was used to scan under the core cover plate for detection of any FSA protrusion. Later, an advanced Under Sodium Ultrasonic Scanner (USUSS) was developed for detection of SA protrusion in PFBR [52].

2.4.7.1 Imaging using a single element ultrasonic probe

In 1990, Swaminathan et al., [50] developed under-sodium viewing system for identification of protrusion in FBTR. This system used theta-Z scanning configuration as shown in Fig 2.5 b to scan Core Cover Plate Mechanism (CCPM) and the space below it for any protrusion of FSAs. The system consists of 6 m long ‘spinner’ tube made up of stainless steel with a diameter of 33 mm. This spinner tube was guided by a 90 mm diameter tube, as shown in Figure 2.32. The spinner tube was rotated by 360° and could move a vertical distance of 350 mm. A side viewing transducer (SVT) was fixed at the bottom of spinner tube for scanning of space below CCPM and FSA tops.

Figure 2.33 shows the deployment of ultrasonic viewer into FBTR. After inserting the viewer into FBTR, theta scanning of SA top area was carried out for detection of SA protrusion. In this way, the entire core plenum area i.e., the interspace (70 mm gap) was scanned for protrusion detection. Figure 2.34 shows the ultrasonic image obtained by scanning the core plenum area between FSA top and thermo well sleeves. The scanning of the interface was carried out at a sodium temperature of 180°C. PZT-5A crystal was used as exciting element with a diameter and thickness of 20 mm and 1 mm, respectively. The central frequency of the transducer was 2 MHz. A Nickel diaphragm was used at the transducer face for quick wetting.

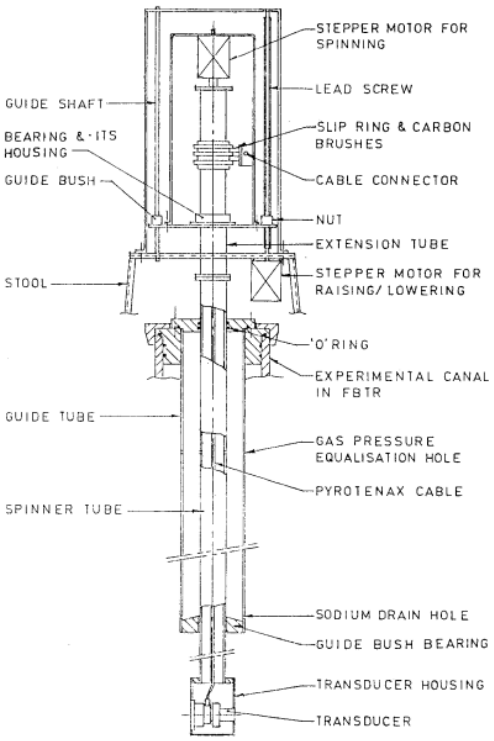

Figure 2.32 Ultrasonic viewer [50]

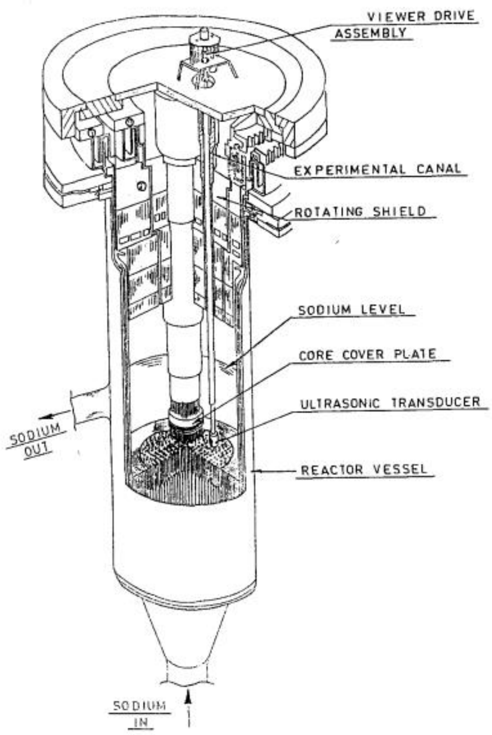

Figure 2.33 Deployment of Ultrasonic viewer in FBTR [50]

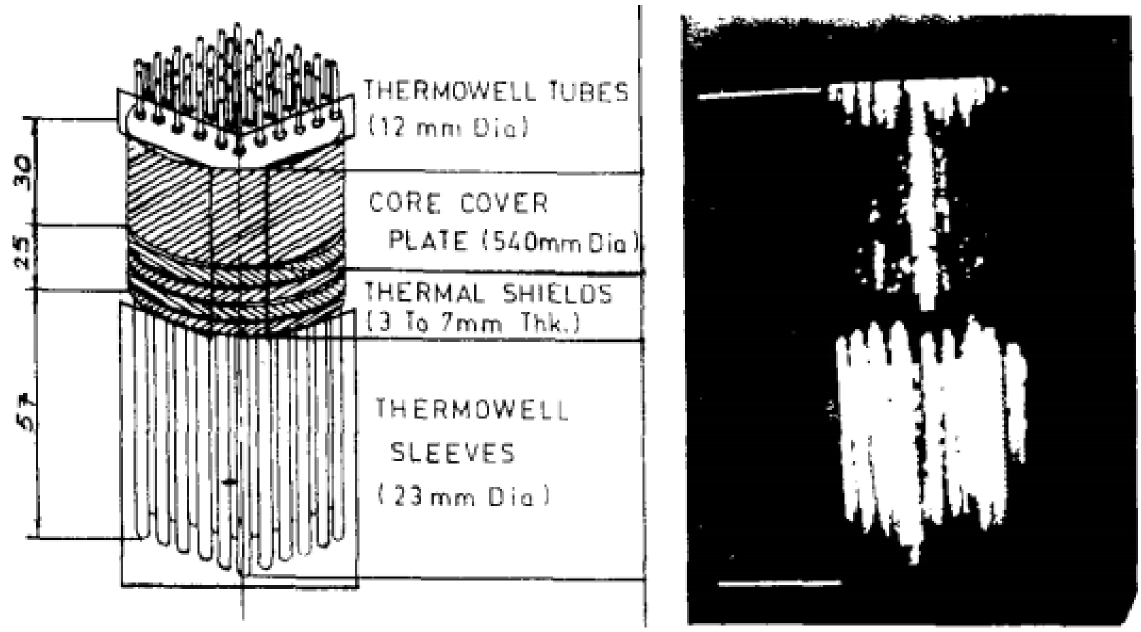

Figure 2.34 Ultrasonic image of the interspace between SA top and thermo well sleeves [50]

2.4.7.2 Imaging using multiple single element probes

Later in 2013, an advanced ultrasonic scanner called Under Sodium Ultrasonic Scanner (USUSS) was developed by Indira Gandhi Centre for Atomic Research (IGCAR) and Bhabha Atomic Research Centre (BARC) for scanning of core plenum in PFBR during shutdown condition. It was developed for identification of protrusion and imaging of FSAs. Ultrasonic Pulse-Echo (PE) technique and configuration shown in Figs 2.5 b and c were used for detection of protrusion and mapping of FSA heads. Scanning of reactor core for protrusion and bowing detection is carried out before every fuel handling operation so that LRP and SRP of PFBR can be rotated without any obstruction [17].

USUSS is a 2-axes (theta and vertical translation) automated mechanical scanner with a conical transducer holder at the bottom of 7.5 m long spinner tube. The diameter of the transducer holder is 400 mm. Transducer holder contains, 4 DVTs (5 MHz), 3 SVTs (1 MHz) and 3 Spare DVTs. The DVTs are used for FSA mapping, whereas SVTs are used for scanning the FSA tops for identification of protrusion, if any. All transducers are sodium compatible. Figure 2.35 a and b show schematic and photograph of USUSS, respectively. Figures 2.36 (a – c) show the bottom head, SVTs and DVTs configuration used in USUSS, respectively [52]. It can be seen from Fig. 2.36 that SVTs are spaced uniformly on the periphery of the transducer holder and are pointing radially away from the holder. During scanning of the PFBR for detection of FSA protrusion, only one of the 4 SVTs will be used, other 3 SVTs are fixed for redundancy situation. DVTs are arranged radially at the bottom of transducer holder with optimized spacing to cover larger area of scanning.

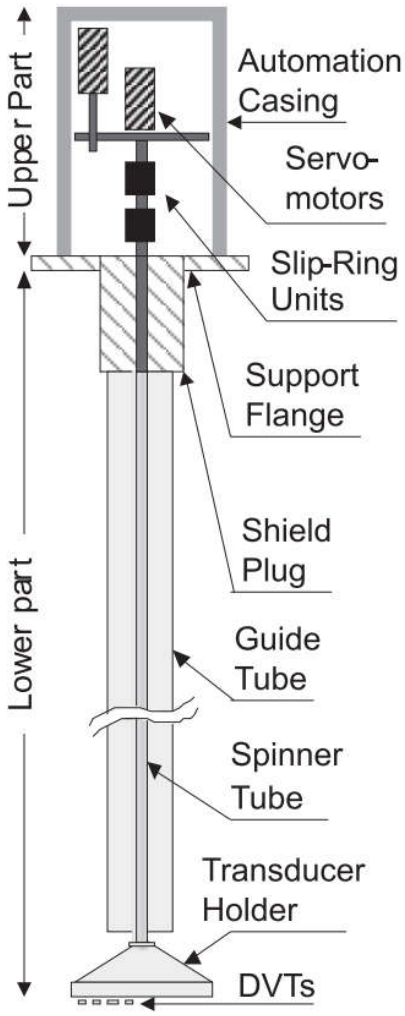

(a)

(b)

Figure 2.35 (a) Schematic and (b) photograph of the USUSS [52]

(a) (b) (c)

Figure 2.36 (a) USUSS transducer assembly head, (b) positioning of SVTs and (c) DVTs in USUSS [52]

Two different methodologies, namely, direct imaging and indirect imaging were proposed for inspection of protrusion in FPBR using USUSS. In PFBR, last row of SAs are cylindrical in shape and are 100 mm taller than all other FSAs. These SAs are called Peripheral Subassemblies (PSA) [53]. To develop the direct and indirect imaging methodologies, PFBR core structure with the PSA was simulated in a large water tank using a single SVT developed for using in USUSS.

➢ **Direct imaging**

When there is no FSA protrusion, ultrasonic reflected echoes from these PSAs are obtained, as shown in Figure 2.37 a. Based on this signal, we can conclude that none of the FSAs are protruded. However, when there is a protrusion of a FSA in favorable orientation to ultrasonic beam, then reflected echo from PSA will be missing but there will a reflected signal from the location of protruded FSA, as shown in Figure 2.37 b, using this echo signature, location of protruded FSA can be identified. This is referred as direct imaging method for FSA protrusion detection.

➢ **Indirect imaging**

When the protruded FSA is not in favorable orientation to the ultrasonic beam, then the amplitude of reflected echo from PSAs reduces, in addition to this, a weak reflected echo from the protruded FSA is obtained as shown in Figure 2.37 c. This method of identifying protrusion of FSA is referred as indirect imaging method.

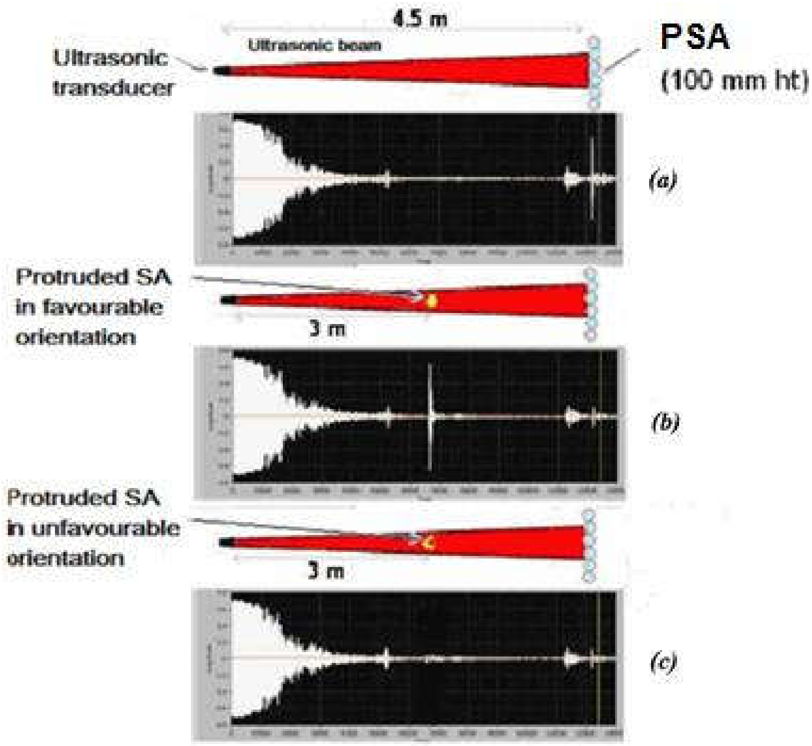

Figure 2.37 (a) Signals obtained from PSA when there was no FSA protrusion, identification of FSA protrusion using (b) direct method and (c) indirect method [48]

Swaminathan et al., 2012 [53] developed In-situ bowing measurements of PFBR FSAs using two methodologies namely, Circle-Fitting method and Data-based method. Under water simulation studies for bowing identification using both methodologies were carried out successfully.

- **Circle-fitting method**

In this method, SA head top rings were scanned using a down viewing transducer as shown in the schematic Figure 2.38 a. The reflected echoes from top ring are circle-fitted and the reconstruction of the SA top ring is carried out using an algorithm as shown in the Figure 2.38 b.

To develop the circle fitting method, honeycomb arrangement of FSAs was placed in a tank filled with water. Then, USUSS was placed at a vertical distance of 100 mm from the FSA top. The 4 DVTs of the USUSS were placed at a distance of 57.5 mm, 120 mm, 160 mm and 187 mm from the central rotating axis of the transducer head of USUSS. When the scanner was rotated on top of the FSA honeycomb arrangement, DVTs make a circular scanning path of different radii corresponding to their placements from the rotating axis.

During scanning, these DVTs were excited with a high voltage pulse. When a DVT was normal to FSA top ring, an ultrasonic echo pulse of maximum amplitude (and least time of flight) was received. Due to the beam divergence, the amplitude of the reflected pulses decreases when the DVT moves towards and away from the top ring of FSA. The amplitudes echo-pulses were converted into proportional DC voltages and were plotted as a pixel on the monitor screen corresponding to the position of each DVT. Thus, an arc of pixels was plotted corresponding to the series of echoes obtained from each SA head. During circular scanning, two-pixel arcs were obtained from each FSA corresponding to different locations using a single DVT.

Four pixel-arcs were obtained from each of the six FSA top rings in the first row of the honeycomb arrangement as shown in the Fig. 2.38 c. The inner radius and outer radius of each FSA is 55 mm and 58 mm, respectively. Then, two concentric circles corresponding to these radii using selectable center co-ordinates were drawn, such that they pass through at least three out of the four pixel-arcs. The distance between the scanner axis and the center of the FSA head can be calculated from which any shift in the lateral position of the FSA (due to ‘bowing’) is determined [16].

Similarly, the last DVT (DVT4), which is placed at a distance of 187 mm from the center of the transducer head is used for identification of FSA bowing and for imaging FSAs located in the second row of the honeycomb arrangement. Based on the fit parameters, the extent of the bowing will be identified.

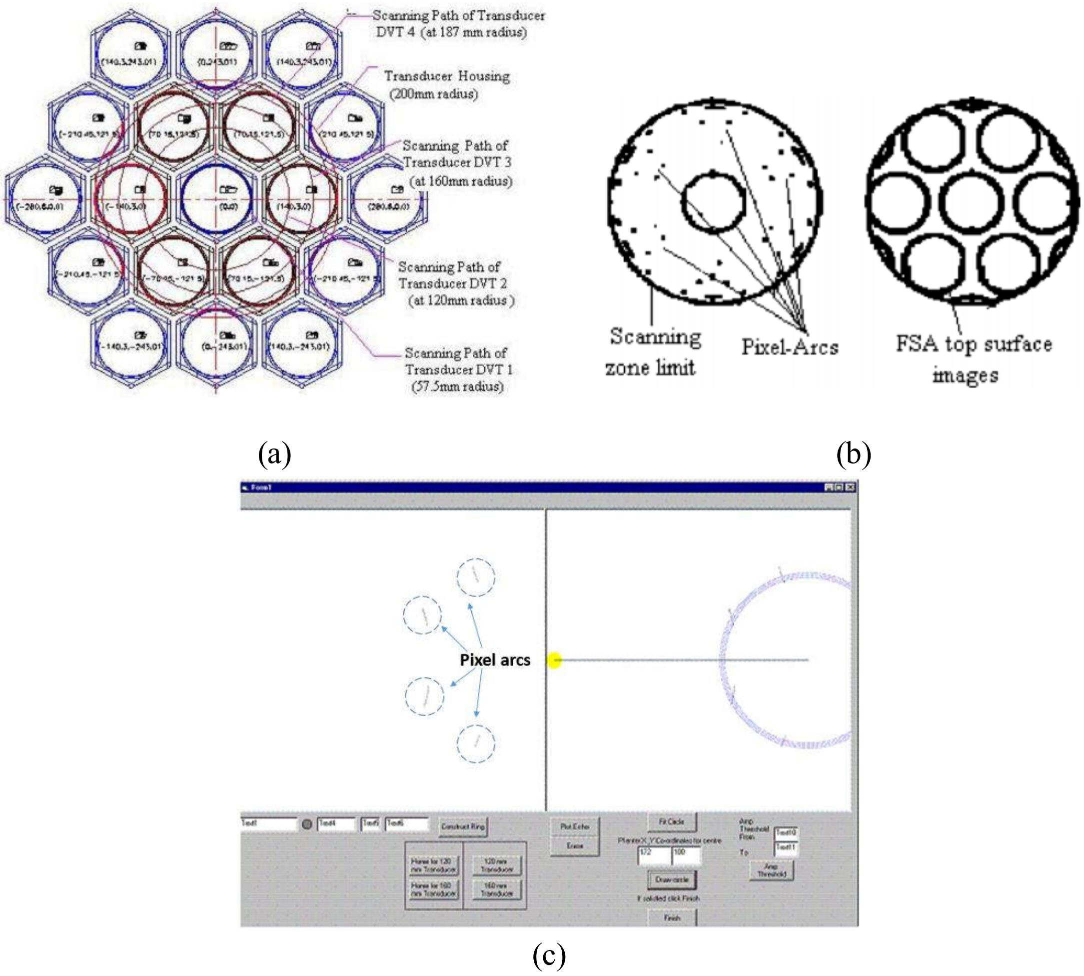

Figure 2.38 (a) Scanning of FSA to get the reflected echoes from the top ring, (b) reconstruction of the top ring to identify the extent of bowing, if any and (c) Graphic User Interface (GUI) of the software used to determine the bowing of FSA [16]

➢ **Data-based method**

The data-based method works on geometric calculation using the stored scan data. As the scanner axis location from where the DVTs were scanning the SA top is known, the reflected echo signals obtained from the top ring of the FSA head while approaching and leaving the SA top are used for identifying the center distance of FSA top ring from scanner axis and from there bowing extent is measured. Figure 2.39 shows the schematic of the distance calculations from FSA center to scanner axis.

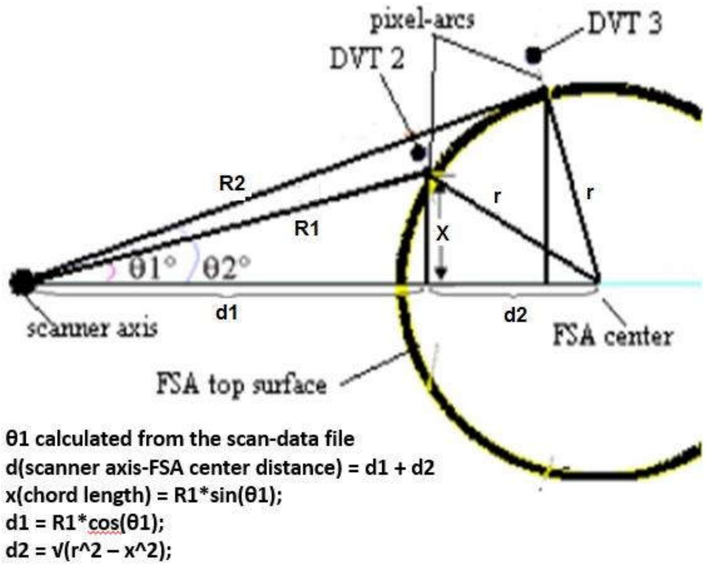

Figure 2.39 Schematic for calculating FSA center distance from the scanner axis [16]

The above-described method is possible when the DVTs fixed to the USUSS header are brought on top of each FSAs. However, in case of PFBR, due to the rotational constraints of the LRP and SRP, USUSS cannot be brought on top of central five rows of FSAs. Hence, mapping of FSA heads and detection of bowing is not possible for central five rows of FSAs using conventional DVTs mounted on USUSS [54].

To overcome this limitation, GAIM is developed to detect protrusion, bowing and for mapping of FSAs without actually going on top of each FSA.

2.5 Summary of scanners and scanning methodologies developed by different countries for under-sodium imaging

Table 2.1 below summarizes ultrasonic scanners and associated scanning methodologies developed by different countries for detection of FSAs protrusion and bowing in FBRs:

Table 2.1 Summary of ultrasonic scanners and associated scanning methodologies developed by different countries

Country	Reactor	Scanner	Type of configuration
USA	FFTF	L-shaped scanning arm	Offset arm with fixed transducers
UK	PFR	VIEWER	Vertical with fixed transducers
	CDFR	Links sweep arm scanner	Offset arm with radially moving transducers
France	Phénix	VISUS	Vertical type NaK filled wave guide
	Super Phénix	IMARSOD	Two perpendicular phased array ultrasonic transducers
	DOLMEN sodium circuit	VENUS scanner	Raster scan using single TUSHT transducer
Japan	Joyo (LMFBR)	Under-sodium Viewer	Vertical scanner with spiral movement of ultrasonic transducer
	DFBR	Phased array system	36 X 36 elements phased array transducer for 3D imaging of reactor internals
Germany	SNR-300	Sweep arm scanner	Offset arm with moving transducers in radial direction
India	FBTR	Under-sodium system	Vertical type scanner with single transducer having 360° rotation and 350 mm transverse movement
	PFBR	Under-sodium Ultrasonic Scanner System (USUSS)	Vertical type scanner with DVTs and SVTs for with rotational (theta) and vertical (z) movement

2.6 Motivation and objectives of present study

The review of literature revealed that numerous under-sodium scanners were developed by many groups for scanning/imaging internals of sodium cooled FBRs at different temperatures. Scanners were developed with different ultrasonic transducers like, single element transducer, linear array of single element transducers, phased array transducers and guided wave transducers based on space restriction and requirement. It can be seen from review of literature that in all under-sodium scanners and associated methodologies, mapping of FSAs can only be performed by keeping the ultrasonic transducer(s) above the FSA.

It is also observed that scanning/imaging of all the nuclear core component may not be possible due to the following reasons [55]:

- Due to the space constrains for inserting the complex scanner and
- Due to the rotational constrains of the rotating plugs that are used to move the scanner to the required locations (as in case of PFBR)

A possible alternative to a complex robotic arm scanner for imaging the inaccessible central FSAs could be a glancing angle-based methodology in which the transducer is not kept above FSA. The glancing angle-based technique was proposed earlier for remote temperature measurements and for ultrasonic thermometry simulation to monitor temperature of sodium flow at the outlet of reactor core in FBRs. The main aim of the study is to measure temperature of sodium from the diffracted echoes obtained from a FSA. Figure 2.40 shows 2D model used in this study. In the model, it was an ultrasonic source ‘S’ with width w. Two solid tubes (blue colour) represent two ends of a FSA separated by a known distance d (diameter of FSA) of 100 mm. The thickness (e) of FSA is 13 mm. It was assumed in the model that sodium flows through ID side of FSA and sodium on OD side of FSA is static. The source was placed at a grazing incidence angle of about 7° to get ultrasonic diffracted echoes from FSA (for the given distances of *a* and *b* equal to 100 mm and 12 mm, respectively). Diffracted echoes were expected from edges E1 and E2 and possibly from E1' and E2'. From the known distance *d* and obtained TOF difference between two edges E1 and E2, velocity of ultrasonic wave was calculated [56].

From the equation given below, temperature of sodium is estimated [57].

$$V = 2723.0 - 0.531 * T(K) \tag{2}$$

where, *V* is the velocity of ultrasonic wave and *T(K)* is the temperature of sodium in Kelvin.

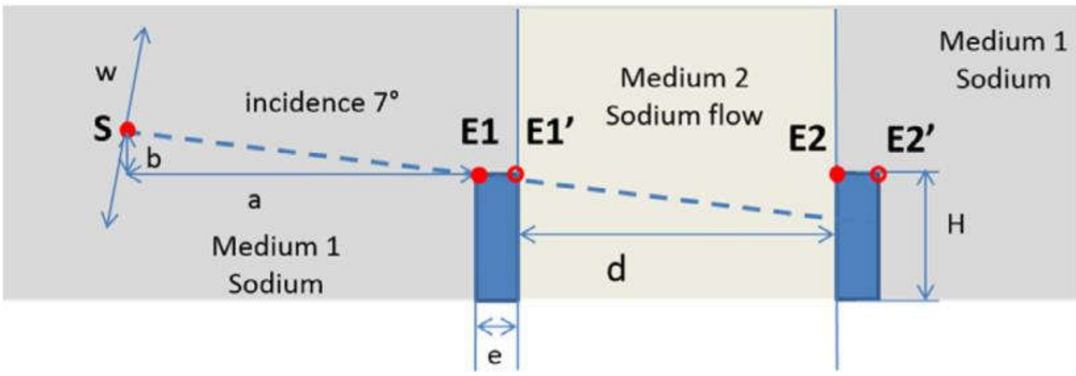

Figure 2.40 2D model of ultrasonic thermometry configuration [56]

In addition to the above work, glancing angle methodology was used to optimize the configuration of edge geometry and ultrasonic tilt angle to obtain the highest diffracted/specular signal amplitude back from a tube end [58].

For this study, various 2D and 3D edge geometries like, right-angle, fillet, 45°-chamfer and 60°-chamfer as shown in Fig. 2.41 a and b were fabricated on a plate (2D) and tube (3D) ends. Then amplitudes of the diffracted/speckle reflected amplitudes were obtained at different glancing angles of the ultrasonic transducer to optimize the shapes of the edges to get maximum diffracted/speckle reflected signals from the plate and tube ends for acoustic thermometry studies of the liquid sodium coming out of FSAs.

From the amplitude data obtained from 2D and 3D edge geometries at different glancing angles of the ultrasonic transducer, it is observed that the amplitude of the reflected/diffracted signal the fillet geometry is roughly twice than the other geometries. Based on this observation, it was concluded that the fillet edge geometry in both is better for obtaining maximum reflected signal for an optimized incident angle of the ultrasonic waves.

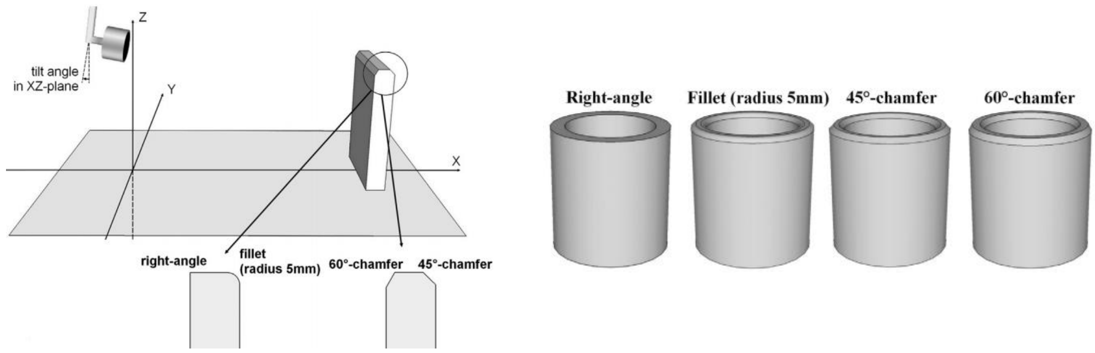

(a) (b)

Figure 2.41*(a) 2D and (b) 3D geometries used for the experimental setup.*

However, application of ultrasonic glancing angle technique for core mapping or detection of SA protrusion / bowing has not been reported so far, to the best of author's knowledge.

Hence, the objectives of present study are thus:

1. to explore possibility of using glancing angle imaging methodology (GAIM) for protrusion, bowing detection and for mapping of FSAs,
2. to study characteristics of signals obtained in GAIM from hexagonal FSA of PFBR at different orientations,
3. qualitative and quantitative detection of FSA protrusion using GAIM,
4. qualitative and quantitative detection of FSA bowing using GAIM,

5. superposition of glancing angle data from two orientations for better visualization of honeycomb arrangement and
6. to explore the possibility of using GAIM in under-sodium environment.

In the next chapter, experimental setups used for achieving above objectives are discussed in detail.

Chapter 3. Experimental details for development of GAIM

3.1 Chapter overview

This chapter describes under water experimental setup used for development of ultrasonic glancing angle imaging methodology (GAIM) for detection of protrusion, bowing and for mapping of FSAs. The details of ultrasonic setup and transducer used are also presented followed by LabVIEW program developed for generating the glancing angle images of SA heads. At the end, experimental setup used for under-sodium experiments are discussed in detail.

3.2 Underwater experimental setup used for development of GAIM

To develop GAIM, under water ultrasonic imaging experiments were carried out using 19 SA heads. These SA heads are geometrically similar to top 150 mm of FSAs used in PFBR. These 19 SA heads were placed in an immersion tank filled with water in form of a honeycomb arrangement as shown in Fig 3.1. Water in the tank was static and temperature of the water was maintained at 25°C (room temperature) throughout the experiments. An under sodium ultrasonic transducer was fixed to an arm of 200 mm length and immersed in water for scanning the honeycomb arrangement. GAIM was developed in such a way that the present methodology can be used with the existing USUSS without making any major modifications to the same. As explained in Chapter 2, USUSS has a 400 mm diameter transducer holder head to place the Side Viewing Transducers (SVTs) and Down viewing Transducers (DVTs) at the bottom to carry out scanning of PFBR core. The arm length of 200 mm simulates fixing the ultrasonic transducer at glancing angles at the periphery of USUSS transducer holder head, i.e., at an arm offset of 200 mm from axis of rotation.

For convenience, all 19 SA heads in the honeycomb arrangement immersed in water were nomenclated from 1-18 with the central SA head nomenclated as SA#C as shown in Fig 3.2. The honeycomb arrangement setup central three rows of FSAs in PFBR which cannot be mapped using DVTs due to constraints in the movement of large rotating plug (LRP) and small rotating plug (SRP). The outer diameter (OD) and the thickness of the top ring of each SA head is 118 mm and 4 mm respectively.

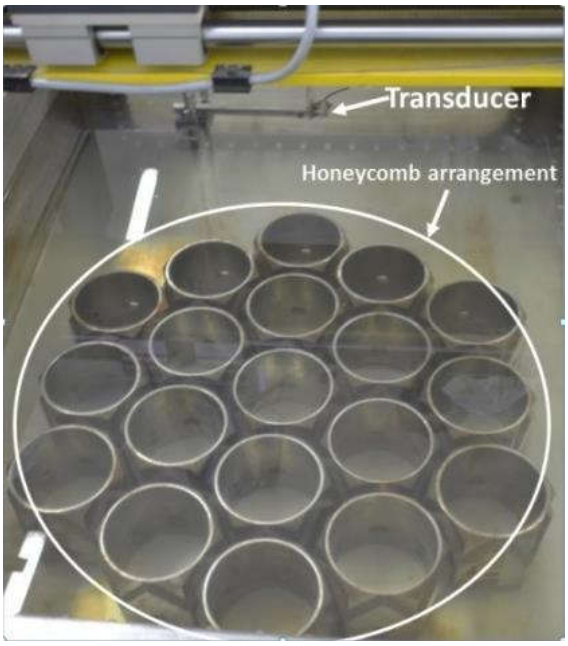

Figure 3.1 Honeycomb arrangement of SA heads

Figure 3.2 Top view and nomenclature of SA heads in honeycomb arrangement

In GAIM, the transducer is inclined at an oblique angle with respect to horizontal plane. This small angle (glancing angle) allows to obtain diffracted signals simultaneously from large number of SAs due to the divergence of the ultrasonic beam. Figures 3.3 a and b show the schematic of glancing angle methodology in side and top view, respectively.

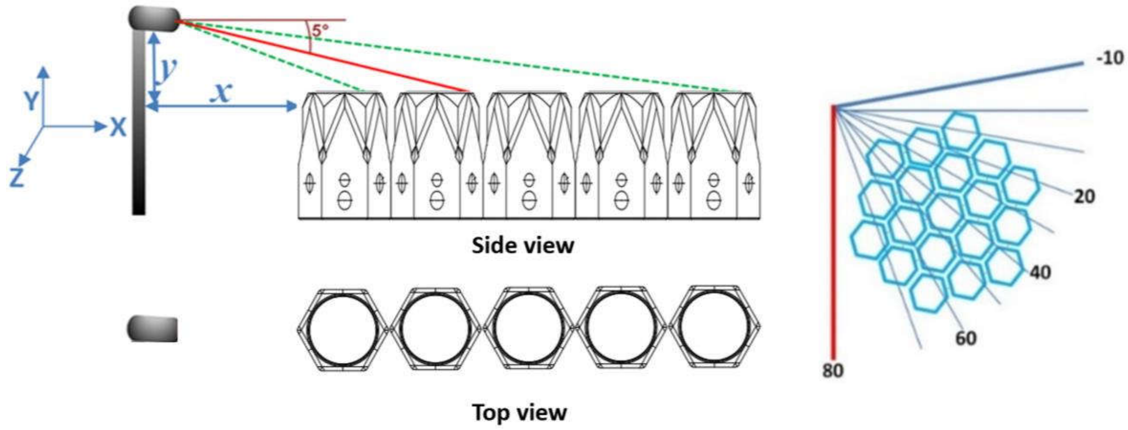

(a) (b)

Figure 3.3 Schematic of glancing angle methodology (a) side and top view and (b) scanning top view

Here, the ultrasonic transducer is placed at horizontal and vertical distances of *'x'* and *'y'*, respectively from the top of the SA heads. Then, by giving a slight tilt to the probe, the entire SA heads is covered due to the divergence of the ultrasonic transducer. For a given *'x'* and *'y',* as the tilt of the ultrasonic transducer increases (with respect to the horizontal axis), the central beam of the ultrasonic transducer falls on the SA heads near to transducer. On the other hand, as the tilt decreases, the central beam of the ultrasonic transducer falls on the rear SA heads. Following section discusses under-water scanner, ultrasonic pulser-receiver and experimental setup used for development of GAIM.

3.2.1 Details about underwater scanner

The details of immersion tank and 5-axes scanner are given below:

The immersion tank was connected to 5-axis scanner (X, Y, Z, θ and Φ) controlled using LabVIEW software. Figure 3.4 shows the immersion tank and associated equipment used for developing GAIM. No air bubbles were observed while performing the experiments.

Immersion tank: The size of the tank is 1100 mm × 1100 mm × 350 mm and it is made up of AISI type 304 austenitic stainless steel. The windows of 12 mm thick glass of size 900 mm ×

250 mm are provided on the sides of immersion tank for clear view of scanning process underway. The leveling screws and sprit level are provided to check parallelism of the bottom level of the tank.

All five stages are stepper motor driven and are controlled by a PC using LabVIEW software. X, Y and Z stage comprise of ball screw (C5 grade accuracy) and anticorrosive linear motion guides. The details of each axis are given below:

X-Axis: The maximum scanning distance in this axis is 800 mm with a resolution of 0.1 mm.

Y-Axis: The maximum scanning distance in this axis is 700 mm with a resolution of 0.1 mm.

Z-Axis: The maximum scanning distance in this axis is 250 mm with a resolution of 0.1 mm.

Θ-Axis: The maximum rotation in this axis is ±360º with a resolution of 0.1º.

Φ-Axis: The maximum gyration in this axis is ±360º with a resolution of 0.1º.

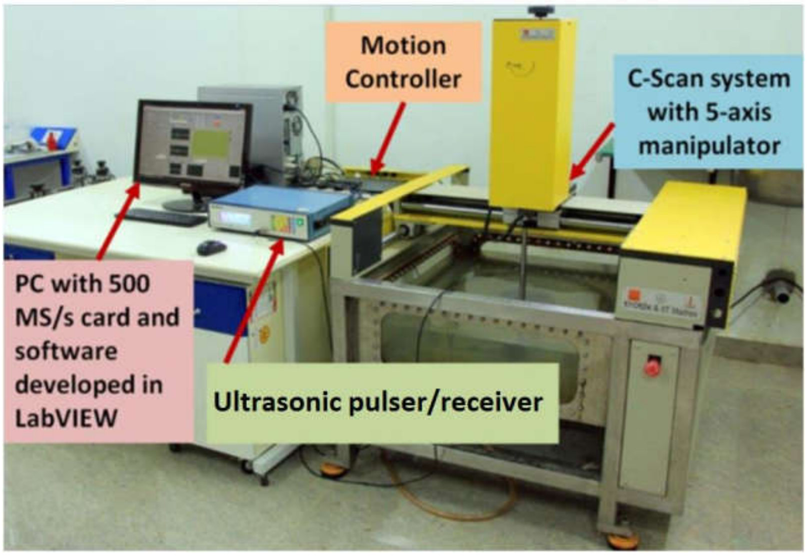

Figure 3.4 Experimental setup used for ultrasonic measurements

For all linear axes, scanning speed is in the range of 1mm/sec - 10mm/sec with user selectable speed range in steps of 1mm/sec. Limit switches are provided for X, Y and Z axes to know the extreme positions of these axes. A special holder is provided to firmly hold the cylindrical ultrasonic transducer during scanning. The maximum weight that the holder can hold is ~150 gm. The holder is generic enough to accommodate sensors of different dimensions. A suitable four axes motor driver (NI MID 7604) and a motion controller (NI PCI 7334) are used. Good quality stepper motors are used for vibration free movement of the scanner.

3.2.2 Details about ultrasonic pulser receiver and transducer

Olympus 5077PR Square wave pulser/receiver and a PCI-based digitizer card placed in C-scan system were used for acquiring ultrasonic signals. The sampling rate of 20 MS/s (50 ns) was used for data acquisition. A 2 MHz unfocused narrowband under-sodium ultrasonic transducer developed by IGCAR, Kalpakkam was used for acquiring the data. The schematic and design details of under-sodium ultrasonic transducer used in the present investigation are similar to those reported by Swaminathan et al. [50]. A broadband transducer is not used for the present study because, an increase in bandwidth of the transducer improves the depth resolution and decreases dead zone also, however this is achieved at a cost of loss in sensitivity due to damping of transducer. In general, it is better to use a transducer that can provide high amplitude diffracted signal up to the required distance (in the present study, I need to inspect a distance of 650 mm for protrusion and bowing identification) with required depth resolution and also have sufficient divergence to allow large coverage. Hence, a narrowband 2 MHz under-sodium transducer with a minimal damping is used in the present study which was developed as a side viewing transducer for long range inspection.

The diameter of the transducer is ~ 20 mm with an element diameter of 10 mm. Figures 3.5 a and b show the time domain A-scan signal and corresponding frequency spectrum obtained by the transducer, respectively. The signals clearly show the narrowband characteristics of transducer with the central frequency at 2 MHz.

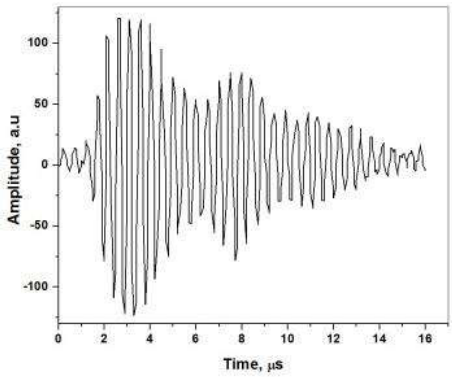

(a)

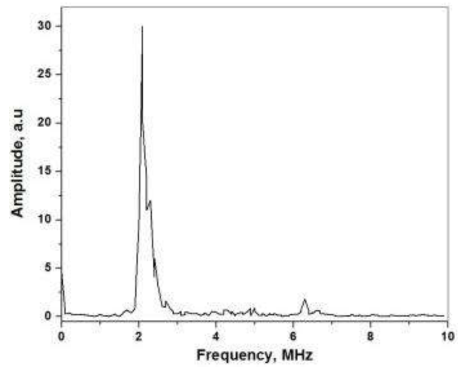

(b)

Figure 3.5 (a) A-scan signal and (b) frequency spectrum of 2 MHz under-sodium ultrasonic transducer

Figure 3.6 shows the beam profile of 2 MHz ultrasonic transducer used in present study. The beam profile of under-sodium transducer was obtained through C-scan imaging. C-scan data was acquired in through-transmission mode using 2 MHz transducer as emitter and a broad-band pinducer (CTS VP – 1063) with frequency range of 10 Hz–10 MHz as receiver. To get the beam profile of the transducer, B-scan data of the transducer was acquired using pinducer by moving the pinducer from one side of the transducer front plate to other side by 100 mm. Then the pinducer was moved away from the transducer front plate by 5 mm and again B-scan data of the emitted field was acquired while moving the pinducer across the transducer. In this way, emitted field of transducer in water was obtained using the pinducer up to a distance of 500 mm from transducer.

-6 dB beam divergence measured from the transducer emitted field was found to be about 2.5°. The -6 dB beam divergence measured from the beam profile is in close agreement with the theoretically calculated -6 dB beam divergence using Eq. (3). The divergence angle of the transducer for reduction of beam intensity to 50 % (-6 dB), is given as [59]:

$$\frac{\propto}{2} = \sin^{-1}\left(\frac{0.51*\lambda}{D}\right) = \sin^{-1}\left(\frac{0.51*v}{f*D}\right) \tag{3}$$

where, λ is wavelength of ultrasonic wave, D is the diameter of piezoelectric element (10 mm), v is the velocity of ultrasonic wave in water (1500 m/s) and f is the frequency of ultrasonic transducer (2 MHz). The theoretically calculated beam divergence (α/2) for 6 dB amplitude reduction is ~2.2°.

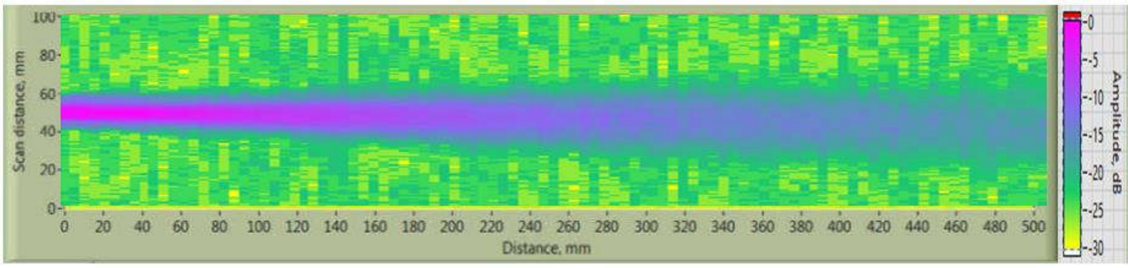

Figure 3.6 Beam profile of 2 MHz ultrasonic transducer

The Near Field (D_{NF}) of the ultrasonic transducer was calculated using the formula;

$$D_{NF} = \frac{r^2}{\lambda} \tag{4}$$

Where, r is the radius of the transducer element and λ is the wavelength of the ultrasound in the medium of propagation. For the ultrasonic transducer used in the present study, the Fresnel Zone/Near Field zone is around 32.5 mm. The effective zone is around 44 mm (4/3 of Fresnel Zone). However, the dead zone of the ultrasonic transducer used in the present study is around 125 mm, hence in the experimental setup, the 1st SA head was placed at a distance of 150 mm from the transducer position which is far away from the initial ringing.

Dead zone is defined as the distance after the initial pulse where the transducer ring down prevents detection or interpretation of reflected energy (echoes).

3.2.3 Experimental set-up for optimizing the position transducer

The horizontal and vertical placements of ultrasonic transducer with respect to SA head (x and y in Fig 3.1a) and the glancing angle (θ) were optimized based on detailed experimental investigations. Initially, the transducer was placed at a judiciously selected height and angle, oriented along 5 SA heads, so that echoes from all 5 SA heads were observed simultaneously due to beam divergence of ultrasonic transducer. Figure 3.7 shows the signals obtained from all 5 SA heads simultaneously.

For the configuration used in present study, the initial ringing of 2 MHz unfocused transducer is 125 mm and the required coverage is ~450 mm (from the end of 1st SA to the end of 5th SA). For the transducer placed at 150 mm away from the 1st SA (to avoid dead zone) coverage of ~450 mm was achieved for ~5° tilt of transducer with respect to horizontal axis.

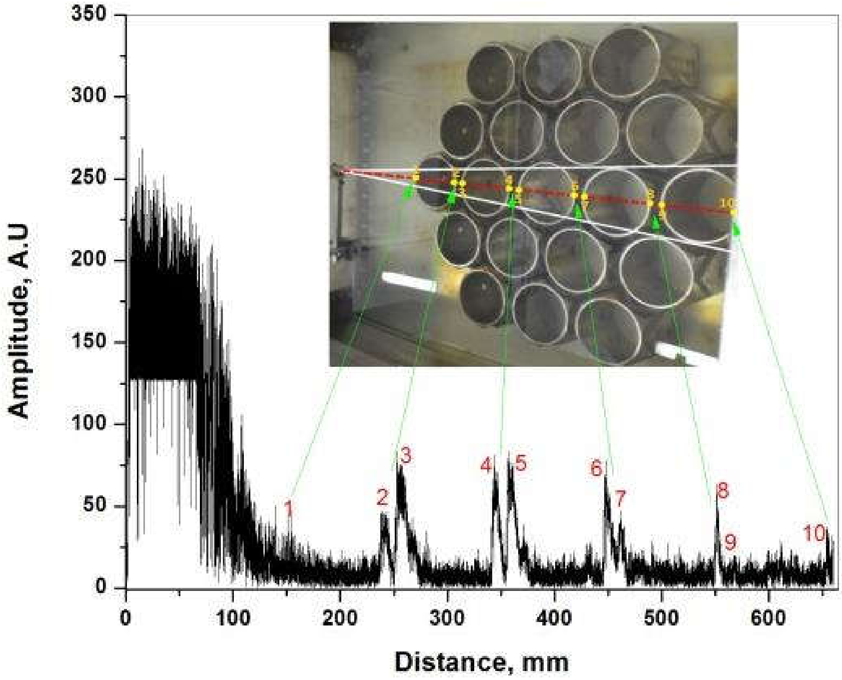

Figure 3.7 A-scan ultrasonic signal comprising of diffracted echoes from edges of the top rings of 5 consecutive SAs along the line of sight of transducer. Yellow dots represent locations corresponding to diffracted echoes

With a slight tilt of ~5° of the transducer, the central beam of the transducer was falling on 2nd – 3rd SA, if transducer was placed at a height of ~40 mm. In addition to this, the entire honeycomb arrangement was covered due to the beam divergence as seen in the typical ultrasonic A-scan signal shown in Fig 3.7. In the A-scan ultrasonic signal, observed peaks (1,2), (3,4), (5,6), (7,8) and (9,10) correspond to diffracted signals from outer diameter (OD) and inner diameter (ID) of top ring of 5 SAs in different rows (SA#7, SA#1, SA#C (central SA), SA#4 and SA#13, respectively) as pointed by the yellow dots in Fig 3.7. Detailed results of systematic optimization study are discussed in Chapter 4.

3.2.4 Development of LabVIEW program for GAIM

The LabVIEW program used for development of GAIM is explained below. Figures 3.8 and 3.9 a show the front panel and control panel of LabVIEW program, respectively used for analyzing B-scan data and generating glancing angle images. Different parameters like, start and end angles, probe location radius, ultrasonic velocity, height of probe and number of data points in a A-scan data were used as input parameters in the front panel of developed LabVIEW program.

In Fig 3.8, glancing angle image can be seen on the right side and corresponding A-scan image can be seen on left side. A-scan signals corresponding to yellow cursor on the un-corrected B-scan image was obtained for further analysis.

Figure 3.9 a, shows the sequence of operation performed on B-scan data for generating glancing angle images. In Fig 3.9 a(i), reading of B-scan data and application of Hilbert Transform on the acquired B-scan signals was performed. Then, by giving different experimental parameters and angle correction as inputs as shown in Fig. 3.9 a(ii), processed B-scan data was plotted as a glancing angle image.

In Fig 3.9 a(iii), 19 nos. of red circles (which represents the top ring of the SA head) were generated and superimposed on the glancing angle image for better visualization of diffracted echoes obtained from different location of the honeycomb arrangement.

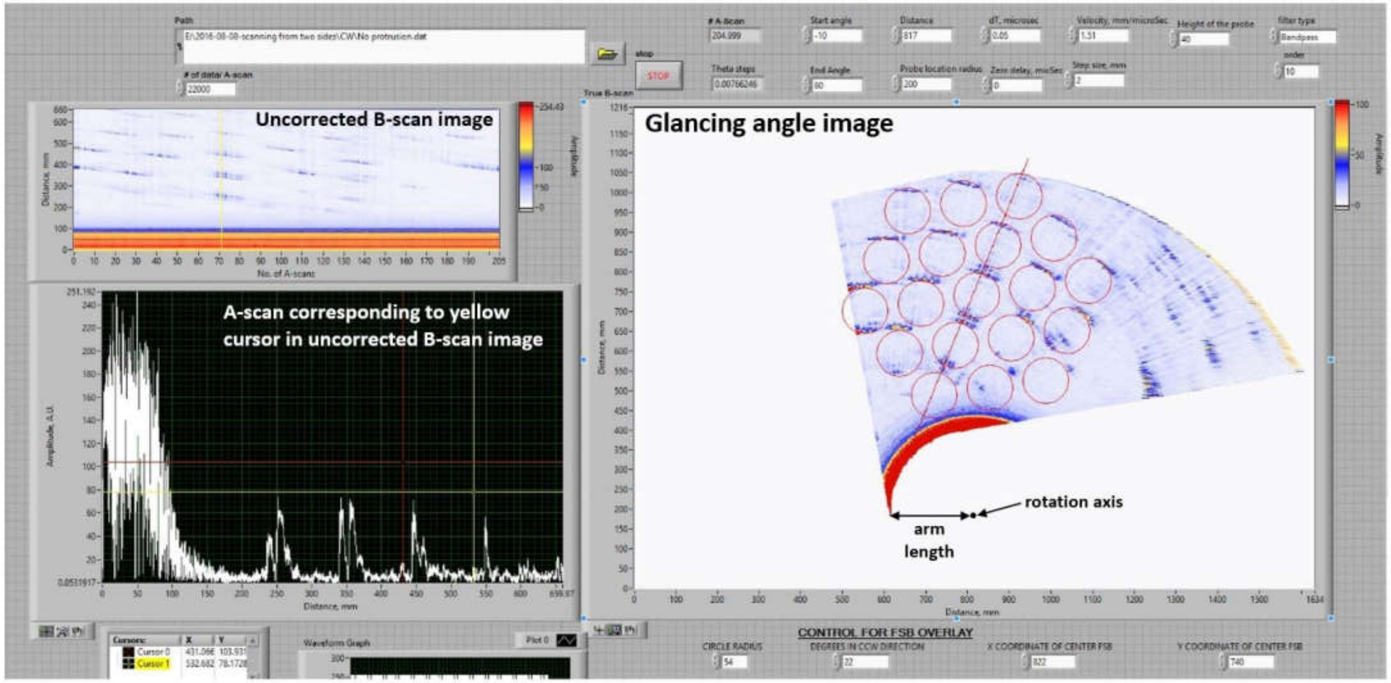

Figure 3.8 Front panel of LabVIEW program developed for generating and analyzing glancing angle images

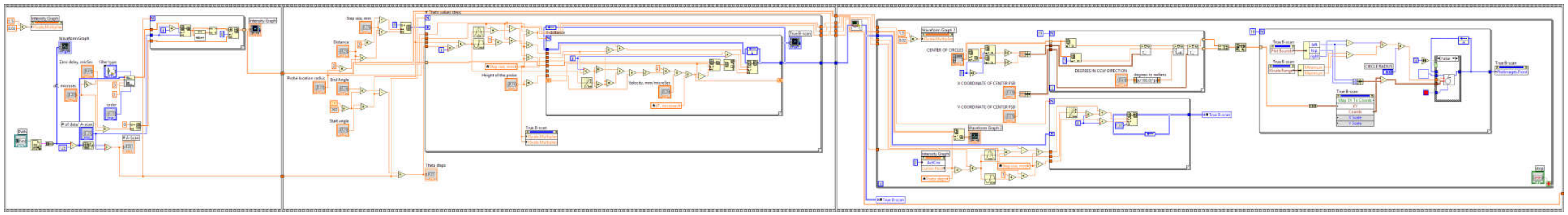

(i) (ii) (iii)

(a)

Figure 3.9 Control panel of LabVIEW program shown in Fig. 3.8

Enlarged images of Figure 3.9 (i) – (iii)

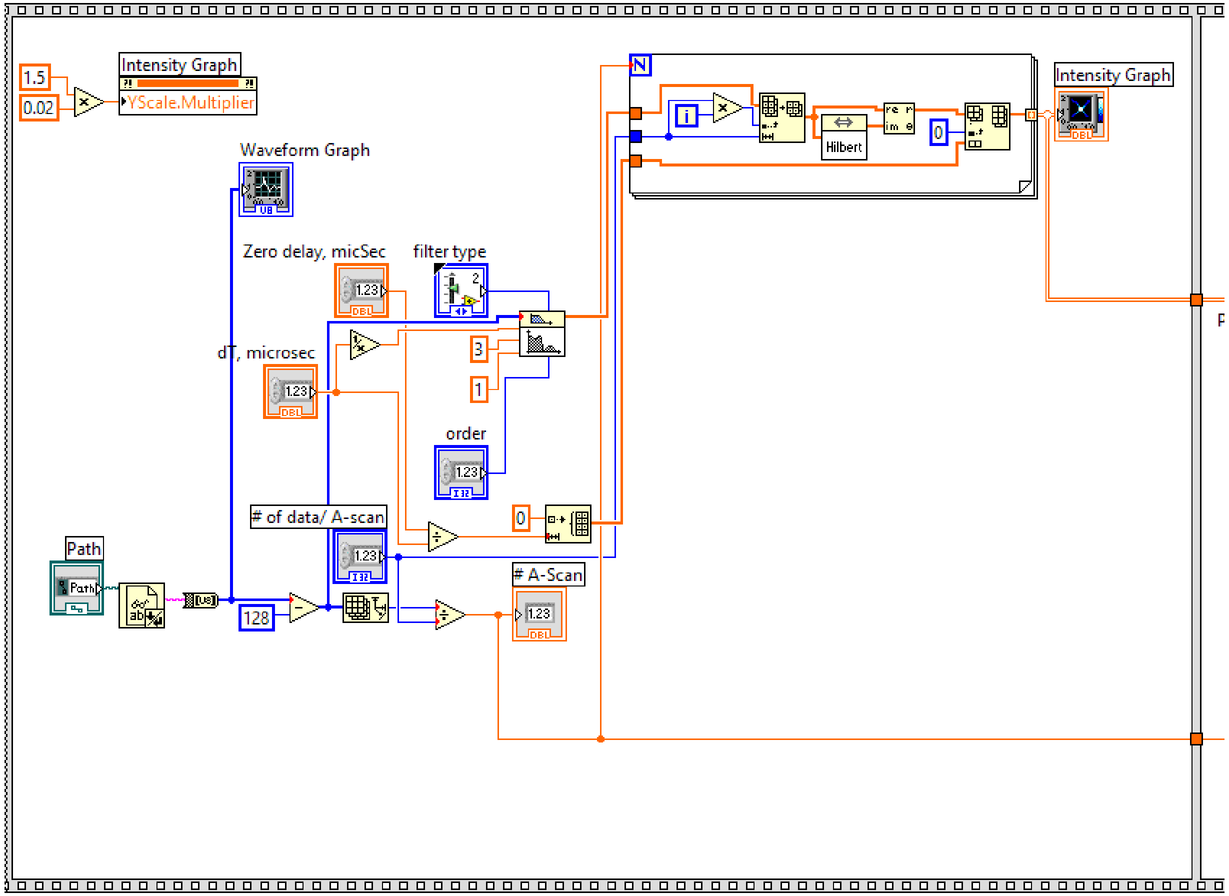

Figure 3.9 a (i)

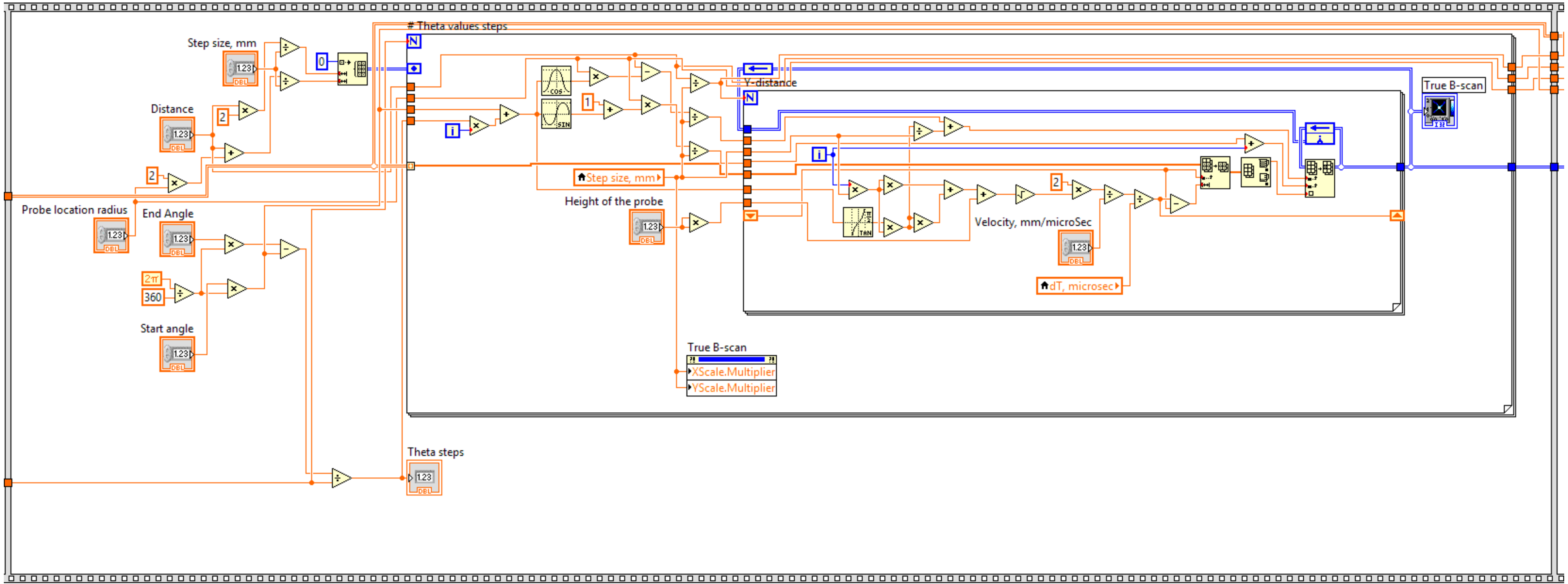

Figure 3.9 a (ii)

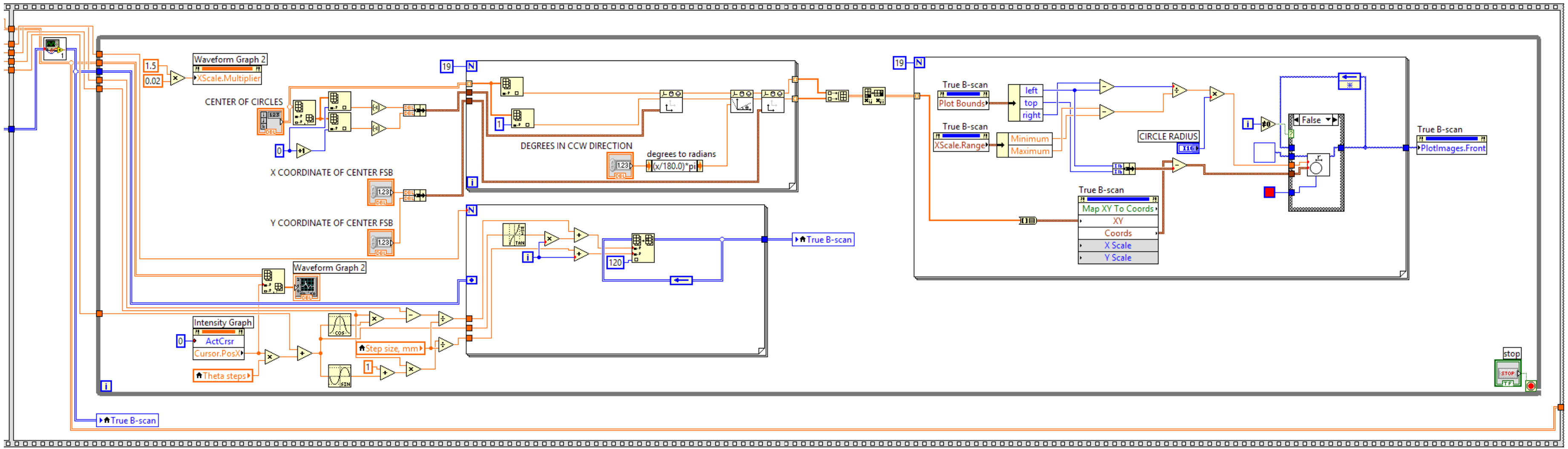

Figure 3.9 a (iii)

3.3 Experimental set-up used for qualitative and quantitative estimation of protrusion

The following sections details about, different experimental setup were used to identify parameters, which can be used for qualitative and quantitative estimation of protrusion.

3.3.1 Experimental set-up used for qualitative estimation of protrusion

Qualitative estimation studies were carried out by keeping the ultrasonic transducer at the optimized position (height at 40 mm and at an angle of 5°) from honeycomb arrangement of 19 SA heads. Positioning of ultrasonic transducer from honeycomb arrangement of SA heads is shown in Fig 3.1. Glancing angle images (through theta-scanning) of entire honeycomb arrangement were obtained for two different scenarios. At first, glancing angle images of entire honeycomb arrangement was carried out without giving protrusion to any of the SA heads. Then, glancing angle images of honeycomb arrangement were acquired by giving 9 mm protrusion to different SAs (SA#1, SA#C and SA#4) in the honeycomb. Then glancing angle images in these two scenarios were compared to obtain the signatures that can be used for detection of protrusion in the honeycomb arrangement.

After comparing and analyzing glancing angle images and the corresponding A-scan signals in these two scenarios, two signatures were identified for qualitative estimation of protrusion. The details about qualitative estimation of protrusion signatures is explained in Chapter – 4.

3.3.2 Experimental set-up used for quantitative estimation of protrusion

Quantitative assessment of protrusion was carried out as per the experimental set-up shown in Figs. 3.10 a and b. In this experimental setup, the ultrasonic transducer was kept at a horizontal of 310 mm from the 1st SA head, as shown in Fig 3.10 a. The transducer was inclined at an angle of 5°. The second SA head was given protrusions in the range of 2 mm – 20 mm at different steps and the amplitude and the time of flight (TOF) of the ultrasonic signal at different protrusion heights were measured. Figure 3.10 b shows the schematic of protrusions given to 2nd SA head (rear SA head). The details about the parameters used for quantitative estimation of protrusion will be discussed in Chapter – 4.

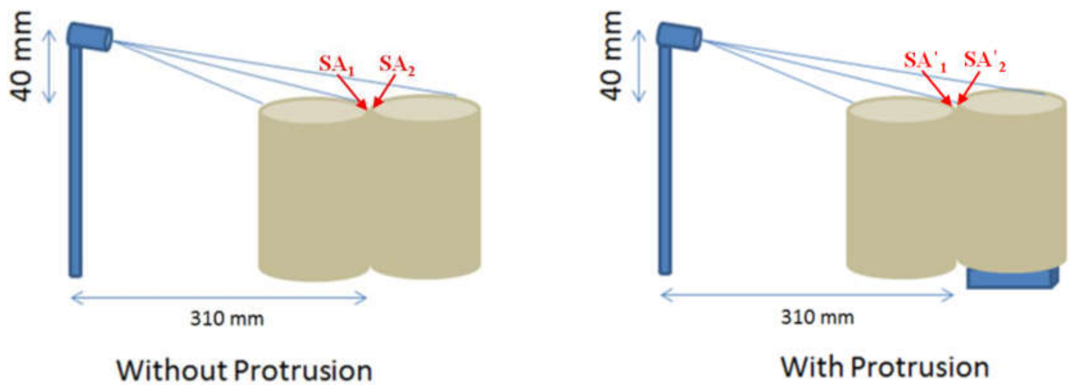

(a) (b)

Figure 3.10 Experimental set-up used for quantitative evaluation of protrusion, (a) without and (b) with protrusion of 8 mm

3.4 Experimental setup used for identification of diffracted echoes from a SA head

A specific experiment was conducted to observe the locations of diffracted signals obtained from the SA head. The schematic of the experimental setup used for this study is shown in Fig 3.11 a. In the experimental set-up, a single SA head was placed on a rotating platform and B-scan data (a series of A-scan ultrasonic signals) was acquired during 360° rotation of SA head. The ultrasonic transducer was placed at a distance of 170 mm from the SA head. In addition to this, SA head was bowed by an angle of 2° and again B-scan data was acquired during 360° rotation to get the signatures for qualitative identification of bowing, the details about the same are explained in Chapter – 5. During 360° rotation of SA head, a total of 795 A-scans were obtained. So, each A-scan was acquired at a rotational step of ~ 0.45°.

Schematic of the bowing experimental setup is shown in Fig 3.11 b. Figure 3.11 c shows the possible locations (6 nos.) from where the diffracted signals were expected from the SA head (indicated by the red circles). This experiment gave an idea of the location of diffracted signals which were obtained during the glancing angle studies. The B-scan signals obtained in this experiment are discussed in Chapter – 5.

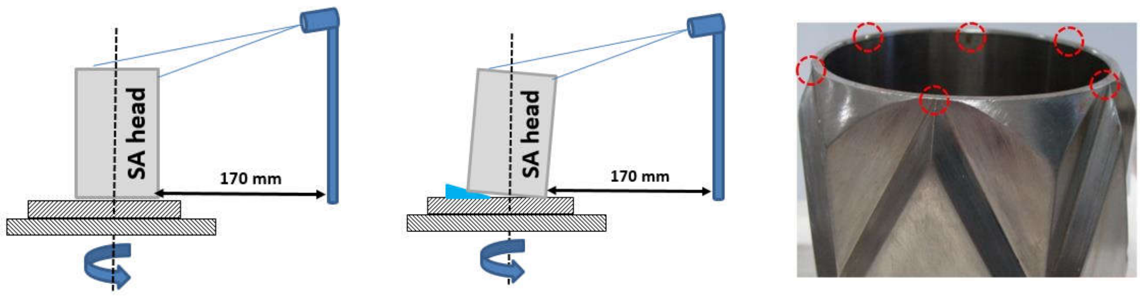

(a) (b) (c)

Figure 3.11 Schematic of experimental setup used for identifying diffracted peaks from the SA head (a) without, (b) with 2° bowing of SA head and (c) possible locations (circled area) from where the diffracted echoes were observed

3.5 Experimental set-up used for superimposition studies

To get better visualization of honeycomb arrangement, glancing angle imaging of honeycomb arrangement was carried out from two different orientations and the same were superimposed. For superimposition studies, transducer was swept by 70° (-10° to 60°) both in the clockwise (CW) and the counter clock-wise (CCW) directions to cover the entire honeycomb arrangement. Figure 3.12 shows the schematic representation (top view) of data acquisition from clock-wise (CW) and counter clock-wise (CCW) orientations and sweeping range of the transducer for obtaining B-scan data from the honeycomb arrangement. Since a single channel pulser/receiver was used, data from CW and CCW directions were acquired from two different orientations using the same ultrasonic transducer. First the transducer was fixed to the left side of the rotating axis and data was obtained by rotating the transducer by 70° (-

10° to 60°) in CW direction. Later, the same transducer was fixed to the right side of the rotating axis and data was obtained by rotating 70° in the CCW direction. Then the data obtained from both the scans (from CW and CCW) were superimposed to get a better visualization of honeycomb arrangement. After θ-scanning, glancing angle images were generated using the in-house developed LabVIEW program as discussed in Section 3.2.4. The results obtained from superimposition data are discussed in Chapter – 5.

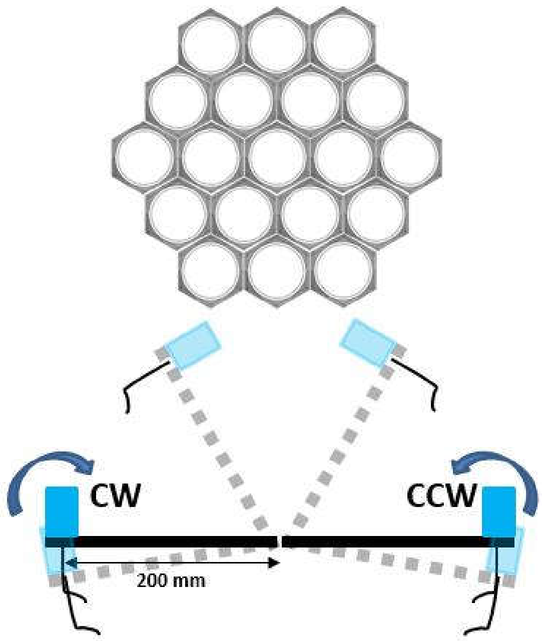

Figure 3.12 Schematic representation (top view) of data acquisition from clock-wise (CW) and counter clock-wise (CCW) orientations

3.6 Experimental procedure for multiple protrusion detection

To identify multiple protrusion detection using GAIM, two SA heads in the honeycomb arrangement were given different protrusions and glancing angle image of the entire honeycomb arrangement was obtained from optimized position of ultrasonic transducer. Figure 3.14 shows the honeycomb arrangement highlighting SA#2 and SA#16 which were protruded by 6 mm and 10 mm, respectively. The glancing angle images and the corresponding A-scan signals with and without protrusion were acquired and analyzed to detect multiple protrusion in the honeycomb arrangement using GAIM. The results of multiple protrusion detection are discussed in Chapter – 4.

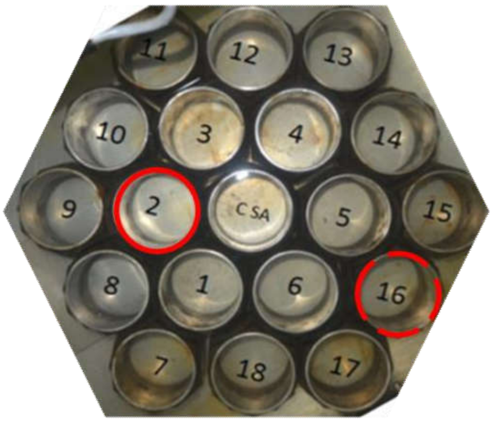

Figure 3.13 Honeycomb arrangement, highlighting SA#2 and SA# 16 protruded SA heads

3.7 Experimental set-up used for qualitative and quantitative estimation of bowing

In addition to protrusion detection, qualitative and quantitative estimation of bowing studies were also performed using GAIM. In contrast to protrusion studies, characterization of bowing must be performed from two different transducer locations, preferably from symmetrically opposite positions around SA head. Below section explains the experimental set-up used for qualitative and quantitative estimation of bowing using GAIM.

3.7.1 Experimental set-up used for qualitative estimation of bowing

Figure 3.15 shows the experimental setup used for signature identification for qualitative estimation of bowing. In the experimental setup, 5 SA heads were placed collinear and ultrasonic transducer was placed in the optimized position, so that the diffracted echoes from all 5 SA heads can be obtained simultaneously.

Figure 3.14 Experimental set-up used for identifying the bowing signatures of the SA heads

All 5 SA heads were uniformly separated by a distance of 3 mm to allow bowing to individual SA heads without disturbing the adjoining SA head. Then, SA heads were given bowing of 2° away and towards the ultrasonic transducer and A-scan signals were saved and compared with no-bowing condition. In addition to this, A-scan signals from symmetrically opposite locations around the SA head (i.e., two different positions separated by an angle of 180° around the SA head) were obtained and compared for different configurations viz., (a) no–protrusion and no-bowing, (b) bowing towards and (c) bowing away from ultrasonic transducer.

Figure 3.15 shows the schematic of experimental setup used for obtaining data from symmetrically opposite positions, say A and B. Q_1 and Q_2 indicate two points on top ring of SA#2 from where diffracted signals were obtained from A and B sides, respectively. When A-scan signals were obtained from position B, then SA#2 became the 4th SA from the transducer. Then, SA#2 was given a bowing of 2° towards ultrasonic transducer positioned at A and A-scan signals from two symmetrically opposite positions were acquired and analyzed. The details about signatures identification for qualitative estimation of bowing are explained in Chapter – 5.

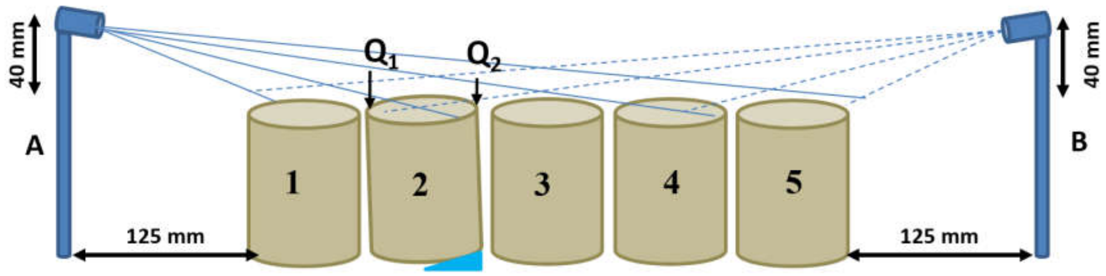

Figure 3.15 Schematic of the experimental setup used for acquiring data from symmetrically opposite positions

3.7.2 Experimental set-up used for quantitative estimation of bowing

In addition to qualitative estimation, quantitative estimation of bowing was also studied using GAIM. The same experimental setup as used for qualitative estimation was used for quantitative estimation of bowing (as shows in Fig 3.15). Quantitative estimation of bowing was achieved by comparing change in TOF of bowed SA head with theoretically calculated TOF change obtained from two different positions separated by 180° about the SA head. Detailed results and comparison of measured and theoretically calculated TOF change for quantitative estimation of bowing are discussed in Chapter – 5.

3.8 Experimental setup used for application of GAIM in sodium environment

After successful development of GAIM for the detection of protrusion and bowing in under-water, GAIM was explored in sodium environment for detection of protrusion and bowing of SA heads. Under-sodium experimental setup consists of sodium test vessel – 5 (TV-5), under-sodium scanner, under-sodium manipulator, ultrasonic transducer, pulser-receiver and the under-sodium honeycomb arrangement setup (UHAS). Below sections gives details about experimental set-up and experimental procedure adopted to check the feasibility of applying GAIM in sodium environment

3.8.1 About sodium test vessel – 5 (TV-5)

Under-sodium experiments were conducted in the test vessel – 5 (TV-5) located in Engineering Hall – 3 of Fast Reactor Technology Group (FRTG), IGCAR. The outer diameter and height of the TV – 5 vessel are 1.73 m (with 10 mm wall thickness) and 13.15 m, respectively. Total sodium holds up in TV-5 is 22433 kg. The vessel was provided with necessary instrumentation like thermocouples, to measure the shell outer temperature, level probes to detect sodium level and leak detectors. The temperature of sodium was maintained at 180°C throughout the experiment. Figures 3.16 a and b show the schematic and photograph of experimental setup used for demonstration of GAIM in sodium environment.

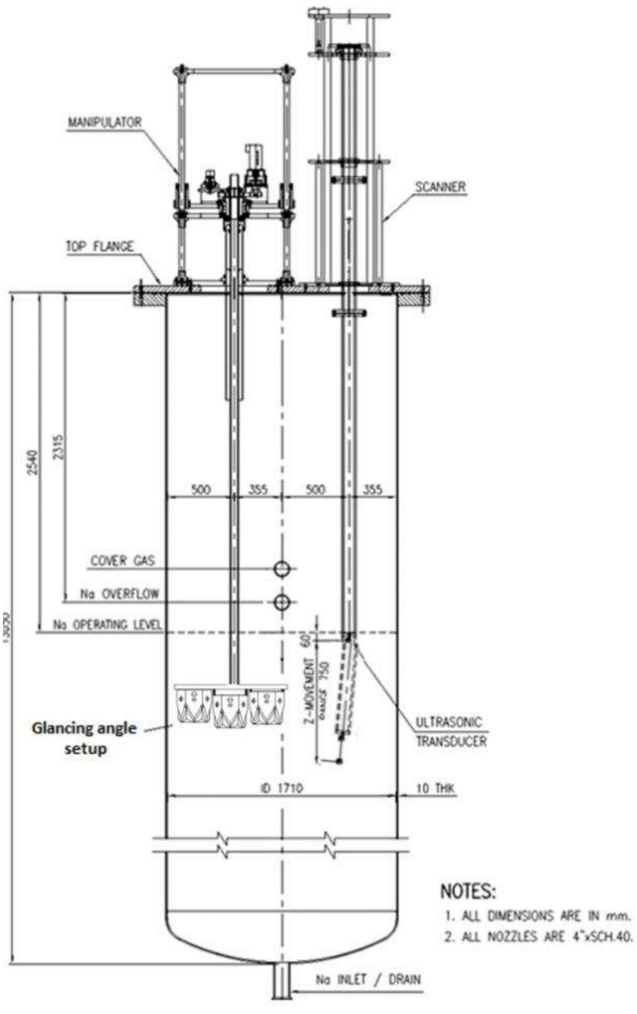

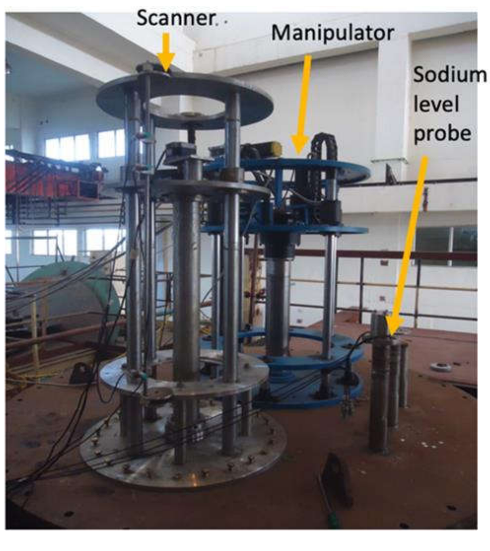

(a) *(b)*

Figure 3.16 (a) Schematic and (b) photograph of the experimental setup

A Mild steel flange of 50 mm was fabricated to close the mouth of TV-5. Two openings of 500 mm and 550 mm diameter were provided as shown in Fig 3.17 to mount under sodium scanner and manipulator on TV-5, respectively. The bottom flanges of scanner and manipulator have deep groove for providing sealing arrangement to avoid argon leak during the experiment.

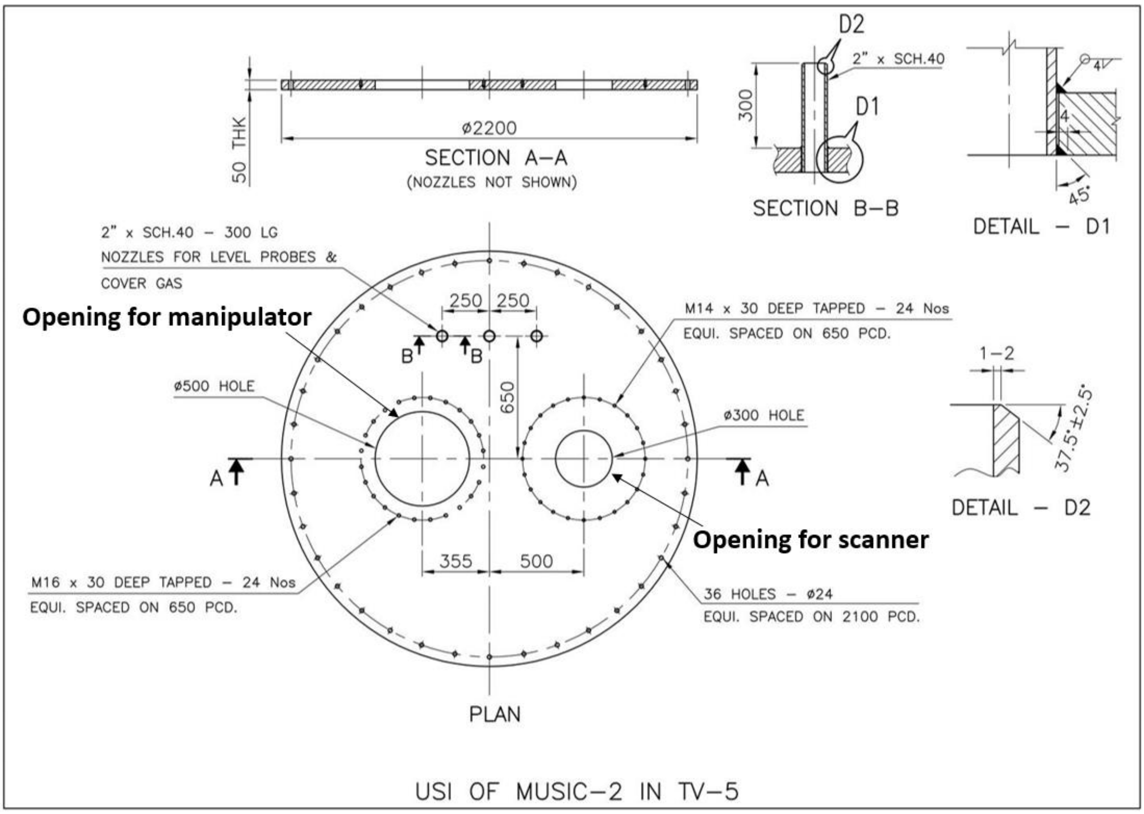

Figure 3.17 Drawing of MS flange for TV-5 showing openings for manipulator and scanner

3.8.2 Under-sodium honeycomb arrangement setup (UHAS)

Customized under-sodium honeycomb arrangement setup (UHAS) was designed to simulate different protrusion and bowing conditions of SA head as can be predicted in a reactor. Figures 3.18 a and b show top view and schematic representation of protrusion of each SA head with respect to base plate.

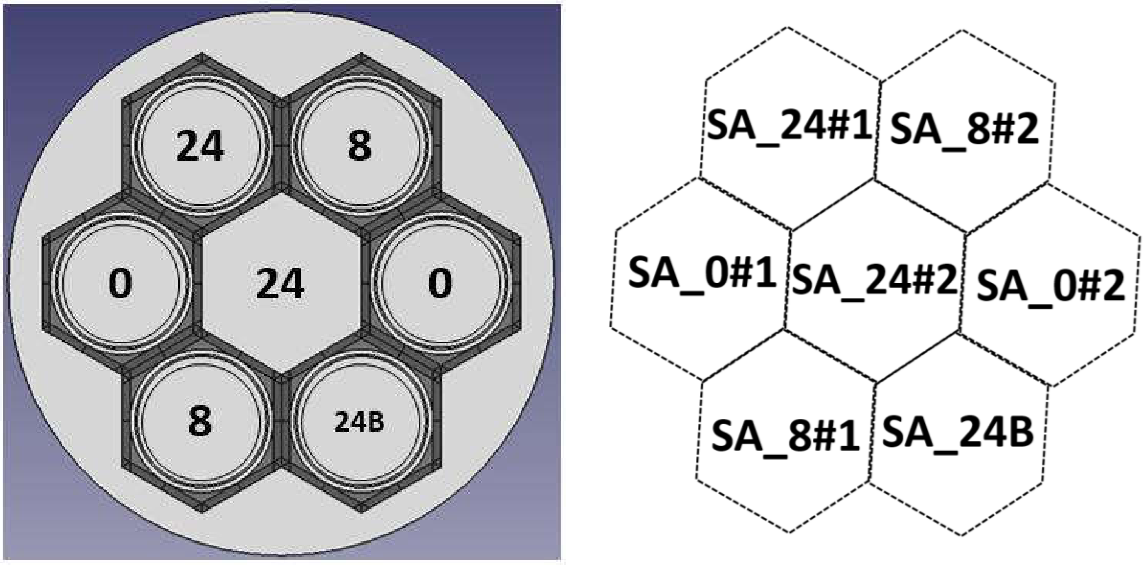

(a) *(b)*

Figure 3.18 (a) Top view and (b) schematic of UHAS simulating different protrusion conditions

In this setup, a total of 7 SA heads were used. These SA heads were bolted to a 10 mm base plate in upside down position. The base plate was made up of SS316 LN. Different combinations of protrusion viz., 0 mm 8 mm, 16 mm and 24 mm were simulated in UHAS. Different protrusion combinations were simulated by bolting each SA head using different bolt length viz., 8 mm and 24 mm. Similarly, 16 mm protrusion was simulated by the height difference of 8 mm and 24 mm protruded SA head. In addition to the SA head protrusion, bowing of 2° was also simulated by tilting one of the SA heads with respect to the adjacent SA head.

This experimental setup is similar to the under-water honeycomb arrangement without the 2nd SA heads ring around the central SA head. Nomenclature and their corresponding representation of subassembly numbers in UHAS are given in the Table 3.1.

Table 3.1 Nomenclature of SA heads used in UHAS

Sl. No.	SA #	Representation	Remarks
1.	SA_0(Z)	no protrusion given to SA head from the base plate (Z - zero)	Relative protrusion of SA head w.r.t SA#0 is 0
2.	SA_8 (E)	8 mm protrusion given to SA head from the base plate (E – eight)	Relative protrusion of SA head w.r.t SA#0 is 8
3.	SA_24 (T)	24 mm protrusion given to SA head from the base plate (T – twenty-four)	Relative protrusion of SA head w.r.t SA#0 is 24
			Relative protrusion of SA head w.r.t SA#8 is 16
4.	SA_24B (TB)	24 mm protrusion given to SA head along with bowing of 5° (TB – twenty-four bowed)	To observe the effect of SA head bowing towards and away from ultrasonic transducer

Figures 3.20 a-d show the photographs of UHAS in different orientations which was fixed at the bottom of under sodium manipulator in the upside-down position. An under-sodium ultrasonic transducer fixed at the bottom of under-sodium scanner was used for sector scanning of UHAS for detection of protrusion and bowing. Correlation-based signal processing was performed on under sodium signals for identification of diffracted echoes from UHAS SA heads. The details of signals processing are explained in Chapter – 6.

(a) *(b)* *(c)* *(d)*

Figure 3.19 a - d. Photographs of UHAS at different orientations

3.8.3 Under-sodium scanner

The under-sodium scanner has two axes (Z and θ) for vertical movement and rotation of transducer. The vertical axis traverse distance is 750 mm with a resolution of 0.1 mm. The θ -axis can rotate by 360° with a resolution of 0.01°. The scanner has an extended shaft of 3500 mm length made up of austenitic stainless steel 316 LN to fix the transducer inside sodium which is at a depth of about 2500 mm from top flange. Both axes were coupled to stepper motors which were controlled by a Galil Motion Control through a LabVIEW software.

3.8.4 Under-sodium manipulator

The manipulator was used to hold and rotate UHAS to different configurations as per the requirement. It has two axes (Z and θ) for vertical movement and rotation. The vertical traverse distance of manipulator is 750 mm with a resolution of 0.1 mm. The θ -axis can rotate by 360° with a resolution of 0.05°. The manipulator has an extended shaft of 4500 mm length made up of 316 LN to hold UHAS. Both axes were coupled to servo motors which were controlled by a Galil Motion Control. Both scanner and manipulator were controlled by the same computer using a single control panel. The bottom flange of under-sodium manipulator was provided with gaskets to avoid leaking of the Argon gas.

3.8.5 Positioning of ultrasonic transducer

The under-sodium ultrasonic transducer was tilted by an angle of 5° to get diffracted signals from UHAS. Figure 3.20 shows the schematic of tilt given to ultrasonic transducer. As the title given to ultrasonic transducer is fixed, translation movement of the scanner is used for obtaining diffracted signals from UHAS.

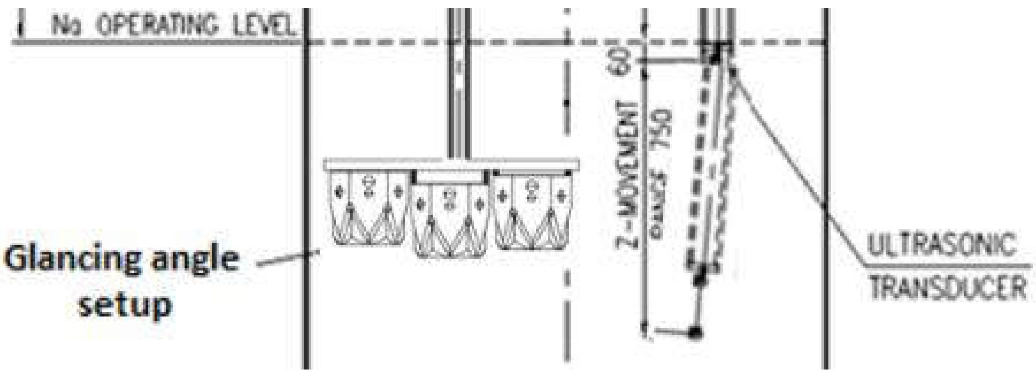

Figure 3.20 Schematic of the tilt given to ultrasonic transducer for under-sodium studies

3.8.6 Under-sodium ultrasonic transducer

The 2 MHz transducer used in underwater studies could not be used for under-sodium study as it was not connected with a Mineral Insulated (MI) cable and not hermetically sealed, even though the transducer was made similar to under-sodium transducer (with a nickel plate in front). Hence, a readily available 1 MHz transducer (same as a side viewing ultrasonic transducer of USUSS) qualified for under-sodium tests was used to perform under-sodium experiments. The transducer was connected with a 10 m long MI cable to withstand high temperature and was mounted on the spinner tube of the scanner. The transducer can withstand temperature up to 200°C. The same pulser-receiver as used in under-water studies was used in the present experiments also.

The wetting of transducer is an important issue for under-sodium viewing. Generally, wetting improves at higher temperatures. The wetting of the transducer took place after about 10 days at a temperature of 180°C of sodium. Results corresponding to under-sodium experiments are discussed in Chapter – 6.

3.9 Conclusions

In this chapter, experimental setup used for development and application of glancing angle imaging methodology (GAIM) in water and sodium environment are discussed. In addition to this, experimental setups used for detection of protrusion and bowing in water and sodium environment are also presented.

- **Experimental set-up used for development of GAIM**
    - For the development of GAIM, 19 Nos. of SA heads are arranged in immersion tank to form honeycomb arrangement. Theta-scanning of a 2 MHz under-sodium transducer was performed to get the diffracted echoes from SA heads in the honeycomb arrangement. Details about pulser receiver and experimental setup used for optimization of parameters are presented. In addition to this, LabVIEW program developed for analyzing the glancing angle data is discussed.
- **Experimental set-up used for qualitative and quantitative estimation of protrusion**

- For qualitative estimation of protrusion, transducer was placed at an optimized horizontal and vertical distances from honeycomb arrangement and glancing angle images obtained in two different scenarios were compared to obtain signatures for detection of SA protrusion.
- For quantitative estimation of protrusion, transducer was placed away from two SA heads and the 2nd SA head (rear SA head) was given protrusions in the range of 2 mm to 20 mm at different steps. The amplitude and time of flight (TOF) of ultrasonic signal obtained at different protrusion heights were used for quantitative estimation of protrusion.

- **Experimental set-ups developed for identification of diffracted echoes and superimposition studies**
  - For identification of diffracted echoes, a single SA head was rotated by 360° and a B-scan data comprising of A-scan signals at different SA orientations was acquired. From this B-scan data, locations of the diffracted echoes from the SA head are identified. Glancing angle images of the honeycomb arrangement obtained from two different orientations were superimposed to get better visualization of the same.
- **Experimental set-up details for qualitative and quantitative estimation of bowing**
  - For qualitative estimation of bowing, 5 SA heads were placed collinearly separated by a distance of 3 mm. Then the SA heads were given bowing of 2° away and towards the ultrasonic transducer.
  - For quantitative estimation of bowing, same experimental setup as in the above case was used. However, for quantitative estimation of bowing, change in the TOF data obtained from symmetrically opposite locations around the SA head was used and compared with the theoretically calculated TOF change.

- **Experimental set-up for application of GAIM in sodium environment**

For the application of GAIM in sodium environment, experimental details about the following were discussed:

- sodium test vessel – 5 (TV-5),
- 1 MHz under-sodium ultrasonic transducer with 10 m long MI cable,
- under-sodium scanner and manipulator and their capabilities,
- fabrication of under-sodium honeycomb arrangement setup (UHAS) and fixing of under-sodium transducer and UHAS to the scanner and manipulator are also discussed
- simulating different protrusion and bowing scenarios in UHAS are discussed. In addition to this, nomenclature of SA heads in UHAS is also discussed,

Chapter 4. Detection and characterization of FSA protrusion using GAIM

4.1 Chapter overview

This chapter describes the details about the detection and characterization of FSA protrusion using ultrasonic glancing angle imaging methodology (GAIM). Optimization of experimental parameters followed by results obtained for qualitative and quantitative estimation of protrusion are presented. In addition to this, sensitivity of GAIM and multiple protrusion detection using GAIM are also discussed.

4.2 Optimization of experimental parameters

To optimize experimental parameters (glancing angle and the vertical height), the ultrasonic transducer (fixed to the 200 mm arm) was moved vertically from 20 mm to 60 mm height above the subassembly (SA) head top in the increment of 2 mm. A-scan signals were saved at each 2 mm step. This procedure was repeated for angles varying from 1°-10° in steps of 1°. The signal to noise ratio (SNR) was determined by taking the ratio of the maximum signal amplitude corresponding to each SA to the maximum value of the noise level within ± 60 mm of the corresponding signal duration at different heights and at different angles of the transducer were measured. However, in the case of SA#1, the noise level after the diffracted signal from SA#1 is only considered for calculating the SNR, as high initial ringing amplitude is observed before the SA#1 signal. Figures 4.1 a-j show the SNR of all 5 SA heads for different angles varying from 1°-10°, respectively.

From Figs. 4.1 a-j, it can be seen that high SNR is obtained for particular glancing incident angle and vertical height of ultrasonic transducer combinations. For example, angles ranging from 1° - 3° (Figs. 4.1 a-c) SNR is high, when vertical distance of the ultrasonic transducer from the SA head is in the range of 20 mm – 35 mm. However, for the same angle ranges, SNR is low in the vertical distance range of 50 – 60 mm. This implies that at lower angles, signals from front SAs can be resolved better when compared to rear SAs. In addition to this, it can also be seen that SNR of rear SA heads is higher than front SA heads for the combination of angles and distances ranging from 6° - 10° and 45 mm – 60 mm (see Figs. 4.1 f-j), respectively. So, at these combinations, signals from the rear SA heads can be better resolved than the front SA heads. Further, it can also be seen that a negative SNR is observed from the front SA heads when the transducer was placed in the vertical distance range of 20 mm – 40 mm. From Figs. 4.1 d and e, it can be observed that SNR from all SA heads is similar for vertical ranges varying from 20 mm – 35 mm. However, at a higher vertical range of 50 mm – 60 mm, the SNR of SA#1 and SA#2 are lower for 4° glancing angle when compared to 5°. So, the glancing angle images of the honeycomb arrangement were acquired at a glancing angle of 5° and at a vertical height of 40 mm from the SA head top.

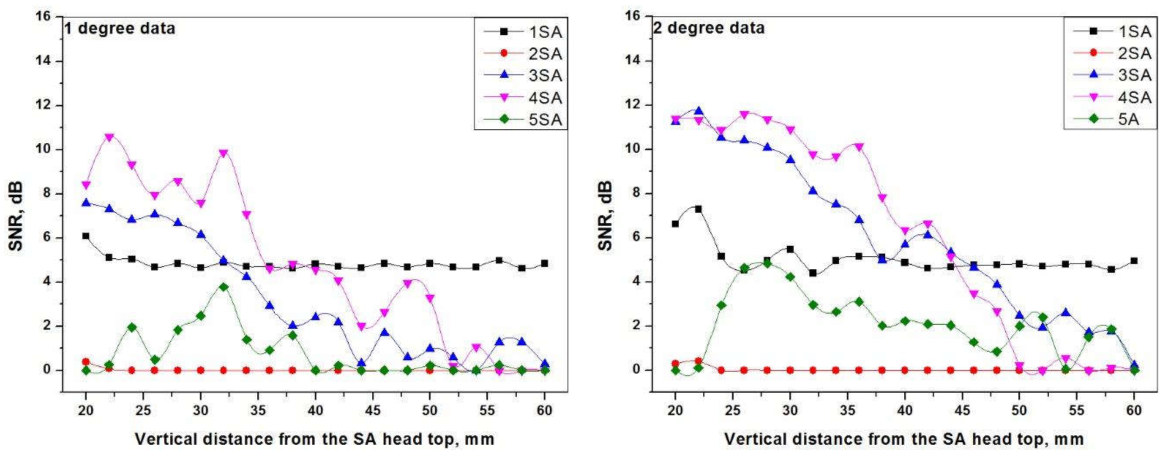

(a) (b)

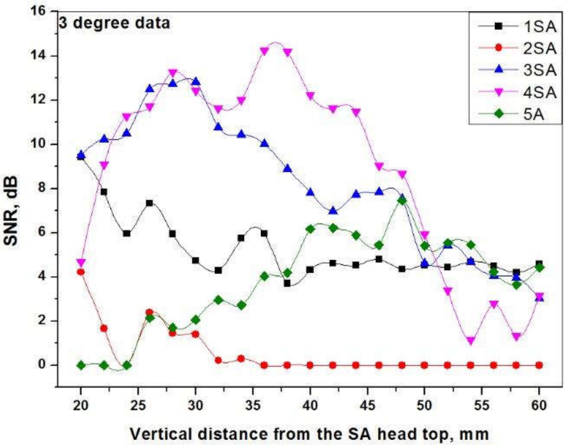
3 degree data
1SA
2SA
3SA
4SA
5A
SNR, dB
Vertical distance from the SA head top, mm

(c)

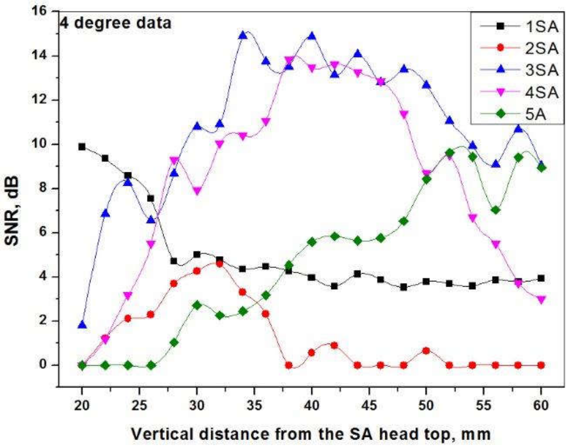
4 degree data
1SA
2SA
3SA
4SA
5A
SNR, dB
Vertical distance from the SA head top, mm

(d)

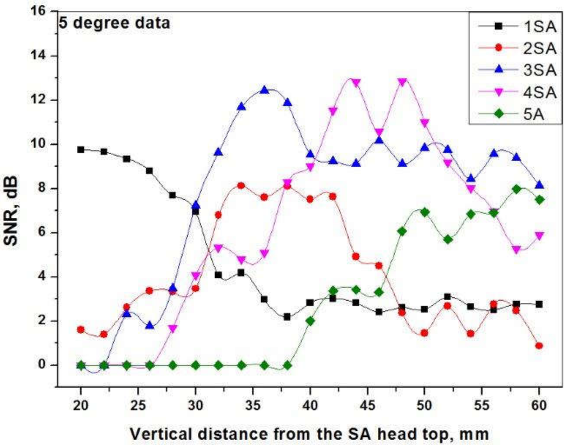
5 degree data
1SA
2SA
3SA
4SA
5A
SNR, dB
Vertical distance from the SA head top, mm

(e)

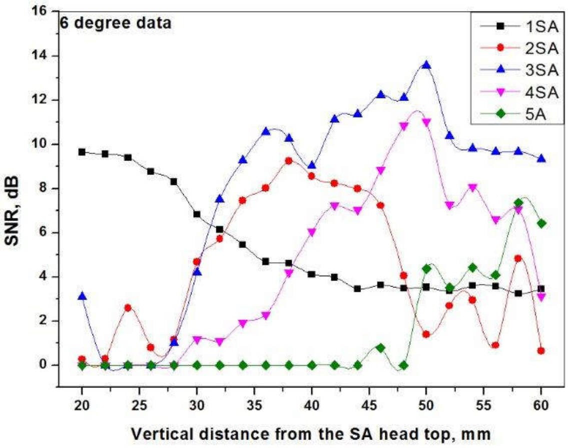
6 degree data
1SA
2SA
3SA
4SA
5A
SNR, dB
Vertical distance from the SA head top, mm

(f)

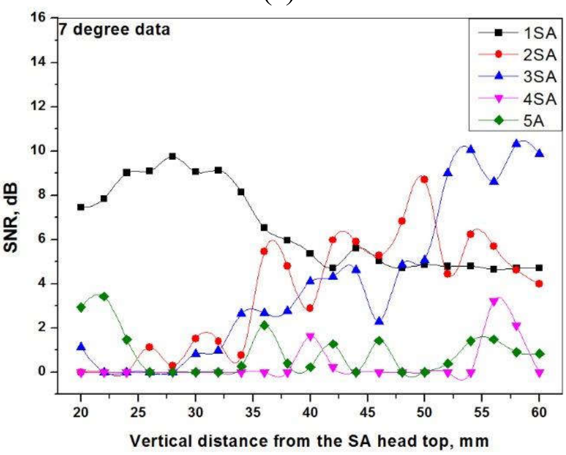
7 degree data
1SA
2SA
3SA
4SA
5A
SNR, dB
Vertical distance from the SA head top, mm

(g)

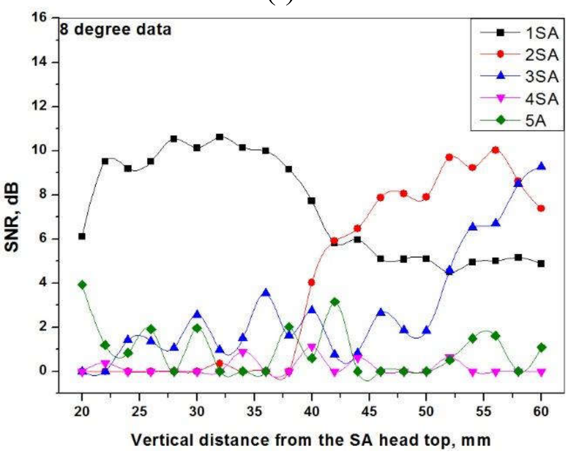
8 degree data
1SA
2SA
3SA
4SA
5A
SNR, dB
Vertical distance from the SA head top, mm

(h)

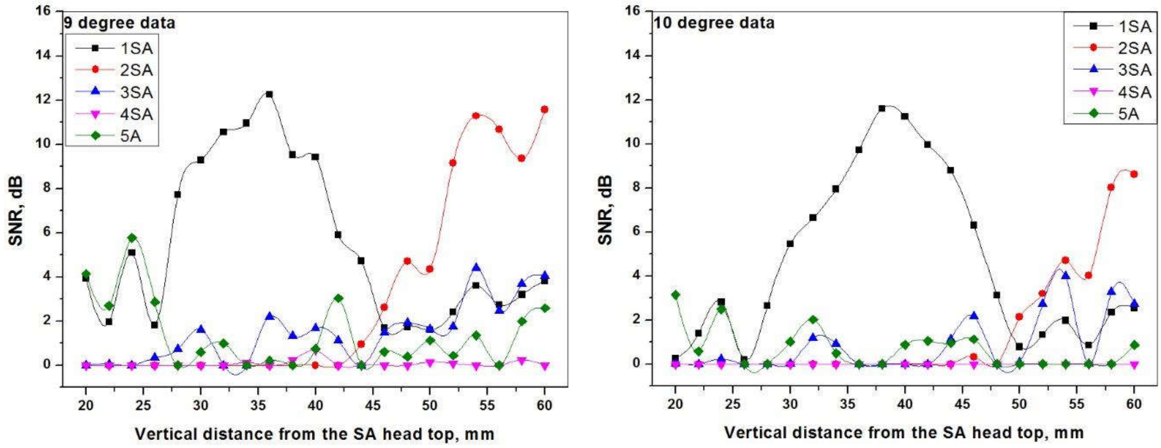

(i) (j)

Figure 4.1 a-j SNR for all 5 SA heads at different glancing angle of the transducer varying from 1°-10°

Data obtained from all 10 angles and at different heights were normalized and added for each of all 5 SA heads to get the optimized SNR. Figure. 4.2 shows the color contour plot of normalized SNR of all 5 SA heads, it is clearly seen that for lower vertical height ranges and higher glancing angle ranges poor SNR is obtained from SA heads. The dotted region in Fig 4.2 shows optimized SNR range for the given honeycomb arrangement.

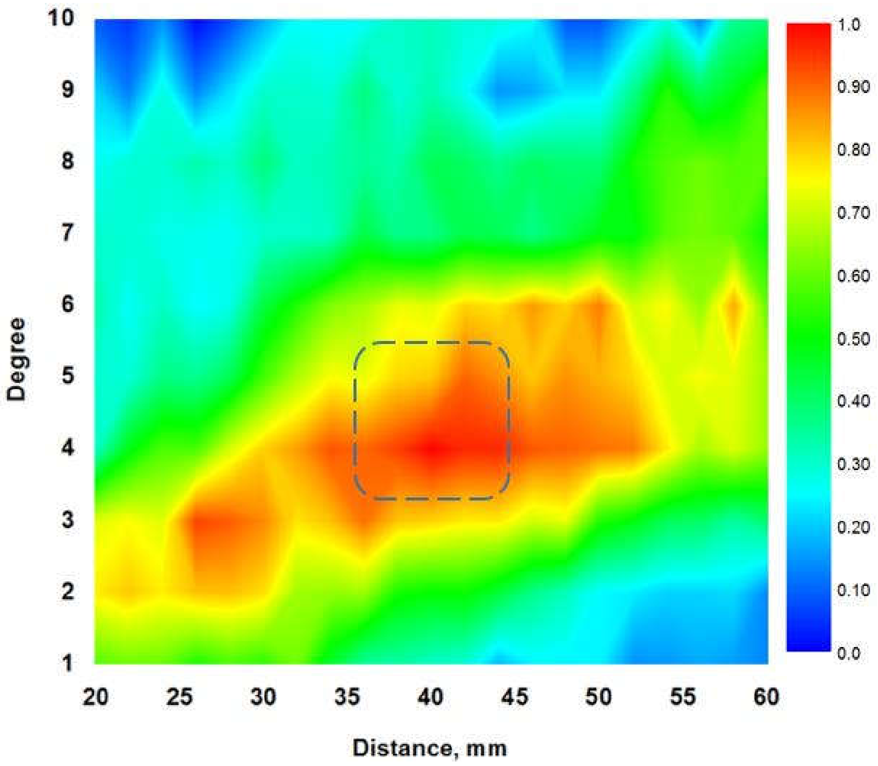

Figure 4.2 Normalized SNR color plot of all 5 SA heads

4.3 Mapping of SA heads in GAIM

After optimizing experimental parameters (height at 40 mm and angle at 5°), glancing angle image of the honeycomb arrangement was acquired by sweeping the transducer by an angle of 80° to cover the entire honeycomb arrangement. Figure 4.3 sows the glancing angle image (superimposed on a honeycomb schematic) of the entire honeycomb arrangement without any protrusion. From the Fig 4.3 it can be observed that the diffracted signals from all the SA heads are identified from the inner diameter (ID) side (rear end). In addition to this, few signals were obtained from the outer diameter (OD) side (front end) of the SA head (as shown by doted circle in the glancing angle image). However, signals from complete top ring of SA head is not observed. To observe the locations of the diffracted signals obtained from SA heads, a turn table experiment was carried out as per the experimental setup shown in Fig 3.11 a.

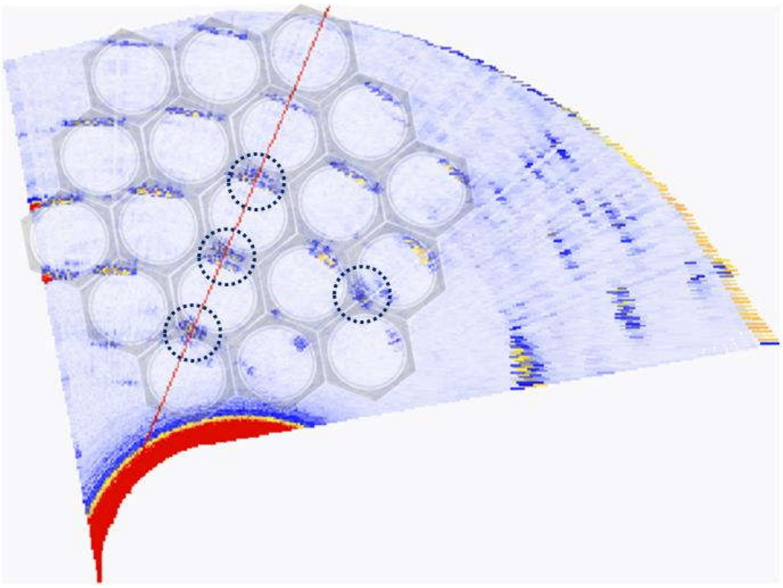

Figure 4.3 Glancing angle image of the honeycomb arrangement

Figure 4.4 shows the B-scan image obtained during 360° rotation of a single SA head. It is clear from the B-scan data that the diffracted signals of almost similar amplitudes are observed from 6 equidistant points on the OD facing the beam. These locations correspond to the sharp edges on the faces of the OD, as shown in Fig 3.11 c (circled at the sharp edge). In addition to this, a signal is observed from ID at all orientations of SA head. This signal corresponds to the diametrically opposite point of the SA head, where the beam is incident radially on the ID, as shown in Fig 3.11c (circled at the backside ID of the SA head). When ultrasonic beam was aligned normal to the front face, signals corresponding to both OD and ID were obtained for all the SA heads in the honeycomb arrangement.

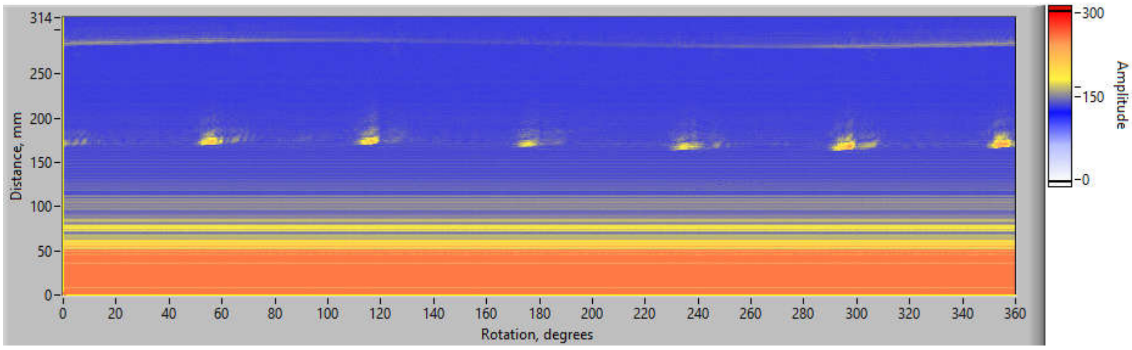

Figure 4.4 B-scan image obtained during 360° rotation of a single SA head

4.4 Qualitative estimation of protrusion

For qualitative estimation of protrusion, identification of signature which indicate the protrusion is important. In the below section, details about identification of protrusion signatures are discussed in detail.

4.4.1 Identification of signatures for qualitative estimation of protrusion

As explained in Section 3.3.1 glancing angle images of entire honeycomb arrangement were obtained with and without giving protrusion of 9 mm to SA heads in the honeycomb arrangement. The SA heads to which protrusion was given are SA#1, SA#C and SA#4. Figures 4.5 (a – d) show the glancing angle images of entire honeycomb arrangement obtained by sweeping the ultrasonic transducer by an angle of 90°, for different protrusion scenarios.

Figure 4.5 a shows the glancing angle image of honeycomb arrangement without any protrusion and Figs. 4.5 (b – d) show the glancing angle image of honeycomb arrangement with a protrusion of 9 mm given to SA#1, SA#C (central SA) and SA#4, respectively. Figure 4.5 e shows the corresponding A-scan signals obtained along the red line shown in the Figs 4.5 (a – d). Red color circles in the glancing angle images represent top rig of SA head, which in-turn represents position of each SA head in the honeycomb arrangement.

From Fig 4.5 (e), an increase in echo amplitude corresponding to protruded SA can be clearly seen. Further, echoes from the SAs behind protruded SAs are masked and multiple reflections from protruded SA are only observed. For example, let us consider the A-scan signals for no–protrusion condition, SA#1 and SA#C protrusion conditions. In no protrusion condition, all 10 peaks (1,2), (3,4), (5,6), (7,8) and (9,10) corresponding to SA heads, SA#7, SA#1, SA#C, SA#4 and SA#13, respectively are observed. In the peak nomenclature (a, b), 'a' represents the peak from front (OD) sharp projection of the SA head and 'b' is from back end ID location of each SA head. When 9 mm protrusion was given to SA#1, peaks (5,6), (7,8) and (9,10) from SA#C, SA#4 and SA#13, respectively were absent. Due to 9 mm protrusion given to SA#1, it blocked ultrasonic beam to reach SA heads behind the SA#1.

Similarly, when SA#C was protruded by 9 mm, peaks (1,2), (3,4) and (5,6) from SA heads SA#7, SA#1 and SA#C, respectively were only present. Other peaks (7,8) and (9,10) from SA heads SA#4 and SA#13, respectively were absent. These two conditions clearly show the masking of echoes behind protruded SA.

In addition to masking of echoes, an increase in amplitude from protruded SA is also observed in Fig 4.5 (e). This is clearly evident by comparing the A-scan signals of no-protrusion and SA#4 protrusion conditions. The peaks (7,8) are from SA#4. The amplitude of peak 7

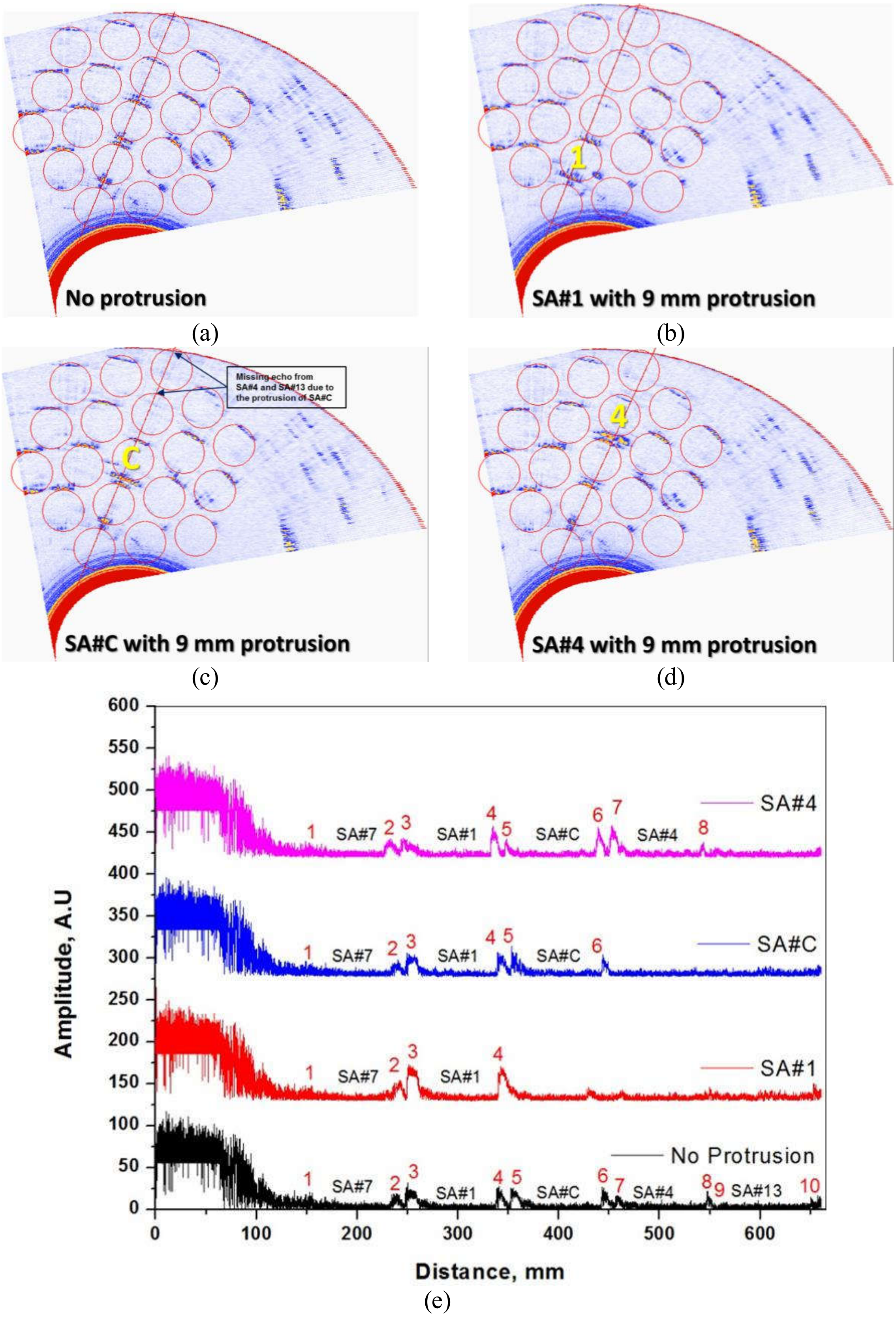

Figure 4.5 (a) – (d) Glancing angle image of the entire honeycomb arrangement for different protrusion scenarios: (a) no protrusion and 9 mm protrusion to (b) SA#1, (c) SA#C, and (d) SA#4. The corresponding A-scan signals obtained along the red cursor line in (a)-(d) are shown in (e)

increased upon protrusion of SA#4, when compared to no-protrusion case. It can also be observed that amplitude of peak 8 decreased in the SA#4 protrusion condition as compared with no-protrusion condition. This is because when SA#4 was protruded, the front face of the SA#4 blocked the ultrasonic beam from reaching to rear face of SA head. Due to which the peak amplitude from the rear end of SA decreased.

In the Fig. 4.5 (e) as the experiments were carried out in water and the velocity of ultrasound in water (1500 m/s) at room temperature is known, distance scale is used in the X-axis. However, for under sodium experimental data, the velocity of the ultrasound varies depending on the temperature of the sodium, so, it will be difficult to mention the scale in distance. If the liquid sodium is maintained at an uniform temperature during the data acquisition in liquid sodium (during shutdown), then the distance scale can be used for representing the A-scan data.

The above discussed signatures indicate that, enhanced echo amplitude corresponding to protruded SA and masking of signals corresponding to SAs behind it can be used as two parameters to detect protrusion of any SA.

4.5 Random and multiple protrusion identification

After identifying signatures which can be used for qualitative estimation of detection, imaging of honeycomb arrangement was performed by giving 9 mm protrusion to random SA heads in the honeycomb arrangement. Glancing angle images and corresponding A-scan signals obtained for the effect of protrusion of SA#5 is shown in Fig 4.6. Figures 4.6 a and b show the glancing angle images of honeycomb arrangement without any protrusion and with 9 mm protrusion given to SA#5, respectively. The corresponding A-scan signals obtained along the line of sight (along the red line shown) in Figs 4.6 a and b are shown in Figs.4.6 c and d, respectively. From Figs. 4.6 c and d, it can be observed that the amplitude of the peaks corresponding to SA#5 increased after protrusion of SA#5 by 9 mm. At the same time, the peak corresponding to SA#14 is missing because of the protrusion of SA#5. The same can be visualized clearly in the glancing angle image (Fig 4.6 (b)) of the honeycomb arrangement obtained by giving 9 mm protrusion to SA#5. This clearly shows that the parameters like, enhanced echo amplitude and missing of the signals behind the protruded SA can be used for the detection of protrusion of any FSA in PFBR reactor.

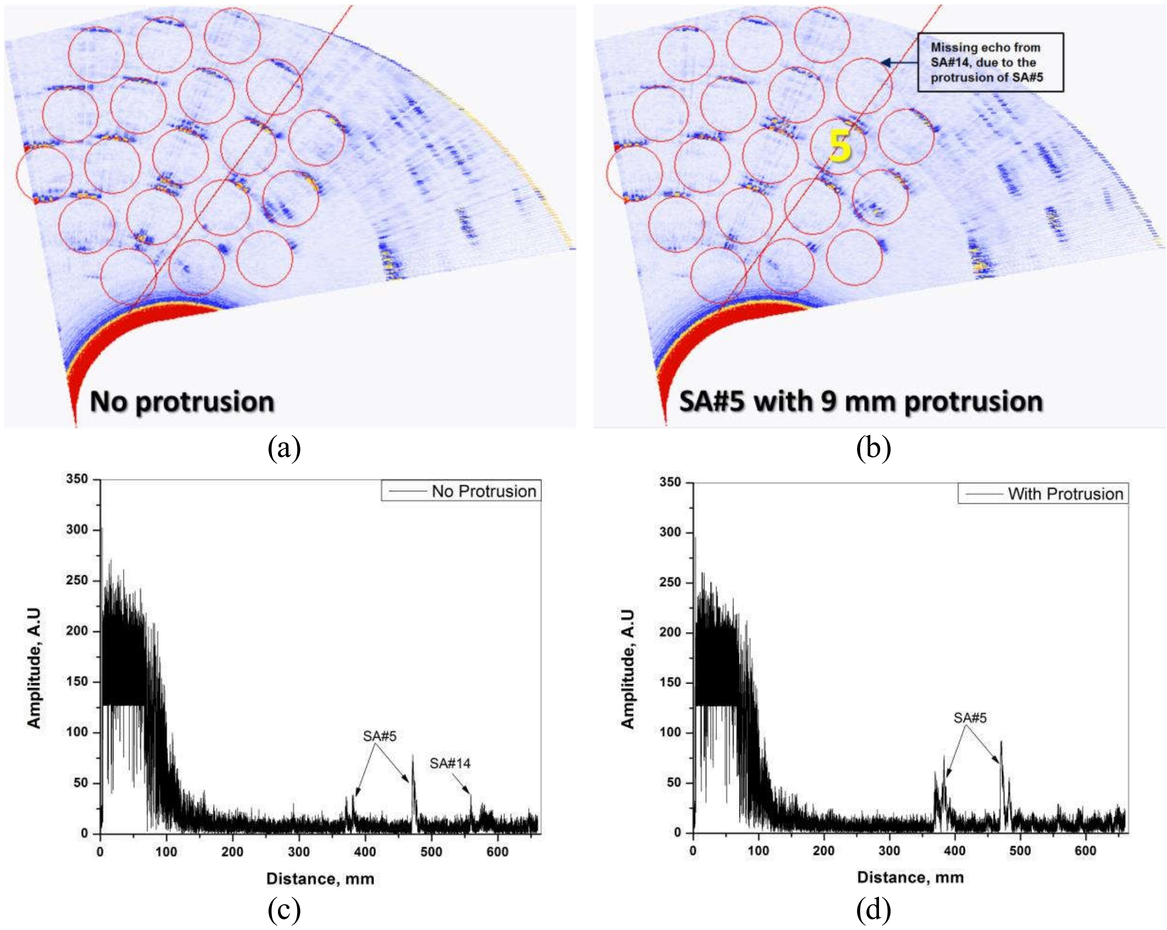

Figure 4.6 (a) Glancing angle image of the honeycomb arrangement for (a) no protrusion and (c) 9 mm protrusion of SA#5. The corresponding A-scan signals obtained along the red cursor line shown in (a) and (c) are given in (b) and (d)

In addition to random protrusion detection, to study possibility of using GAIM for multiple protrusion detection, SA#2 and SA#16 were protruded by 6 mm and 10 mm respectively in the honeycomb arrangement. Then, the glancing angle images were acquired without and with protrusion given to above mentioned SA heads. The corresponding A-scan signals of both the SAs before and after protrusion were compared in addition to the glancing angle images for identifying multiple protrusion in the honeycomb arrangement.

Figures 4.7 a and c show glancing angle images of honeycomb arrangement without and with protrusions given to SA#2 (6 mm protrusion) and SA#16 (10 mm protrusion), respectively. Figures 4.7 b and d show the A-scan signals corresponding to red cursor shown in Figs. 4.7 a and c. From the A-scan signals, it can be observed that intensity of diffracted echo from SA#2 increased due to protrusion. A drop in amplitude corresponding to SA#3 can be clearly seen in the GAIM image due to shadowing effect.

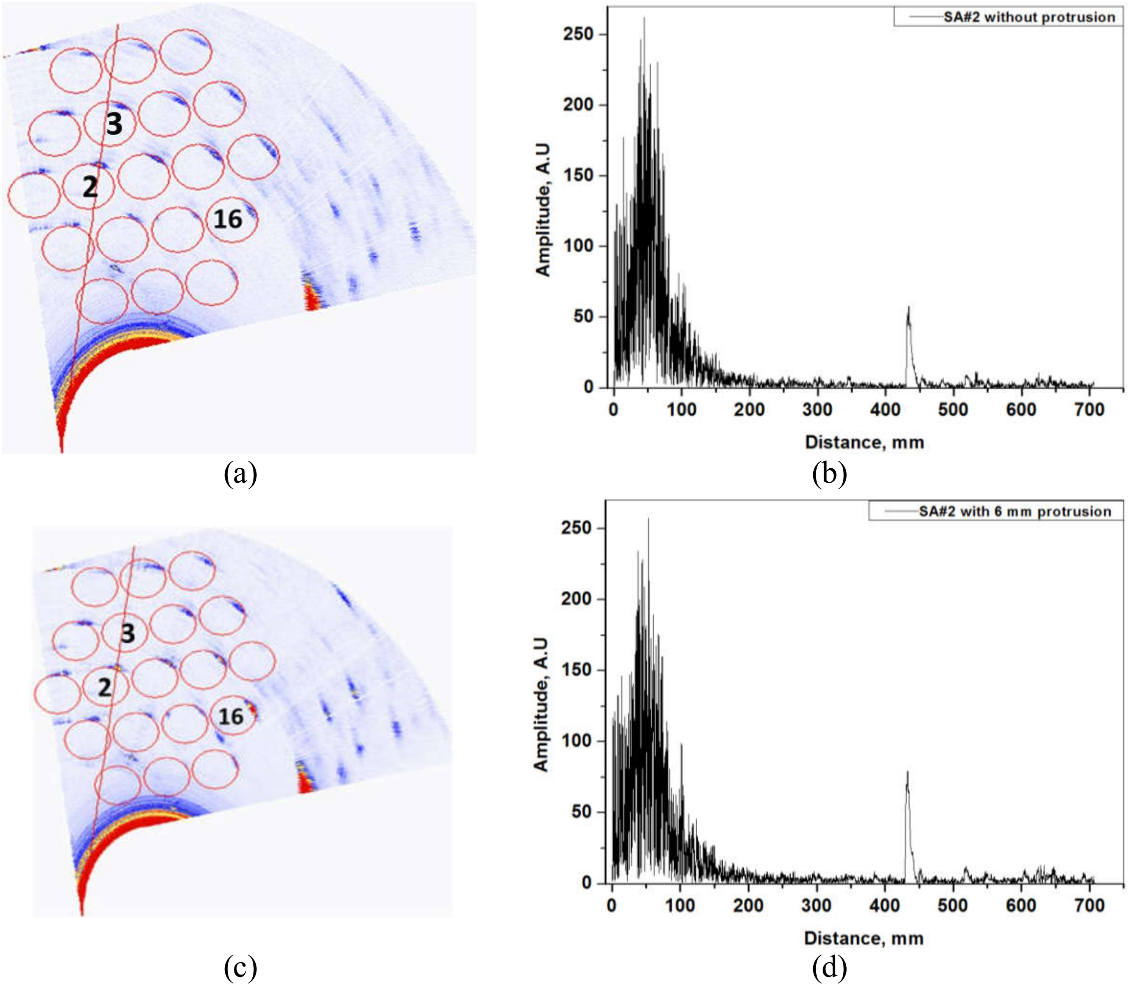

Figure 4.7 (a) Glancing angle image of the honeycomb arrangement for (a) no protrusion and (c) 6 mm protrusion of SA#2. The corresponding A-scan signals obtained along the red cursor line shown in (a) and (c) are given in (b) and (d)

In addition to this, it can be observed from the glancing angle images, that there is an intensity increase from the SA#16 due to 10 mm protrusion given to the same. Figures 4.8 a and b show the A-scan signals (without and with 10 mm protrusion) obtained along the cursor when it is orthogonal to SA#16. It can be seen from Fig. 4.8 b, diffracted echo from ID was obtained (due to 10 mm protrusion given to SA#16) which was absent in no-protrusion condition.

From the above studies it is clear that multiple protrusion can also be detected with a single sweep of the ultrasonic transducer using GAIM.

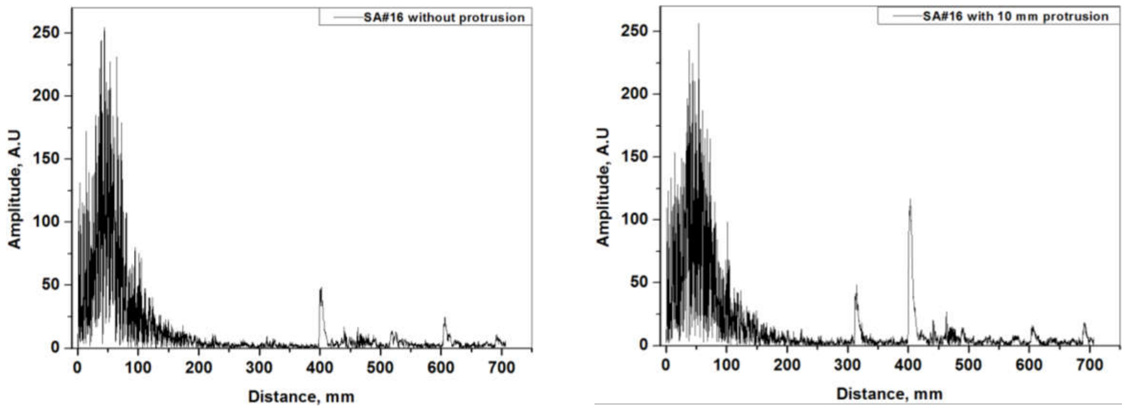

(a) (b)

Figure 4.8 A-scan signals obtained along the cursor when it is orthogonal to SA#16 (a) without protrusion and (b) with 10 mm protrusion

4.6 Quantitative estimation of protrusion using GAIM

Quantitative assessment of protrusion was carried out as per the experimental set-up shown in Figs. 3.10 a and b. The 2nd SA head was given protrusions in the range of 2 mm – 20 mm at different steps and the amplitude and the time of flight (TOF) of the ultrasonic signal at different protrusion heights were measured for quantitative estimation of protrusion. Figures 4.9 a and b show the A-scan signals obtained without and with 8 mm protrusion given to 2nd SA head (from the ultrasonic transducer), respectively. The peaks SA_1 and SA_2 in Fig 4.9 a are from the rear end of the 1st SA head and front end of the 2nd SA head respectively, as mentioned in Fig 3.10 a. The peaks SA'_1 and SA'_2 in Fig 4.9 b are the corresponding peaks upon protrusion of SA#2 by 8 mm as shown in Fig 3.10 b. It can be observed that amplitude of peak from the 2nd SA head in the protrusion case is almost double than that for no-protrusion case.

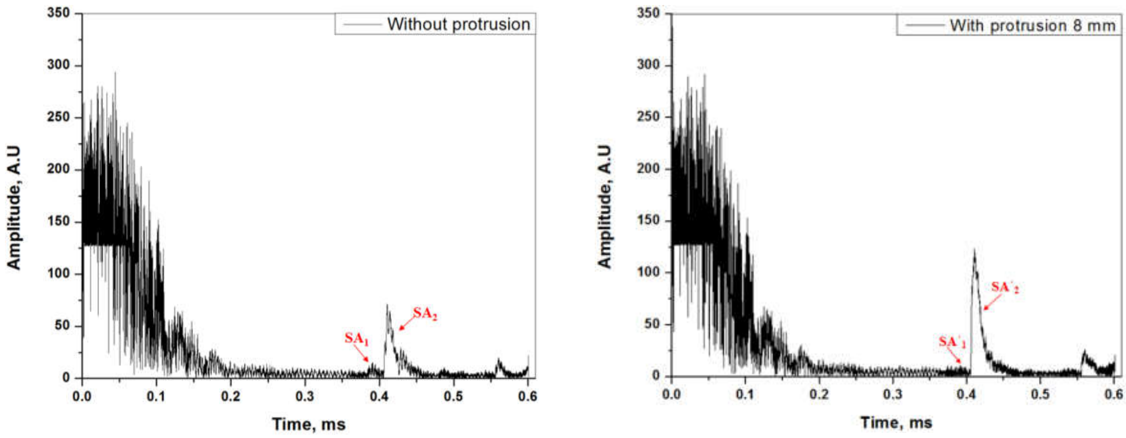

(a) (b)

Figure 4.9 A-scan signals from the experimental set-up used for quantitative evaluation (a) without and (b) with protrusion

Figures 4.10 a and b show variations in the absolute and relative amplitude corresponding to protruded SA head (SA'_2) with the extent of protrusion, respectively. A continuous increase in amplitude is observed with the extent of protrusion. As the SA head top has a complex structure with six fold symmetry (Figs.4.11 a and b), the orientation of SA is also expected to influence the correlation between maximum amplitude and the extent of protrusion. In view of this, measurements were performed for different orientations of SA viz, 0°, 10°, 20° and 30°. In case of 0° orientation, flat surface of the SA is perpendicular to the incident beam, as shown in Fig 4.11 a. It can be seen from Fig 4.10 a, that the absolute amplitude is maximum at 0° orientation of SA head without any protrusion. In addition to this the absolute amplitude is maximum for 10° and 0° orientations and minimum for 30° orientation of the SA head.

While carrying out in-service-inspection of reactor core for detection of protrusion in FSAs, a relative amplitude comparison will give an idea about the effective protrusion extent of a particular FSA. So, a variations in relative amplitude corresponding to the extent of protrusion was plotted as shown in Fig 4.10 b. It can be seen in Fig 4.10 b that increase in relative amplitude is minimum for 0° and 30° orientations of the SA and maximum for 10° orientation.

The relative amplitude at each protrusion is the ratio of amplitude at a particular protrusion of the SA head with respect to the no protrusion amplitude. It is mathematically represented as;

$$RA_p = \frac{A_p}{A_0} \tag{5}$$

Here, RA_p is the relative amplitude for a given protrusion of p. A_p stands for amplitude of the diffracted echo for the given protrusion of p to the rear SA head and A_0 stands for the amplitude of the diffracted echo from the rear SA head without any protrusion (i.e., 0 mm protrusion).

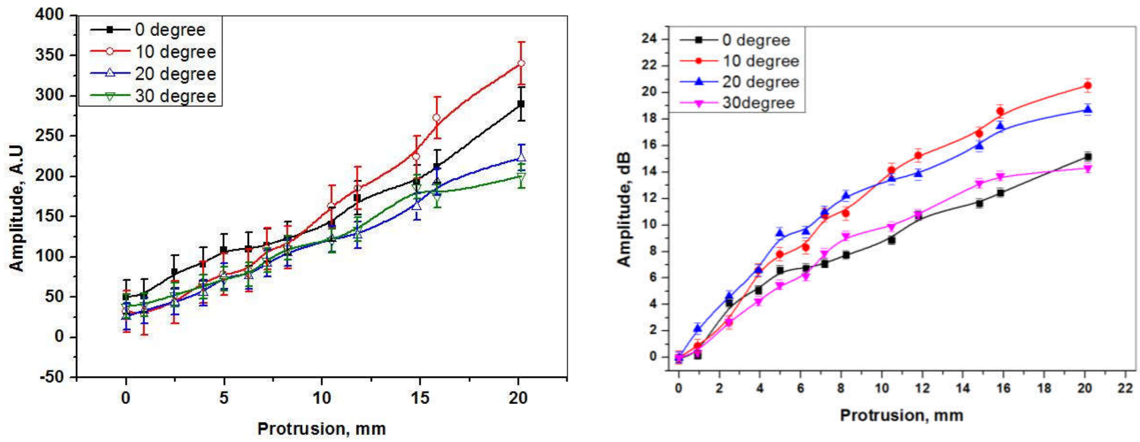

(a) (b)

Figure 4.10 Variaiton in (a) absolute and (b) relative amplitude of ultrasonic signal with the extent of protrusion for four orientations of SA head

(a) (b)

Figure 4.11 SA at (a) 0° and (b) 30° orientation (circled portion on top of SA head shows flat surfaces at different angles)

In addition to amplitude of signal SA'_2, time of flight (TOF) of arrival of the signal is also found to be influenced by SA protrusion. Figure 4.12 shows the variation in TOF signal with extent of protrusion of 2nd SA head for different orientations. The TOF decreased with increasing extent of protrusion for all SA head orientations.

The time of flight (TOF) is defined as the time necessary for an ultrasonic wave to travel from the transmitter to the receiver after being reflected from the target. In the present work, peak in the signal envelop is considered for TOF measurements.

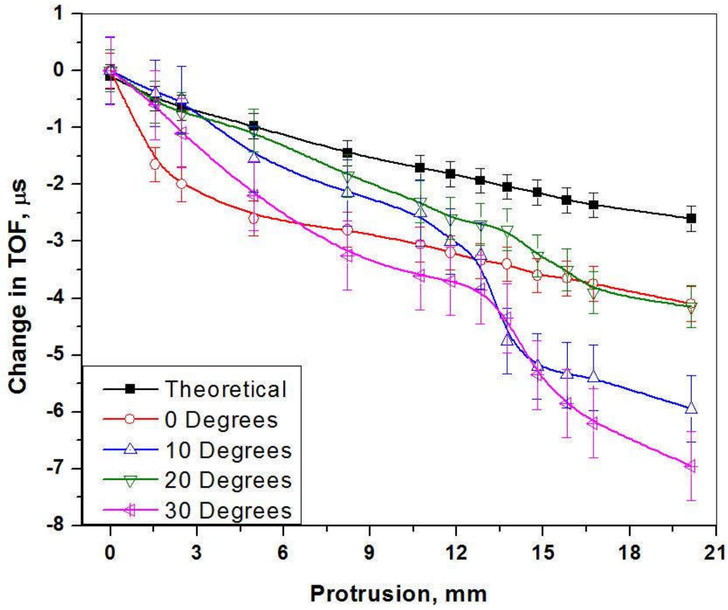

Figure 4.12 Variation in time of flight (TOF) of ultrasonic signal with the extent of protrusion for four orientations of SA head

The decrease in TOF with increasing protrusion can be understood using the schematic shown in Fig 4.13. '*A*' in Fig 4.13 corresponds to a point in the top ring of 2nd SA head, from where the diffracted signal is observed and the TOF corresponding to distance Z from the transducer. Upon protrusion of SA by height *p*, the point shifts to A_p leading to decrease in TOF because of the reduced distance from transducer (Z_p), as given below:

$$z = \sqrt{X^2 + Y^2} \qquad (6)$$

$$z = \sqrt{X^2 + (Y - p)^2} \qquad (7)$$

$$TOF_p = \frac{2 \times Z_p}{v} \qquad (8)$$

where, v is the velocity of ultrasound in water.

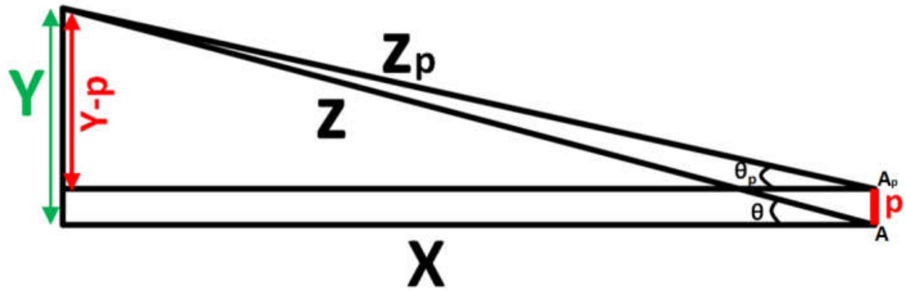

Figure 4.13 Schematic used for calculating theoretical TOF

The calculated values of TOF_p as a function of protrusion p for the configuration shown in Fig 3.10 b is also shown in Fig 4.12 (theoretical). A continuous decrease in TOF was observed with increasing protrusion. The experimental results show better sensitivity for change in TOF with protrusion as compared to the calculated values. Further, different rates of change in TOF with the extent of protrusion is observed for SA heads with different orientations. This is attributed to complex FSA top with different flat surfaces (Figs. 4.11 a and b) at different angles, which may change source of the signal from diffraction from the top ring to reflection from the flat surfaces upon protrusion, leading to sudden change in the TOF values.

4.7 Minimum protrusion detection using GAIM

The sensitivity of the GAIM was obtained by giving protrusion to SA#6 and observing change in amplitude of the diffracted echoes from SA#5 and SA#6 heads. In the honeycomb arrangement SA#5 is behind SA#6, as shown in Fig 3.13. Figure 4.14 shows the amplitudes from SA#6 and SA#5 at different protrusion conditions.

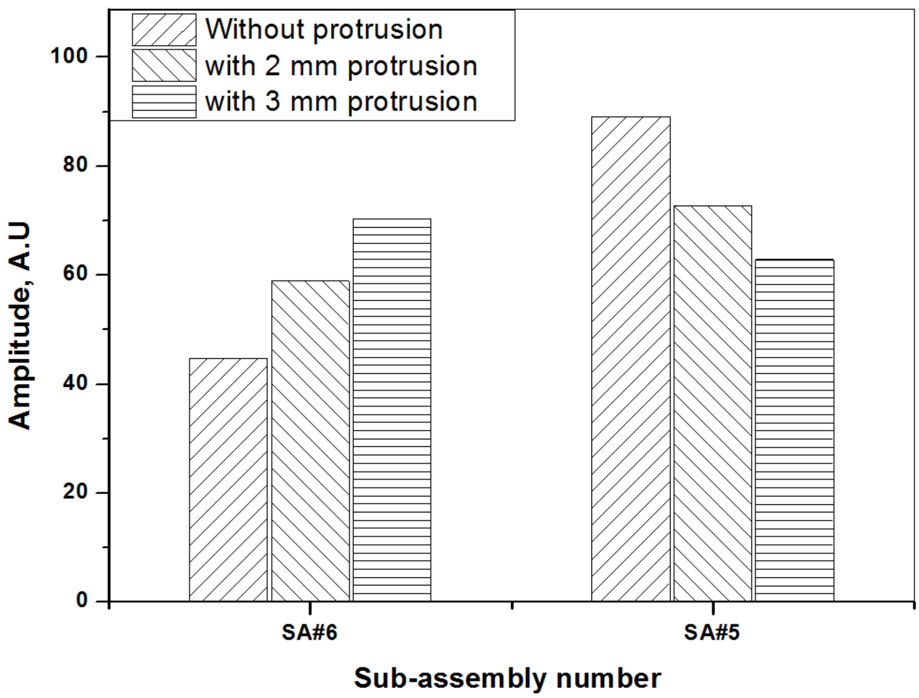

Figure 4.14 Amplitudes of SA#6 and SA#5 for different protrusion conditions

From Fig 4.14, it can be seen that the amplitude of the SA#6 increased from 44.8 A.U. to 58.9 A.U. when the protrusion was increased from 0 to 2 mm. There is a variation of 14.1 A.U. observed when SA#6 is protruded by 2 mm. In the next step, when 3 mm protrusion was given to SA#6, the amplitude increased from 58.9 A.U. to 70.4 A.U. A variation of 11.5 A.U. is observed when the SA# was protruded by 1 mm more.

On the other hand, the intensity of SA#5 which was behind SA#6 decreased gradually as the height of the protrusion (given to SA#6) increased from 2 mm to 3 mm. In the case of SA#5, the intensity decreased from 89.1 A.U. to 72.7 A.U., i.e., there is a variation of 16.4 A.U. observed due to 2 mm protrusion. The intensity further decreased to 62.9 A.U. when protrusion was increased by 1 mm. In this case, variation in the intensity found to be 9.8 A.U.

From the above observations it can be concluded that the sensitivity of the GAIM is around 1 mm for the given configuration and transducer in ideal conditions.

4.8 Conclusions

In this chapter, optimized experimental parameters for the GAIM are presented systematically. The glancing angle imaging of the honeycomb arrangement and the signature identified for qualitative and quantitative estimation of protrusion are discussed in detail. In addition to this, the details about imaging of the honeycomb arrangement and the identification of the diffracted locations from the SA head are discussed in detail.

- **Optimization of the experimental parameters**

For optimizing the experimental parameters, A-scan signals at different vertical height varying from 20 mm to 60 mm from the SA head and at different angles varying from 1° to 10° are obtained from the honeycomb arrangement. The SNR of all 5 SA heads was determined for each of this A-scan signal and the corresponding color contour plot of the normalized SNR of all 5 SA heads was plotted. From the normalized SNR plots it is observed that the optimized vertical height and glancing angle of the ultrasonic transducer are 40 mm and 5°, respectively. As the dead zone of the 2 MHz ultrasonic transducer is 125 mm, the transducer was placed at a distance of 150 mm from the 1st SA head.

- **Imaging of the honeycomb arrangement and the identification of the diffracted locations**

From the optimized position, glancing angle images of the honeycomb arrangement was acquired by sweeping the transducer by an angle of 80° to cover the entire honeycomb arrangement. In the glancing angle image, diffracted signals were observed from the ID and OD sides of the SA heads in the honeycomb arrangement. Locations of these diffracted signals were identified by the B-scan image obtained during the 360° rotation of a single SA head. The B-scan signal revealed that the diffracted signals from the OD side of the SA head are observed from 6 equidistant locations (sharp edges on the top of the SA head separated by an angular distance of 60°) on the top of each SA head and the signal from the ID side of the SA head is observed when the beam is incident radially on the rear side ID of each SA head.

- **Qualitative and quantitative estimation of protrusion**

For qualitative estimation of the protrusion, glancing angle images of the entire honeycomb arrangement was obtained with and without giving protrusion of 9 mm to particular SA heads in the honeycomb arrangement. From the A-scan signals obtained with and without protrusion, following signatures were identified which can be used for qualitative estimation of protrusion:

1. enhanced echo amplitude corresponding to the protruded SA and
2. masking of signals corresponding to the SAs behind the protruded SA.

Multiple protrusion detection (qualitative) in the honeycomb arrangement was performed using the GAIM by giving random protrusion to SA#2 and SA#16. From the glancing angle images and the corresponding A-scan signals of both SA head signals, protrusion signatures were identified clearly. In addition to the multiple protrusion detection, sensitivity of the GAIM is found to be around 1 mm for the current configuration.

Quantitative estimation of protrusion was studied using the amplitude and time of flight (TOF) of the ultrasonic signal at different protrusion heights. As the SA head top has a complex structure with six fold symmetry, the orientation of SA is also expected to influence the correlation between the maximum amplitude and extent of protrusion. In view of this, measurements were performed for different orientations of SA viz, 0°, 10°, 20° and 30°.

A continuous increase in the amplitude and decrease in TOF is observed with the extent of protrusion for all the SA head orientations. However, different rates of change in TOF with the extent of protrusion is observed for SAs with different orientations. This is attributed to the complex SA top with different flat surfaces at different angles, which may change the source of the signal from diffraction from the top ring to reflection from the flat surfaces upon protrusion, leading to sudden change in the TOF values. In addition to this, measured TOF values were compared with the theoretically calculated values and they are found to be in good agreement.

Chapter 5. Detection and characterization of FSA bowing using GAIM

5.1 Chapter overview

This chapter describes the application of GAIM for detection and characterization of FSA bowing. The signatures identified for qualitative estimation of bowing is explained in this chapter. The superimposition of glancing angle data obtained from two different orientations is presented. Further, quantitative estimation of bowing and comparison of experimentally measured bowing with the theoretically calculated value is discussed. The detection of bowing of random SA heads in the honeycomb arrangement is presented.

5.2 Qualitative estimation of bowing

In order to identify signatures of SA bowing in GAIM, results obtained in two specific experiments are described in this section:

(i) by placing 5 collinear SA heads and giving bowing to individual SAs towards and away from the transducer and

(ii) by rotating a single SA head with bowing of 2° mounted on a turntable by 360°.

5.2.1 Identification of signatures for qualitative estimation of bowing

Figure 5.1 shows the A-scan signals obtained from positions A and B (separated by an angle of 180° around the SA head) corresponding to different configurations (a) – (c). The experimental setup of these A-scan signals is shown in Figure 3.16.

Signals (a) and (b) in Fig 5.1, show the A-scan signals obtained from probe position A for all SA heads without any bowing and with bowing of 2° given to SA#2 towards transducer, respectively. In case of bowing towards transducer, decrease in TOF of both signals corresponding to SA#2 can be seen in Fig 5.1 b as compared to Fig 5.1a. Further, the signal corresponding to the front side of SA#3 was absent due to the shadowing effect. A-scan signal shown in Figure 5.1 c was obtained by placing the ultrasonic transducer at position B, i.e., after SA#5 as shown in Fig 3.16. Hence, this data corresponds to bowing away from the transducer for SA#2, i.e. the 4th SA from the transducer side (from position B). Hence, the signal is plotted from right to left side in Fig 5.1 c. A high amplitude signal was observed corresponding to SA#2 at the 4th SA place. Due to the shadowing effect, no signal is observed for the back side of SA#2 (Q1) and from the 1st SA. This clearly indicates that the amplitude and TOF of signals corresponding to a FSA can be used to detect its bowing, if any.

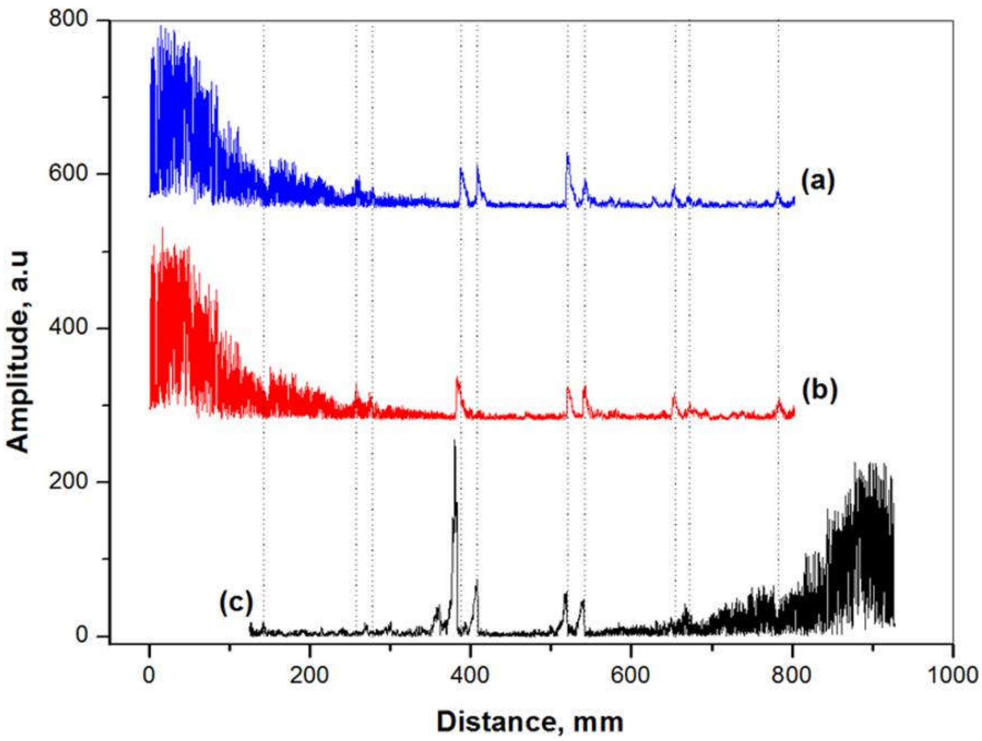

Figure 5.1 A-scan signals obtained by the transducer at Position A for (a) un-bowed and un-protruded condition, (b) for SA#2 bowed by 2° towards the transducer at A and (c) corresponds to the signal obtained from position B for the same SA condition as in (b).

5.2.2 Identification of diffracted signal locations from a SA head

In order to understand the effect of orientation of a SA on the characteristics of diffracted signal from a bowed SA, a single SA head was placed on a turntable with a bowing of 2° rotated by 360° as shown in Figs. 3.11 b. Figure 5.2 a shows the B-scan image obtained for the SA head with 2° bowing. B-scan image for a SA without protrusion/bowing (as shown in Fig 4.4) is also shown here for ready comparison. It is clear from the experimental data that diffracted signals of almost similar amplitudes are observed from 6 equidistant points on the outer diameter (OD) facing the beam.

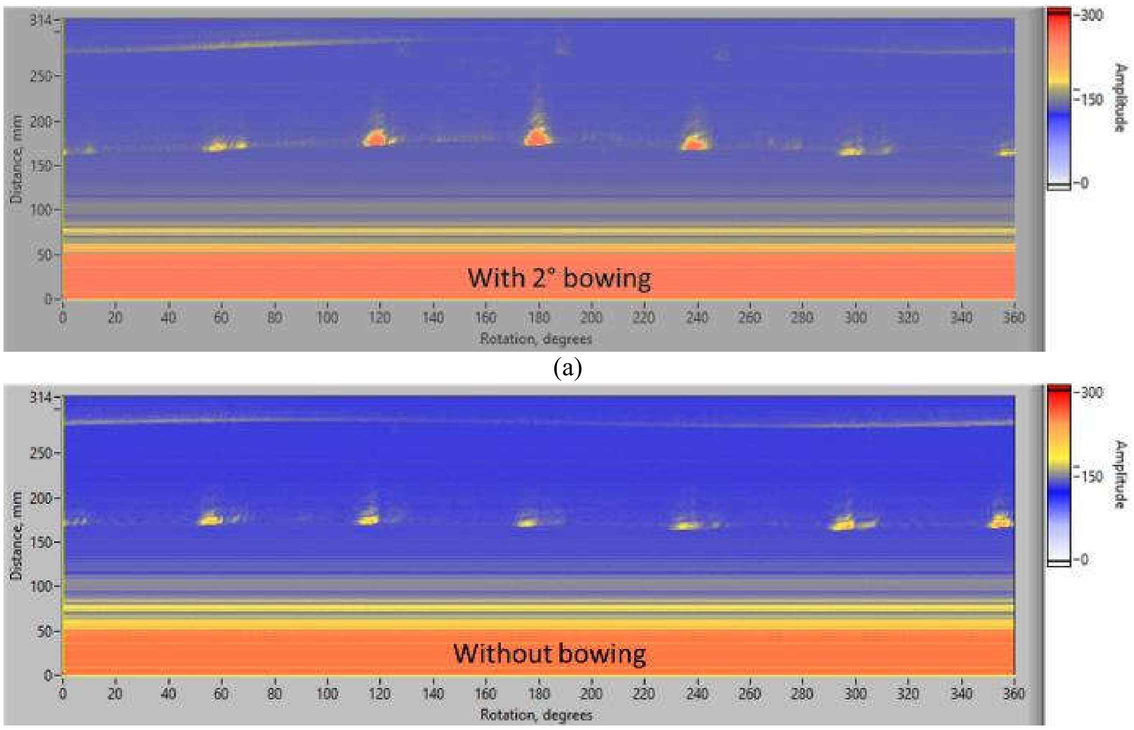

(a)

(b)

Figure 5.2 B-scan image obtained during 360° rotation of a single SA head (a) without bowing and (b) with 2° bowing

With 2° bowing given to SA head, the diffracted amplitudes become a function of the angle of the beam incidence on SA head with respect to direction of bowing. When the SA head was bowed away from transducer/incident beam (~180° in Fig 5.2 b), the diffracted signal amplitude from the OD point increases and the diffracted signal from the ID was not observed due to shadowing effect. This is in line with that observed in Fig 5.1 c. However, when the SA head was bowed in the opposite direction i.e. towards the transducer (~0° in Fig 5.2b), signal amplitude from the OD point decreases and signal from the ID is clearly observed. These results provide the clues for using the signal characteristics for detection of bowing and possible qualitative methods for detection of extent as well as direction of bowing. In addition to signal amplitude, change in TOF of signals i.e. increase in TOF (as observed in Fig 5.2b) in case of bowing away from the transducer and vice-versa, can also be used as a parameter for quantitative measurement of bowing.

From the experimental data change in TOF due to bowing of SA head by an angle of 2° was found to be ~8.95 μs and the theoretically calculated change in TOF due to bowing of 2° was found to be around ~8.4 μs. It is clear from the data that the measured change in TOF due to bowing is in good agreement with theoretically calculated change in TOF. The error of about 6% is attributed to complicated geometry of SA head which may lead to small shift in location corresponding to reflection/ diffraction of ultrasonic signals in case of bowing.

5.3 Superimposition studies using GAIM

As mentioned earlier, bowing leads to lateral displacement of upper portion of the FSAs (SA handling head) in addition to their vertical growth unlike one dimensional growth in the case of protrusion of FSAs. Hence, data acquisition from more than one transducer location is required for characterization of bowing and its differentiation from a simple protrusion scenario. Further, superimposition of data acquired from different probe positions may provide better visualization of FSAs condition. Hence, superimposition of data acquired from clockwise (CW) and counter clockwise (CCW) directions with respect to mean position as shown in Fig 3.12 for from a single location of the scanner was performed. The distance of

400 mm between two transducers corresponds to diameter of probe holder of USUSS on which Side Viewing Transducers (SVTs) are mounted. By mounting a pair of transducers at glancing angle at these two diametrically opposite locations, information from two different transducer orientations can be obtained from a single location of the scanner. After keeping the ultrasonic transducer at optimized position, glancing angle images of honeycomb arrangement were obtained from the two different orientations for without and with bowing configurations. These glancing angle images obtained from the two orientations were superimposed to obtain better visualization of the honeycomb arrangement of SAs.

Figures 5.3 a and b show the glancing angle images of entire honeycomb arrangement obtained by sweeping the ultrasonic transducers by an angle of 70° viz. without bowing given to any of the SA heads in the honeycomb arrangement. CW and CCW directions (from the same scanner locations), respectively. It can be seen in Figs. 5.3 a and b that signals from ID are obtained for all SAs for both orientations of transducer, when the beam is radially incident to the ID, similar to that observed in Fig 5.2 b. However, signals corresponding to ODs are observed only for a few SAs viz. SA#7, SA#1, SA#C, SA#4, SA#13 and SA#9 for CW sweeping of left transducer and for SA#18, SA#1, SA#2 and SA#10 for CCW sweeping of right transducer, for which the incident beam is normal to sharpe OD edges on the top of each SA head as shown in Fig. 3.11 c.

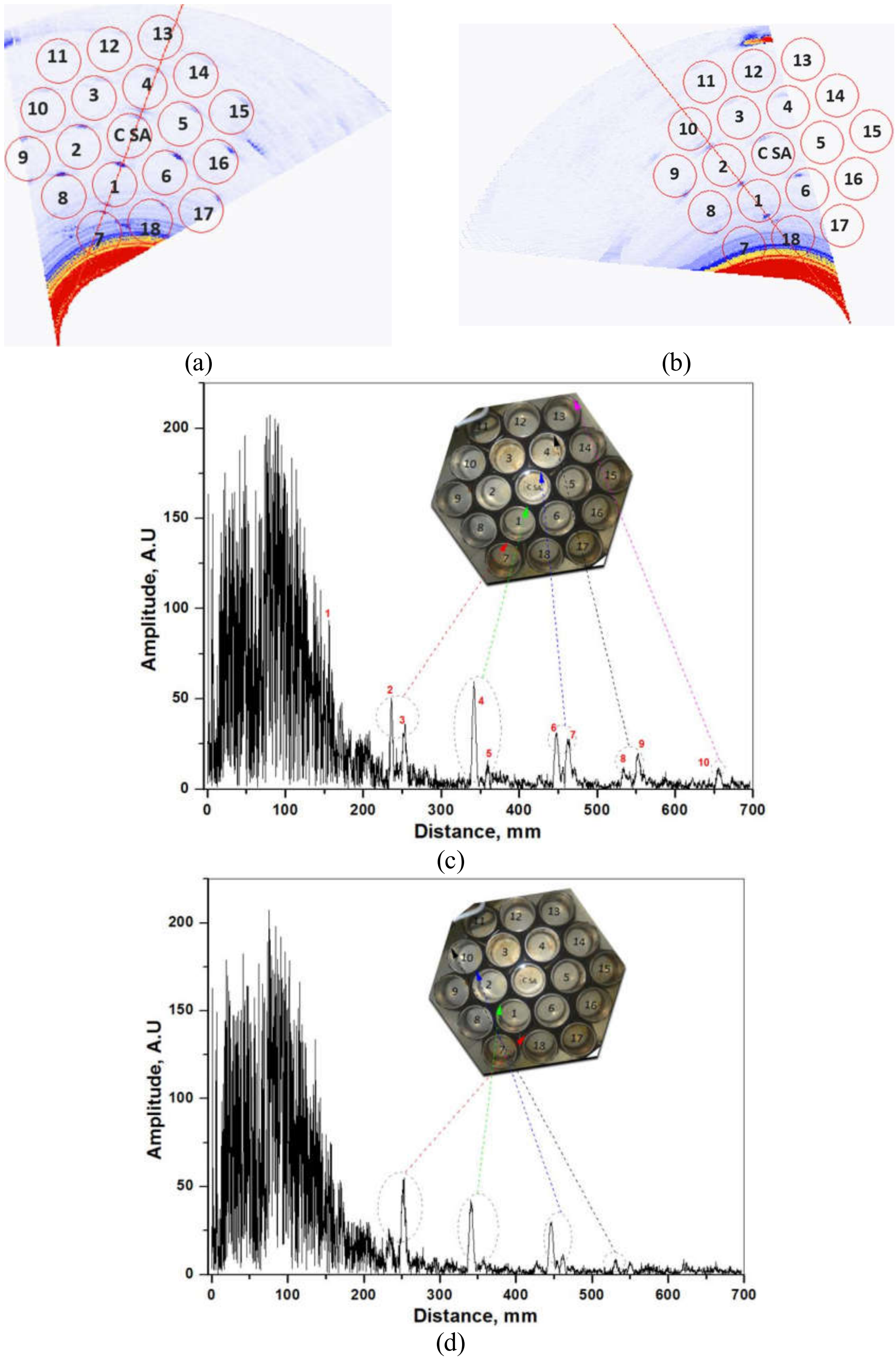

Figure 5.3 Glancing angle images of honeycomb arrangement obtained from (a) CW and (b) CCW directions with no bowing condition and (c and d) A-scan signals corresponding to the red cursor in (a) and (b). Arrow marks show the locations from which the diffracted echoes are being observed

Figures 5.3 c and d show the corresponding A-scan signals obtained along the red lines shown in Figs. 5.3 a and b, respectively. Figure 5.3c shows the A-scan signal comprising of the diffracted signals from the sharp edges at the top of SA heads on OD and from ID of SA heads in different rows. In the A-scan ultrasonic signals, the observed peaks (1,2), (3,4), (5,6), (7,8) and (9,10) are from SA#7, SA#1, SA#C (central SA), SA#4 and SA#13, respectively. The corresponding locations are indicated using arrows in the photograph of the honeycomb arrangement shown in Fig 5.3 c. Similarly, Fig 5.3 d shows the A-scan signals comprising of diffracted signals obtained from different locations as indicated by the arrows, while scanning from CCW direction.

Figure 5.4 a shows the superimposition of data obtained from both CW and CCW orientations without bowing of any SA head in the honeycomb arrangement. From Fig 5.4 a, it can be clearly seen that points ***a*** and ***b*** are echoes obtained from sharp curvature present on the OD head of SA#1, as shown by the dotted circle in Fig 3.11c. Echoes ***c*** and ***d*** are obtained from the ID of SA#1 where the beam was incident radially.

Figures 5.4 b and c show the superimposed images for SA#1 given a bowing of 2° away from ultrasonic probe and the same SA head given a bowing of 2° towards ultrasonic probe, respectively. It can be seen in Fig 5.4b that, when SA#1 was bowed by an angle of 2° away from the transducer, echoes ***a*** and ***b*** were shifted away from ultrasonic transducer (shifted upwards from the initial position). In addition to this as explained in the previous section, there is an increase in the amplitude of two signals because of more surface area exposed to ultrasonic beam.

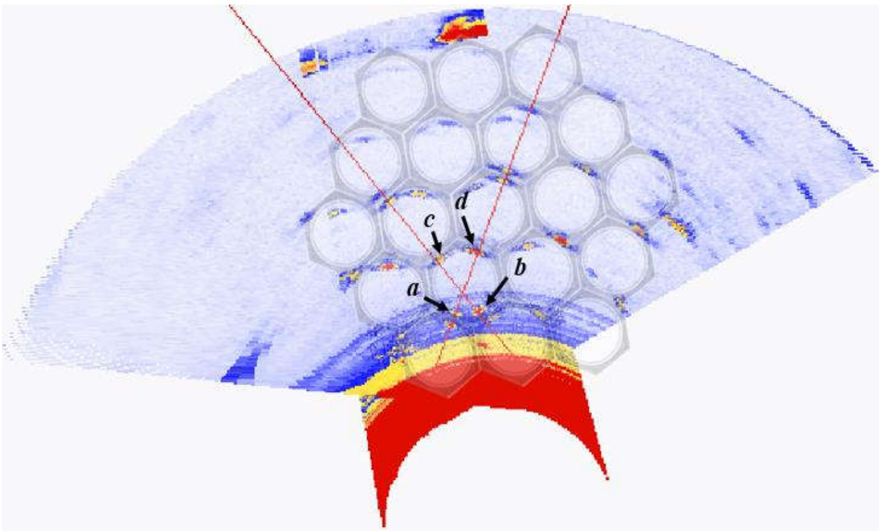

(a)

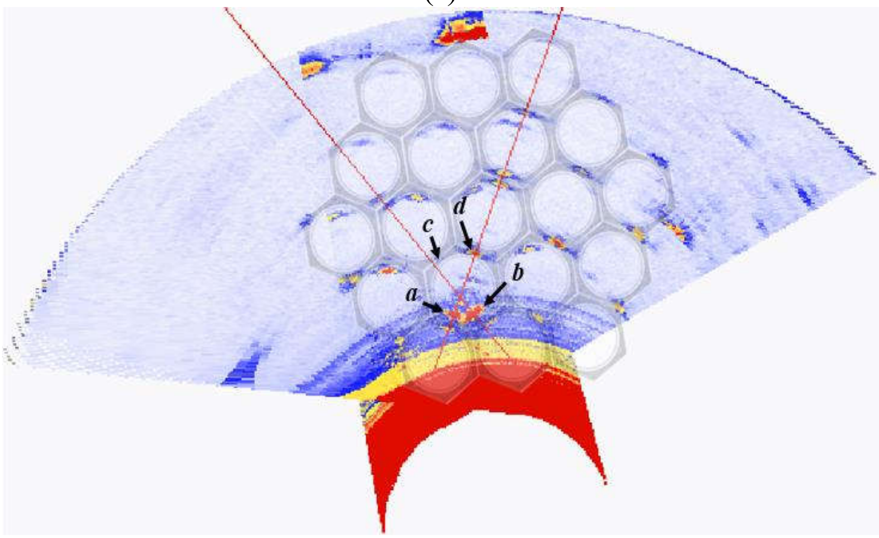

(b)

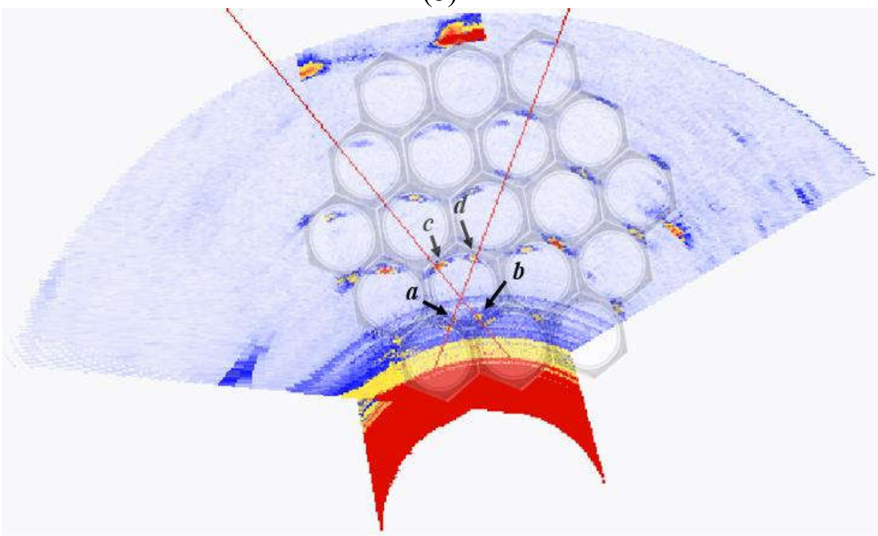

(c)

Figure 5.4 Superimposed image of honeycomb arrangement (a) without and with 2° bowing of SA#1 (b) away and (c) towards the ultrasonic transducer

The region of interest (SA#1 region, where the labels are pointed) in Figs. 5.4 (a) – (c) are zoomed for better visualization as shows in Figs 5.5 (a) – (c). These figures correspond to superimposed images of honeycomb arrangement without any bowing, with 2° bowing of SA#1 given away and towards ultrasonic transducer, respectively.

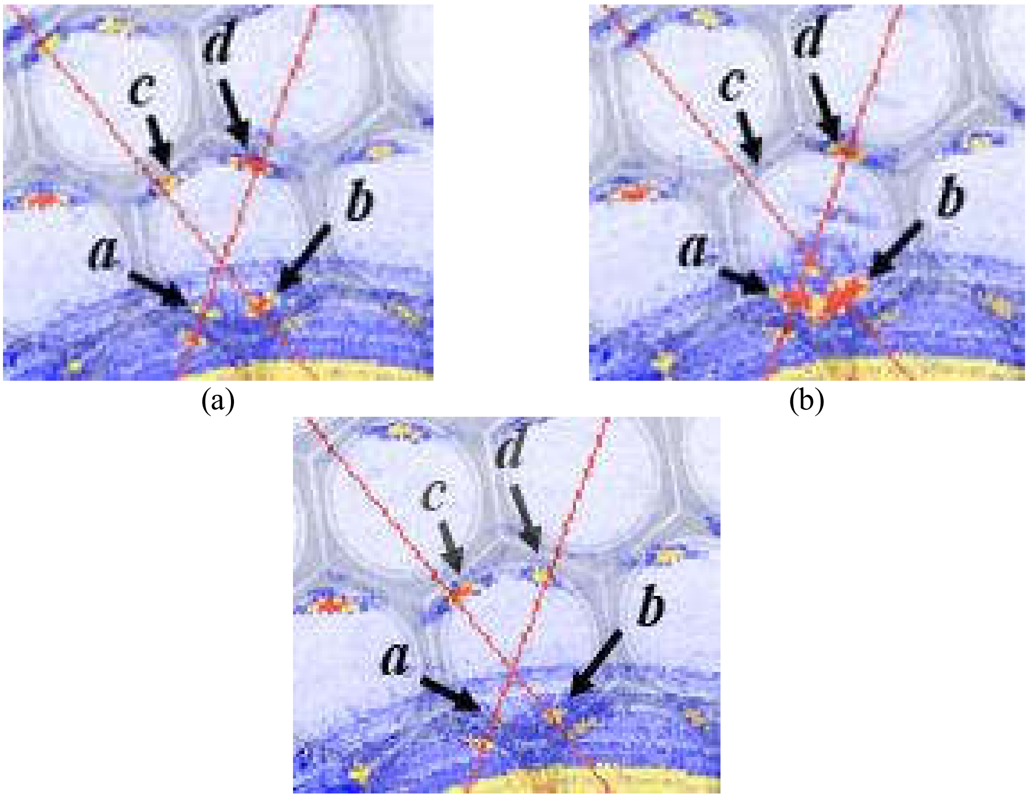

(a) (b) (c)

Figure 5.5 Zoomed region of interest of Fig 5.4 (a) without and with 2° bowing of SA#1 (b) away and (c) towards the ultrasonic transducer

Figures 5.6 a and b show A-scan signals obtained along red cursors shown in Figs. 5.4 a (without bowing) and b (2° bowing away) in CW and CCW directions, respectively. From A-scan signals, it is clearly seen that amplitude of echo from OD side of SA#1 is high due to a larger surface area exposed to ultrasonic beam when the SA head was bowed away from transducer.

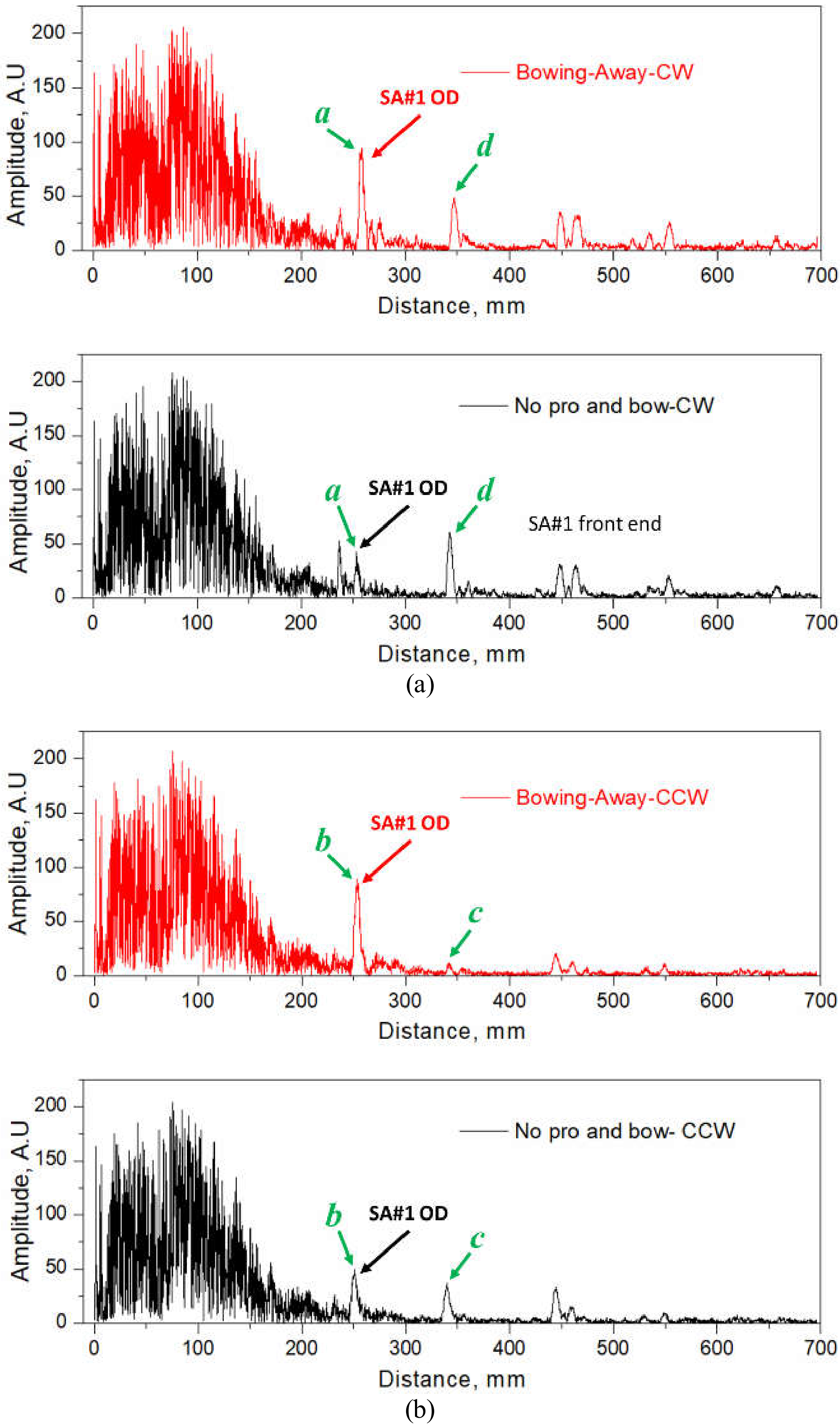

Figure 5.6 A-scan signals obtained along the red cursors shown in Figs. 5.4 a (without bowing) and b (2° bowing away) in (a) CW and (b) CCW directions. Echoes from the OD side of SA#1 are marked with arrows

The echoes ***c*** and ***d*** also shifted away from transducer. However, intensities of echoes ***c*** and ***d*** decreased due to shadowing effect of front end of SA#1. Similarly, when SA#1 was bowed towards ultrasonic transducer by an angle of 2°, the echoes ***a*** and ***b*** shifted towards transducer and also there is a decrease in the intensities of these two echoes due to the fact that front end of SA#1 was blocked by rear end of SA#7. In addition to this, echoes ***c*** and ***d*** shifted towards ultrasonic transducer (shifted downwards from the initial position) and slight increase in intensities of these echoes can be observed.

With the help of above signatures, qualitative estimation of SA head bowing (towards or away from the ultrasonic transducer) can be identified using GAIM. An automated image analysis for protrusion or bowing detection using GAIM will be beneficial for the operator to readily identify protrusion or bowing detection. This can be achieved by subtracting the glancing angle images obtained before and after protrusion/bowing.

5.4 Random bowing detection honeycomb arrangement

To check the reliability of GAIM in the detection of SA bowing in the honeycomb arrangement, SA#4 in the honeycomb arrangement was bowed towards and away from the ultrasonic transducer and the corresponding glancing angle images were generated. In addition to the glancing angle images, A-scan signal were compared to get a better identification of bowing in the honeycomb arrangement.

Figures 5.7 a-c show glancing angle images of honeycomb arrangement without bowing of SA#4 and with bowing away and towards ultrasonic transducer respectively. The scanning was carried out in CW direction by an angle of 70°. In the present case SA head bowing was observed from the same direction without going to 180° symmetrically opposite direction. This is to simulate a condition where if the access to a different position (separated by an angle of 180° around the SA head) is not possible due to the space constraint in the reactor. In this case, at least the qualitative estimation of the FSA can be identified. However, if there is no space constraint during the inspection, then one must obtain the diffracted echoes from two locations preferably separated by an angle of 180° around the SA head to qualify and quantify the extent of FSA bowing.

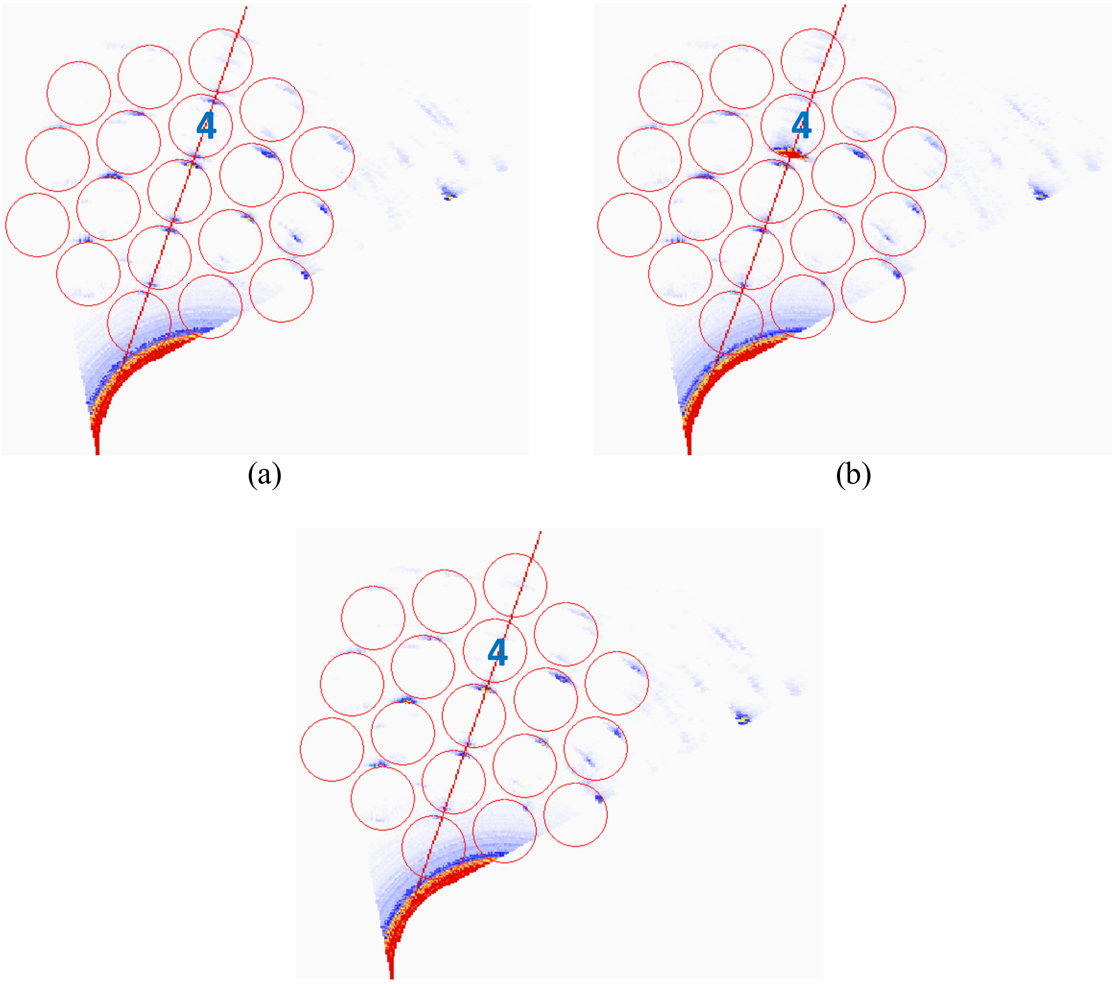

(a) (b) (c)

Figure 5.7 Glancing angle images of the honeycomb arrangement (a) without and with 2° bowing of SA#4 (b) away and (c) towards ultrasonic transducer

Figure 5.8 shows the corresponding A-scan signals along the red cursor line in the glancing angle images shown in Fig 5.7 (a-c). The vertical dotted line represents the front end of SA#4. From Fig 5.8 it can be seen that two signatures namely, increased intensity of SA head bowing away from transducer and shifting of diffracted signal away and towards from transducer is observed clearly. The inserts in the Fig 5.8 shows the zoomed images of the shift in the peak of diffracted signals of the bowed SA head (for better clarity).

From the above results, it can be concluded that the qualitative and quantitative estimation of bowing can be carried out without actually going on to the top of each SA head.

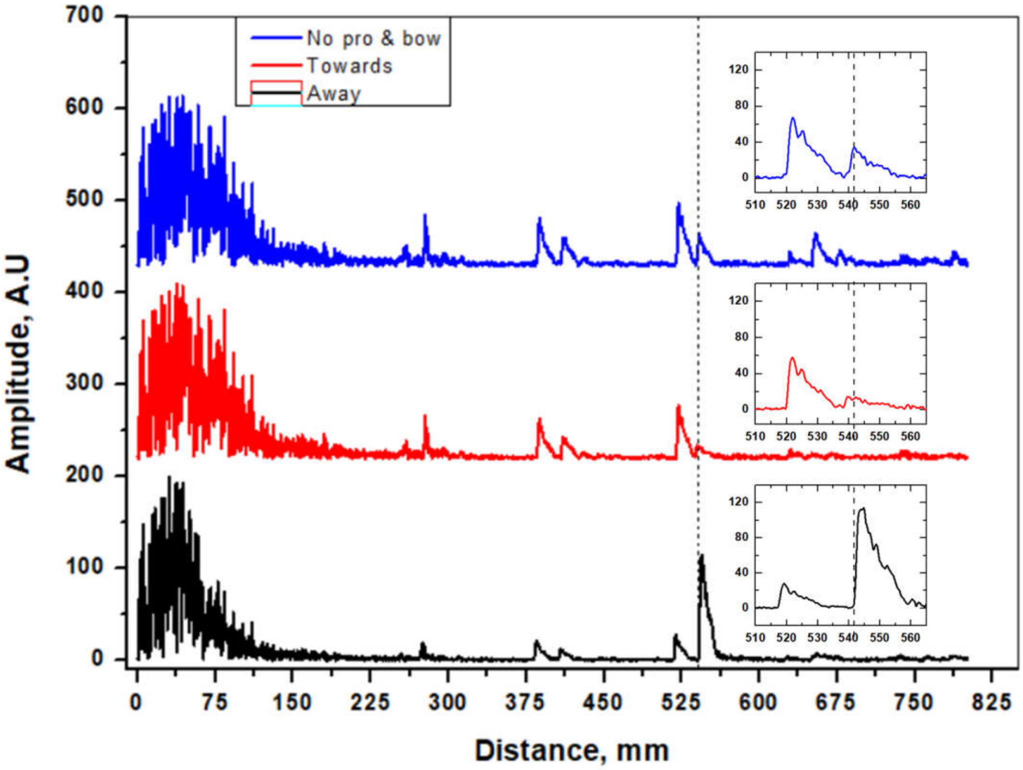

Figure 5.8 A-scan signals corresponding to red cursor line shown in Figs. 5.7 (a-c)

In the same way, few more under water bowing simulations were performed by giving bowing to random SA heads in the honeycomb arrangement. Figures 5.9 a-c show glancing angle images of honeycomb arrangement without bowing of SA#C and with bowing away and towards ultrasonic transducer respectively. The scanning was carried out in CW direction by an angle of 70°. Similarly, Figures 5.10 a-c show glancing angle images of honeycomb arrangement without bowing of SA#13 and with bowing away and towards ultrasonic transducer respectively. The scanning was carried out in CW direction by an angle of 70°. In the present case SA head bowing was observed from the same direction without going to 180° symmetrically opposite direction.

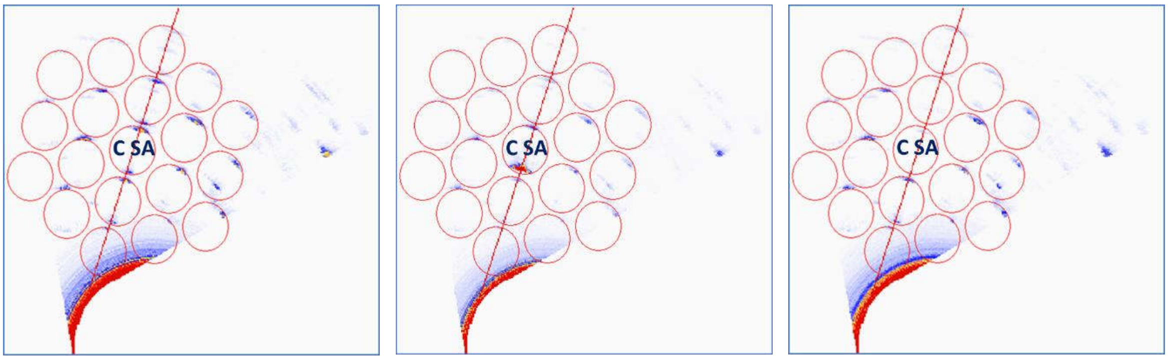

(a) *(b)* *(c)*

Figure 5.9 *Glancing angle images of the honeycomb arrangement (a) without and with 2° bowing of SA#C (b) away and (c) towards ultrasonic transducer*

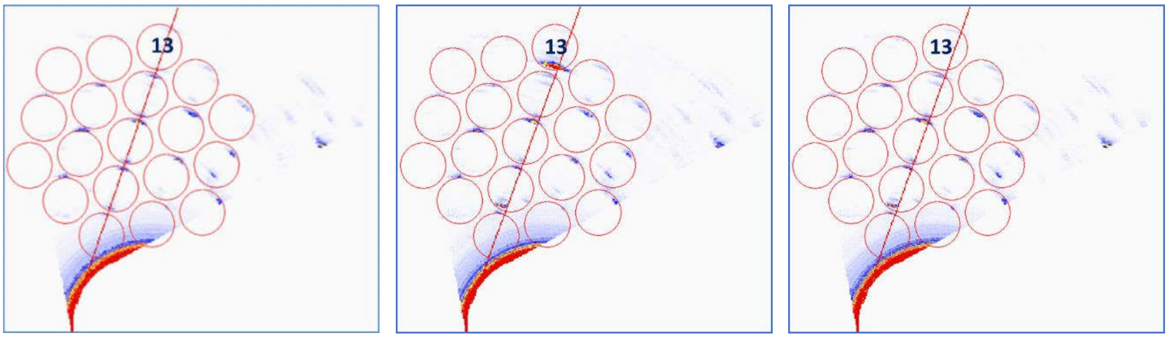

(a) *(b)* *(c)*

Figure 5.10 *Glancing angle images of the honeycomb arrangement (a) without and with 2° bowing of SA#13 (b) away and (c) towards ultrasonic transducer*

Figure 5.11 shows the corresponding A-scan signals along the red cursor line in the glancing angle images shown in Fig 5.9 (a-c). The vertical dotted line represents the front end of SA#C. From Fig 5.11 it can be seen that two signatures are observed namely, increased intensity of SA head bowing away from transducer and shifting of diffracted signal away and towards from transducer.

Similarly, Fig 5.12 shows the corresponding A-scan signals along the red cursor line in the glancing angle images shown in Fig 5.10 (a-c). The vertical dotted line represents the front end of SA#13. Here also the two signatures are observed namely, increased intensity of SA head bowing away from transducer and shifting of diffracted signal away and towards from transducer.

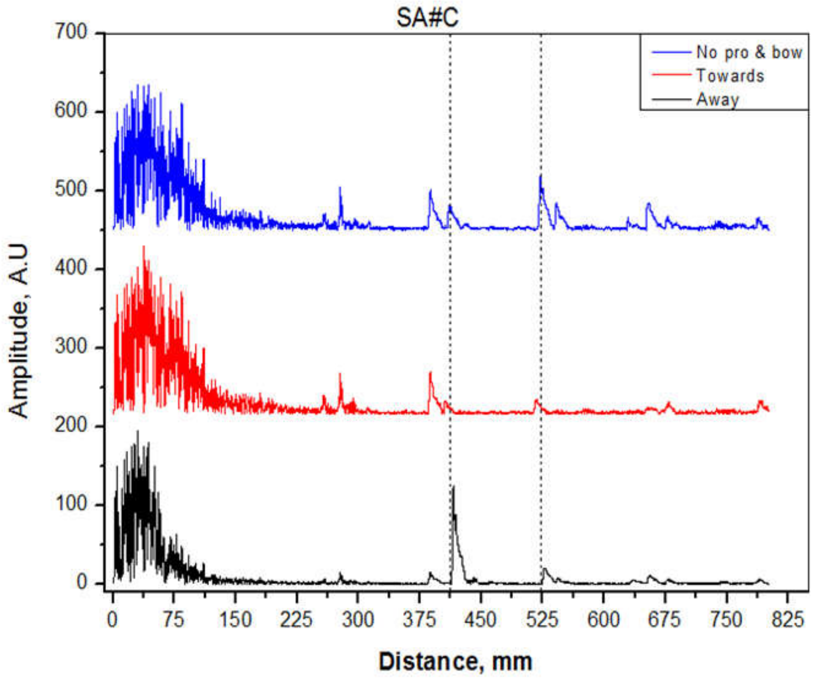

Figure 5.11 A-scan signals corresponding to red cursor line shown in Figs. 5.9 (a-c)

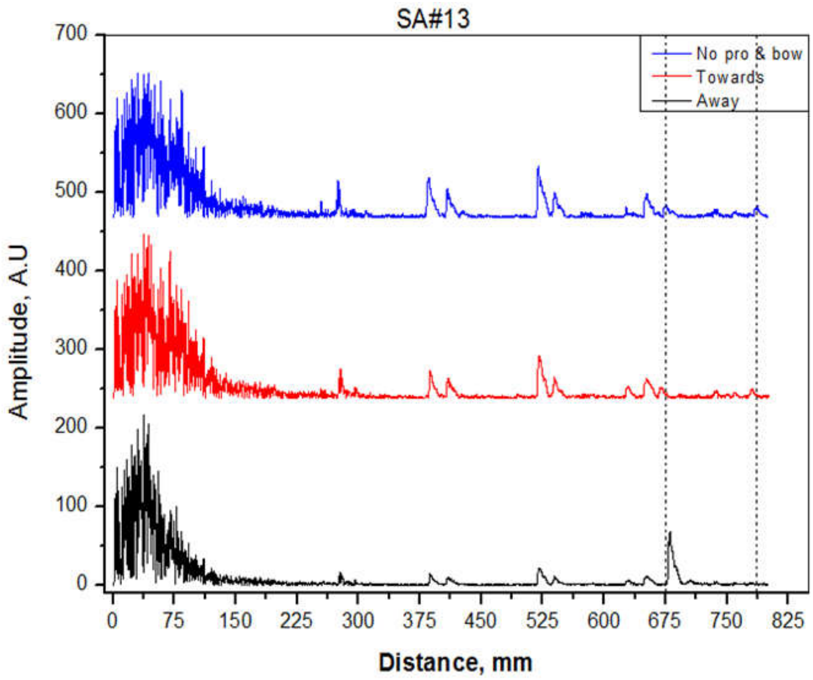

Figure 5.12 A-scan signals corresponding to red cursor line shown in Figs. 5.10 (a-c)

5.5 Quantitative estimation of bowing using GAIM

In addition to qualitative estimation of bowing using signatures mentioned above, quantitative estimation of bowing was also studied using GAIM. Quantitative estimation of the bowing was achieved by comparing change in TOF of bowed SA head with theoretically calculated TOF change obtained from two different positions separated by 180° about the SA head. Figure 5.13 shows the schematic used for calculating the lateral shift in the SA head top ring theoretically when the SA head was bowed by an angle of 2°. The schematic is similar to that shown in Fig 3.16.

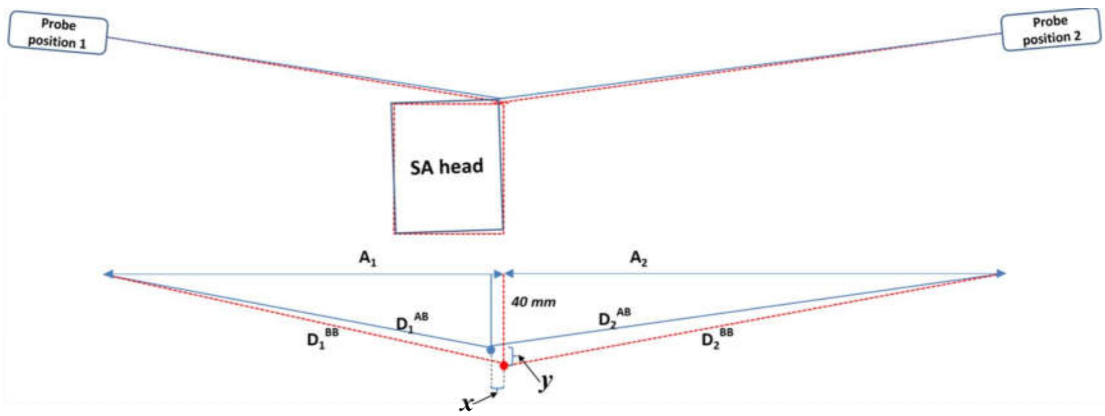

Figure 5.13 Schematic of side view (cross section) used for theoretically calculating the lateral shift (x) of a SA head due to bowing

Red and blue dots represent the locations of point Q_2 on the SA head ring before and after bowing, respectively. The red dotted line and the blue solid line represents the beam paths from the transducers to point Q_2 before and after bowing, respectively. The bottom portion of Fig 5.9 shows the ray diagram of the experimental setup with zoomed view. Here, A_1 and A_2 represent the physical horizontal distances of point Q_2 from probe positions 1 and 2 before bowing, respectively. D_1^{BB} and D_2^{BB} are the distances (beam paths) from probe positions 1 and 2 before bowing of the SA, respectively. Similarly, D_1^{AB} and D_2^{AB} represent the distances from probe positions 1 and 2 after bowing of the SA, respectively. *v* and *x* are the vertical and later shifts of SA head at point Q_2 due to bowing, respectively. As the probe was placed at the optimized height, the vertical distance between the probe and point Q_2 is 40 mm before bowing.

The distances A_1 and A_2 are known (which can be measured physically). From the geometry of the ray drawing, the following equations can be derived:

$$(D_1^{AB})^2 = (A_1 - x)^2 + (40 - y)^2 \qquad (9)$$

$$(D_2^{AB})^2 = (A_2 + x)^2 + (40 - y)^2 \qquad (10)$$

Subtracting Eq. (2) from Eq. (1) gives,

$$(D_2^{AB})^2 - (D_1^{AB})^2 = (A_2)^2 - (A_1)^2 + 2x(A_1 + A_2)$$

During the application of GAIM in the reactor condition, D_2^{AB} and D_1^{AB} can be obtained from the ultrasonic signals and, A_2 and A_1 can be obtained from the scanner locations and a priori knowledge of the SA positions without bowing.

By substituting values corresponding to present experimental setup in the above equation, lateral shift (*x*) of SA head due to bowing was obtained to be 5.12 mm. Whereas, the physically measured lateral shift was found to be 6.3 mm. The difference of around 1 mm is attributed to the fact that when transducer was at position 1, the diffracted signal was obtained from the ID of the SA head, whereas when transducer was at position 2, the diffracted signal was obtained from the OD of the SA head. The present study was performed with SA heads of 150 mm height only. If the same 2° bowing is observed in the real full length SA, the lateral shift will be much more (~30 mm) and hence can be measured very accurately. The same signatures can be used for identifying the bowing in a honeycomb arrangement of SA heads by sweeping the ultrasonic transducer.

5.6 Influence of various experimental parameters on detection of protrusion and bowing using GAIM

The methodology developed in the present study is towards application in a FBR during shutdown condition. The acoustic impedance of liquid sodium at ~200°C (in the shutdown condition) is similar to that of water at room temperature. Hence, the efficacy of the developed methodology is demonstrated through under water studies for logistical reasons. Keeping the final application in consideration, an under-sodium ultrasonic transducer was utilized in the present under water demonstration study.

The transducer characteristics may influence the effectiveness of GAIM. With increase in the frequency, attenuation of ultrasonic beam increases and the divergence decreases. Further, with decreasing frequency, the dead zone increases and the depth resolution (to resolve echoes from neighboring subassemblies) decreases. An increase in bandwidth of the transducer improves the depth resolution and decreases dead zone also, however this is achieved at a cost of loss in sensitivity due to damping of transducer. In general, we should use a transducer that can provide high amplitude diffracted signal up to the required distance with required depth resolution and also have sufficient divergence to allow large coverage. This can be achieved by a 2 MHz under-sodium transducer of about 10-20 mm diameter and with minimal damping, as used in the present study.

The distance between the probe and the subassemblies were maintained similar to that required in PFBR. In sodium at ~200°C, the ultrasonic velocity will be higher (~2500 m/s) as compared to 1500 m/s in water at room temperature. This will lead to slightly larger beam divergence for the same transducer in the reactor condition as compared to that in water. This will be advantageous for the present methodology as it will allow better coverage. With increased ultrasonic velocity, the time of flight for corresponding echoes will decrease. This may decrease the measurement accuracy slightly. For example, the distance measurement accuracy corresponding to an echo signal digitized at 20 MHz sampling frequency is 0.038 mm in water, whereas the same in sodium at ~200°C is ~0.060 mm. In the present study, bowing of a single SA head is considered at a time. However, the same methodology can be utilized suitably for the case of bowing of multiple SAs also. In the reactor condition, DVTs in the scanner can be utilized for getting heights and locations of the SA heads just below the scanner. These can be used as reference to find the relative heights and locations of FSAs under evaluation. In the shutdown condition, variation in sodium temperature is expected to be very minimal and sodium flow is also negligible. Hence, these are not expected to affect the methodology described in the present study.

5.7 Conclusions

In this chapter, signatures identified for qualitative and quantitative estimation of bowing are discussed in detail. In addition to this, details about superimposition of glancing angle images and random SA bowing detection are also discussed. At the end of the chapter, the influence of various experimental parameter on detection of protrusion and bowing are discussed.

- **Qualitative and quantitative estimation of bowing**

Bowing leads to lateral displacement of the upper portion of the FSAs (SA handling head) in addition to their vertical growth, unlike one dimensional growth in the case of FSA protrusion. Hence, data acquisition from more than one transducer location is required for characterization of bowing and its differentiation from a simple protrusion scenario.

Signatures for qualitative estimation of bowing were identified using A-scan signals obtained from 5 collinear SA heads. A-scan signals from these SA heads were acquired from two different positions separated by an angle of 180°. A-scan signals from all SA heads were acquired with and without 2° bowing given to each SA head. A turn table experiment was performed to understand the effect of orientation of a SA head on the characteristics of diffracted signals. In this experiment, a single SA head was placed on a turntable with a bowing of 2° give to the SA head and rotated by 360°. B-scan data was acquired during the 360° rotation of SA head. From these A-scan signals, the following signatures were identified for qualitative estimation of bowing:

* increase in the amplitude of the SA head, bowed away from the transducer
* change in the TOF of bowed SA head (decrease in the TOF when bowed towards the transducer and increase in the TOF when bowed away from the transducer) and
* in addition to this, when the SA head is bowed away from the transducer, no signal is observed behind the bowed SA head due to the shadowing effect.

Random SA head bowing detection in the honeycomb arrangement was carried out by giving 2° bowing (towards and away from the ultrasonic transducer) to SA#4. Then, the glancing angle images of the entire honeycomb arrangement with and without bowing were generated. From the signatures observed in the A-scan signals corresponding to SA#4, the qualitative estimation of bowing was identified.

Quantitative estimation of bowing was achieved by comparing experimentally measured change in TOF of bowed SA head with theoretically calculated TOF change obtained from two different positions separated by 180° about the SA head. When a SA head was bowed by an angle of 2°, then the theoretically calculated lateral shift of the SA head top was obtained to be 5.12 mm. Whereas, the physically measured lateral shift was found to be 6.3 mm. The difference is attributed to the fact that diffracted signal were obtained from ID and OD sides of the SA head from two different positions. From these results, it is concluded that the qualitative and quantitative estimation of bowing can be carried out without actually going on to the top of the each SA head.

- **Superimposition of glancing angle images and random SA bowing detection**

In addition to the qualitative and quantitative estimation of bowing without actually going on to the top of the each SA head, better visualization of the honeycomb arrangement was performed by acquiring and superimposing glancing angle images acquired from two different orientations viz., CW and CCW.

Chapter 6. Feasibility studies on implementation of GAIM in sodium environment for the detection of SA protrusion and bowing

6.1 Chapter overview

With the confidence gained in detection of SA protrusion and bowing using GAIM in Chapters 4 and 5, the feasibility of using GAIM in sodium environment was studied and presented in this chapter. In the present chapter, results of attempt made in implementation of ultrasonic GAIM in sodium environment are discussed. In addition to this, comparison of the ultrasonic signals obtained using under-sodium transducers in water and sodium are also discussed. At the end, the ultrasonic signals obtained in the sodium environment using 1 MHz under-sodium transducer and signal processing of the data to identify diffracted signals from under-sodium honeycomb arrangement setup (UHAS) are discussed.

As explained in Section 3.8.6, the 2 MHz transducer used in underwater studies was not hermetically sealed and qualified for under-sodium tests. So, a readily available, 1 MHz transducer connected with a 10 m long Mineral Insulated (MI) cable (same as a side viewing ultrasonic transducer of Under-sodium Ultrasonic Scanner System (USUSS)) qualified for under-sodium tests was used to perform under-sodium experiments. All signals shown in this chapter were obtained at the same instrument gain of 30 dB.

6.2 Under water ultrasonic signals

Before inserting the 1 MHz transducer into sodium environment, ultrasonic signals of under-sodium transducer were acquired in water at room temperature of 25°C and compared with those of 2 MHz ultrasonic transducer which was used in Chapter 4 and 5 for the development of GAIM.

6.2.1 Comparison of response of 1 MHz and 2 MHz ultrasonic transducers

Same pulser receiver and same experimental parameters as detailed in Chapter 3 were used for acquiring ultrasonic signals from both 1 MHz and 2 MHz transducers. However, the sampling rate of 10 MS/s (100 ns) and 20 MS/s (50 ns) were used for data acquisition of 1 MHz and 2 MHz transducers, respectively. Figures 6.1 a and b show underwater ultrasonic signals of 1 MHz and 2 MHz ultrasonic transducers, respectively. Ultrasonic signals were acquired up to a distance of 480 mm water path. It can be observed from ultrasonic signals that initial ringing of both transducers are similar in water. In the 1 MHz ultrasonic signal (Fig 6.1 a), many characteristic peaks are observed. However, in the case of 2 MHz signal (Fig 6.1b), the intensity is gradually decreasing without any characteristic peak.

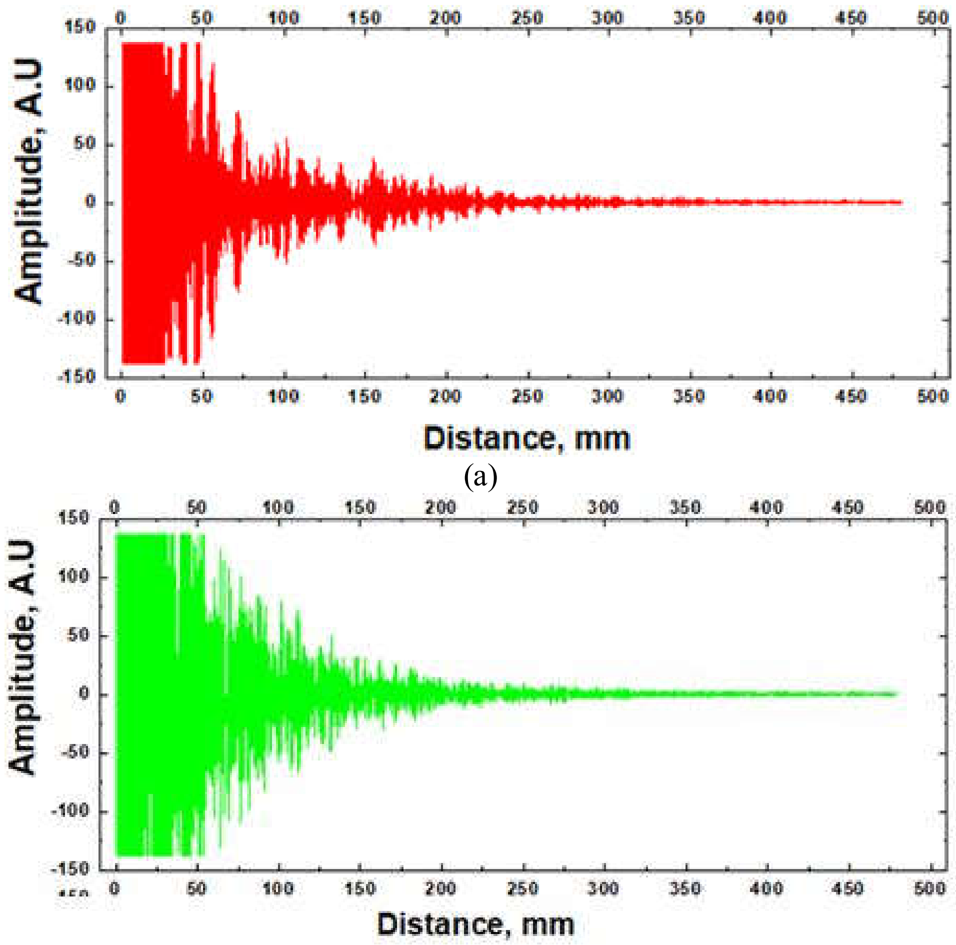

Figure 6.1 Under water ultrasonic signals of (a) 1 MHz and (b) 2 MHz

To analyze the sensitivity of transducers, ultrasonic signals were acquired by placing an austenitic stainless steel (SS) reflector plate at a distance of 140 mm from transducers. Figures 6.2 a and b show the ultrasonic signals obtained from a SS plate using 1 MHz and 2 MHz transducers, respectively. From Fig 6.2 a, it can be observed that the amplitude of the signal from the SS plate for 1 MHz probe is higher than that for the 2 MHz probe. In addition to this, many peaks adjacent to the peak at 140 mm are observed in the 1 MHz probe ultrasonic signal. In the case of 2 MHz signal, sharp echoes can be observed and the location and intensity of the multiple echoes of the 2 MHz are higher and are very distinct than that for the 1 MHz transducer. This is attributed to less divergence at higher frequency.

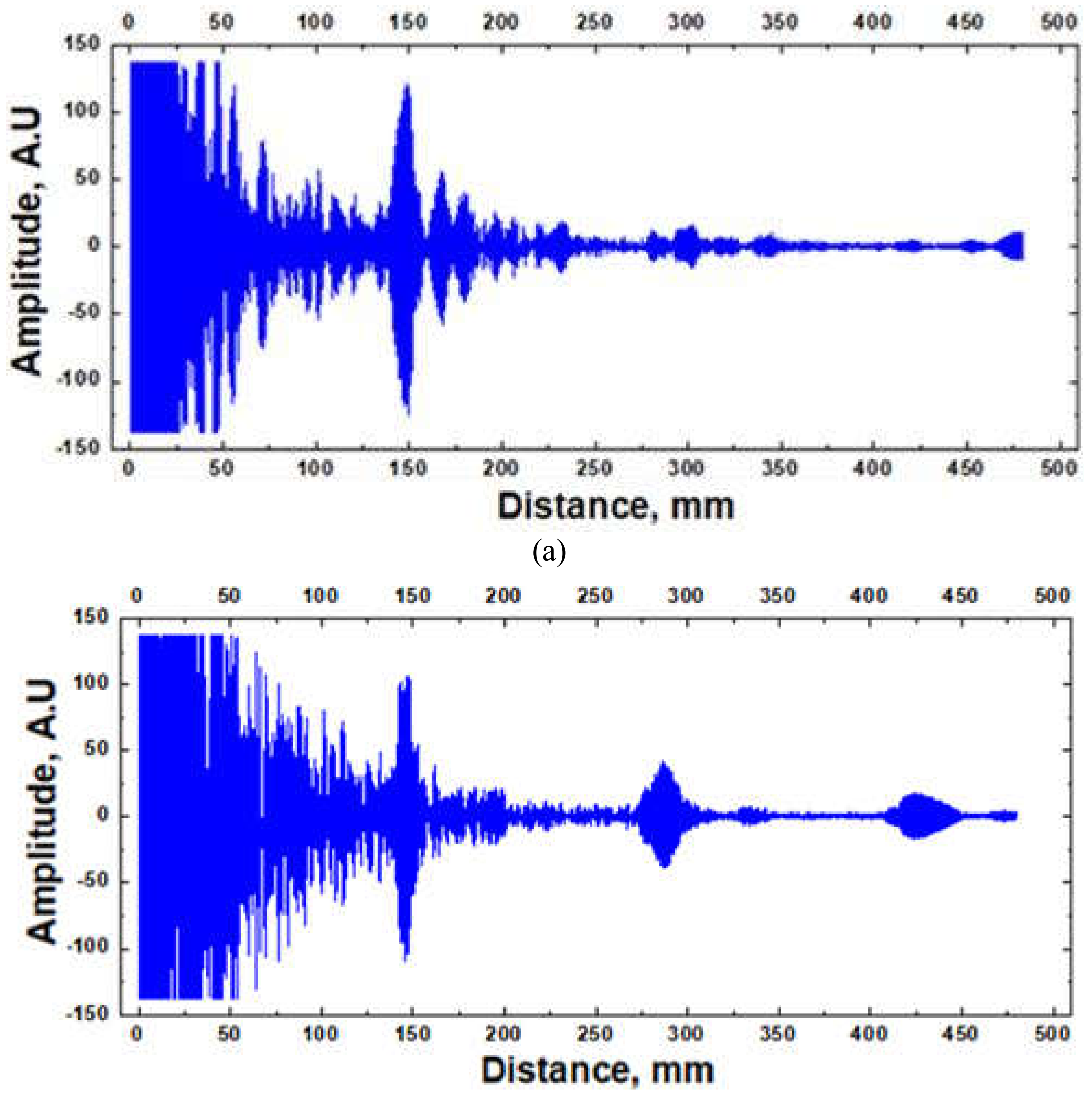

Figure 6.2 Ultrasonic signals obtained from a reflector placed at a distance of 140 mm using (a) 1 MHz and (b) 2 MHz transducer

6.3 Under-sodium ultrasonic signals

The wetting of transducer is an important issue for under-sodium viewing. Generally, the wetting improves at higher temperatures or by keeping the transducer at a particular temperature for long time. In the present study also, the wetting of the transducer took place after about 10 days at a temperature of 180°C in sodium. At this temperature, the velocity of the ultrasonic waves is found to be around 2400 m/s. Figures 6.3 a - c show the under-sodium signals obtained using 1 MHz transducer after first exposure, after 10 days of sodium exposure and the relative noise amplitude of the ultrasonic signal obtained over the period of 10 days, respectively. For calculating the relative noise level, the root mean square (RMS) values of the amplitude of the underwater and under sodium signals in the distance range of 500 mm to 600 mm is considered. The RMS amplitude values in the above-mentioned range is calculated for different days for the under-sodium signal. The relative noise level of the sodium signal is plotted and compared with the underwater signal. The RMS amplitude of the underwater signal in the same distance range is calculated and the ratio of RMS amplitude of the underwater signal and the maximum value of the under-sodium signal is considered for calculating the relative noise level of underwater signal. The value is found to be 0.175.

It can be observed from Fig 6.3 a that the initial ringing of the 1 MHz transducer is very high (up to around 500 mm) before wetting of the transducer in the sodium environment. The wetting of the ultrasonic transducer improved with time and the initial ringing got reduced. The same can be observed from relative noise amplitude shown in Fig. 6.3 c.

From Fig. 6.3 c it can be clearly seen that relative noise amplitude of ultrasonic signal reduced to half, after 5 days of sodium exposure. It can also be seen from Fig. 6.3 c that even after sodium exposure for 10 days the noise level is higher than that of underwater signal noise level (red line). After wetting of ultrasonic transducer for 10 days, ringing had reduced to around 100 mm. In this case also, peaks characteristic to 1 MHz transducer is clearly observed even after wetting (see Fig 6.3 b).

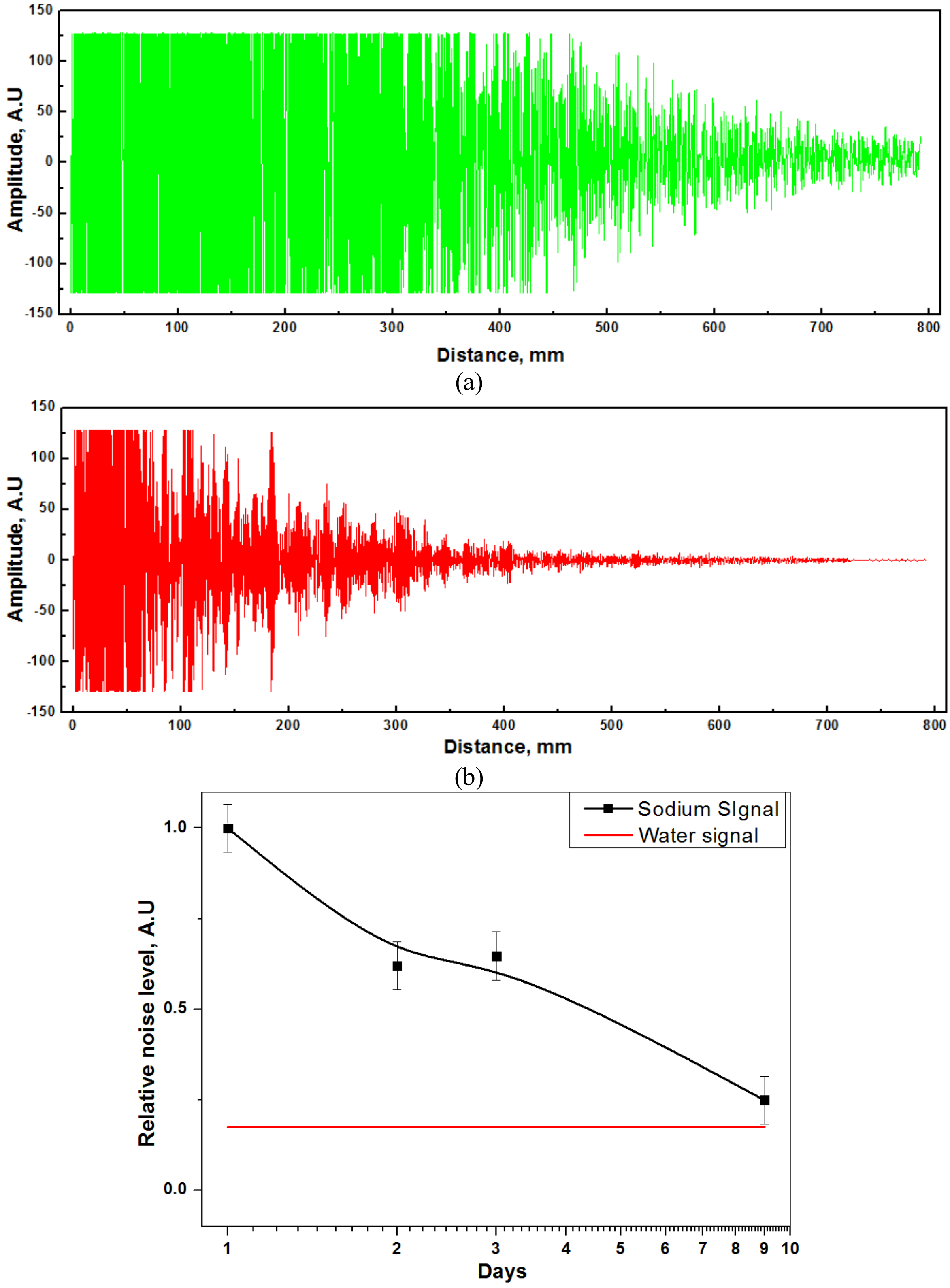

Figure 6.3 Under-sodium signals of 1 MHz transducer (a) before, (b) after wetting and (c) comparison of relative noise amplitude of ultrasonic signals of 1 MHz transducer in sodium (over a period of 10 days) and in water

As in the case of underwater studies, in sodium environment also a reflector plate (SS) was placed at a distance of 140 mm from the transducer and data was acquired without plate and with plate. The data in sodium environment was acquired using the same pulser receiver and at same voltage and gain as in the case of underwater studies. Figures 6.4 a and b show the ultrasonic signals obtained using 1 MHz transducer in sodium environment with and without reflector plate, respectively.

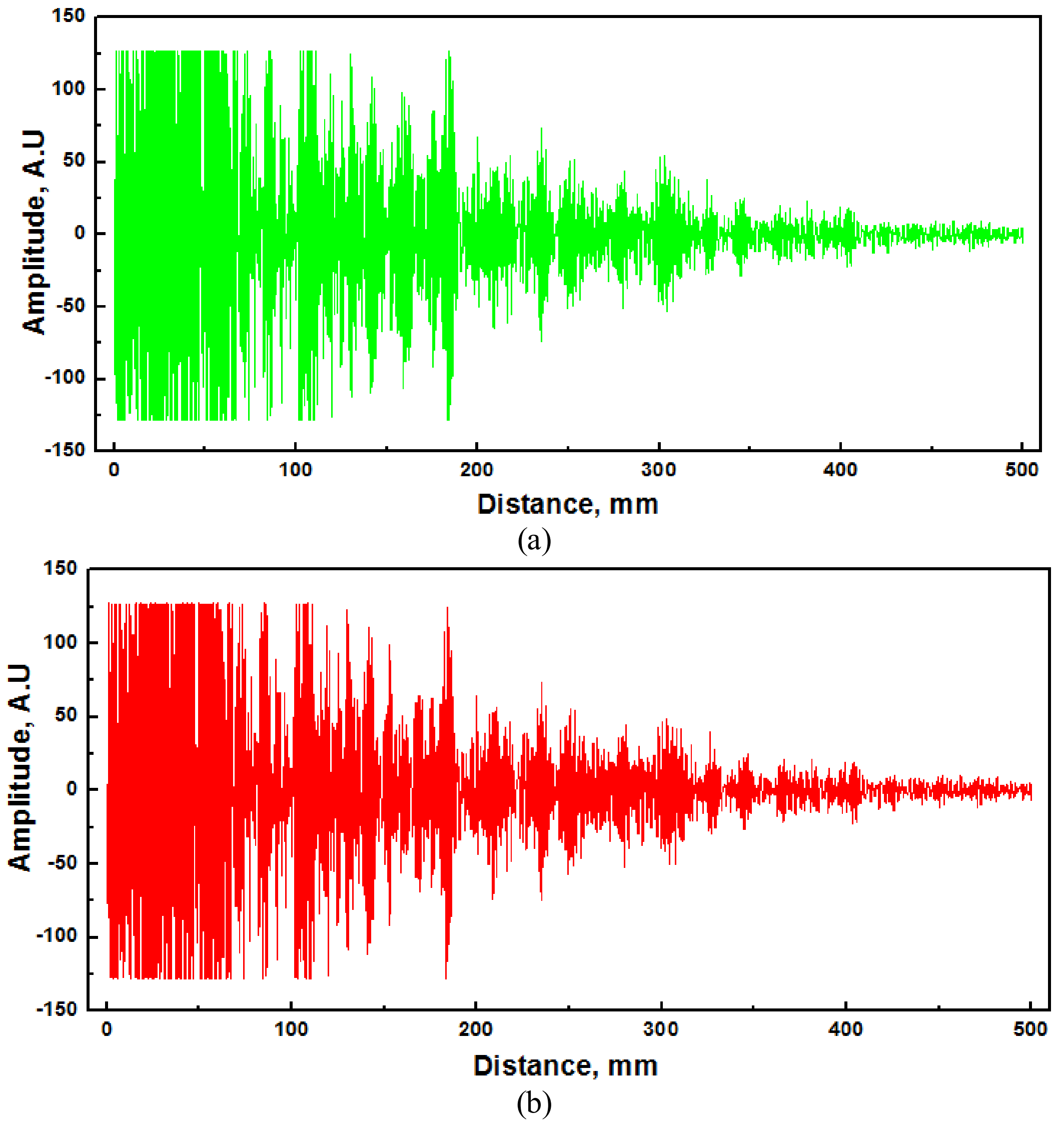

Figure 6.4 Ultrasonic signal obtained using 1 MHz transducer (a) with and (b) without plate

From Fig 6.4 a, it can be observed that signal from the reflector plate placed at a distance of 140 mm from transducer front surface is merged inside the initial ringing. To extract the merged signal from reflector plate, signal processing of raw signal was performed to get improved SNR. For this, a reference signal was acquired and subtracted from plate and without plate signals. Reference signal was a random signal without any obstructions in the line of propagation of ultrasound in sodium environment. Figure 6.5 shows the reference signal which is subtracted from signals shown in Figs 6.4 a and b.

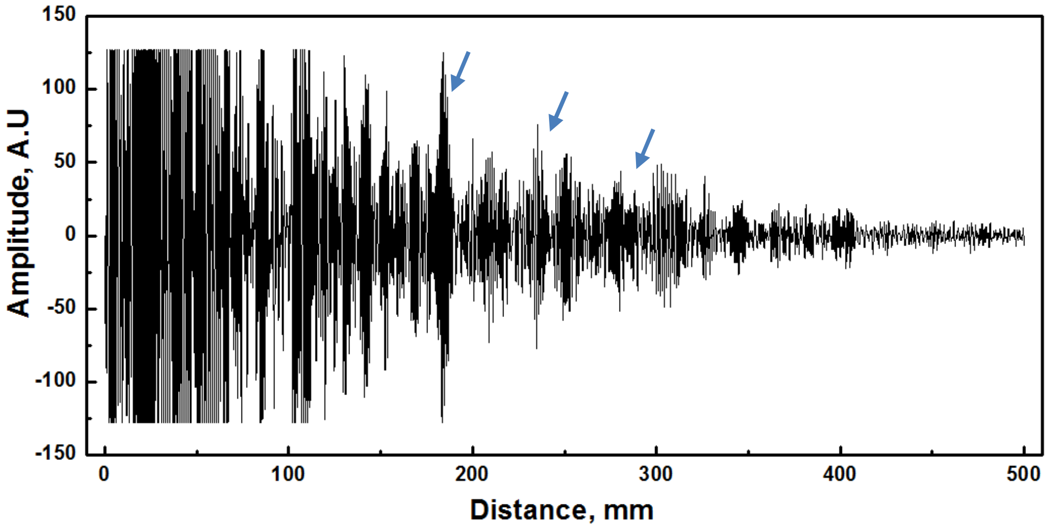

Figure 6.5 Reference signal obtained in sodium environment using 1 MHz transducer

The blue arrows in Fig 6.5 shows to the characteristic peak signals in 1 MHz under-sodium transducer. These peaks are repeated in all the signals irrespective of presence or absence reflector plate.

Figures 6.6 a and b show the processed signal obtained by subtracting the reference signal (Fig 6.5) from signals shown in Figs 6.4 a and b, respectively. From Fig 6.6a, the signal from the reflector plate (at 140 mm) can be seen clearly after processing the raw data. As in the case of underwater signal, the intensity of the multiple reflections (see Fig 6.6a) is very low, even after signal processing of the under-sodium signal. In addition to this, signal from the plate is broad and many adjacent peaks (see Fig 6.6a) can be observed as in the case of underwater signal obtained using 1 MHz transducer.

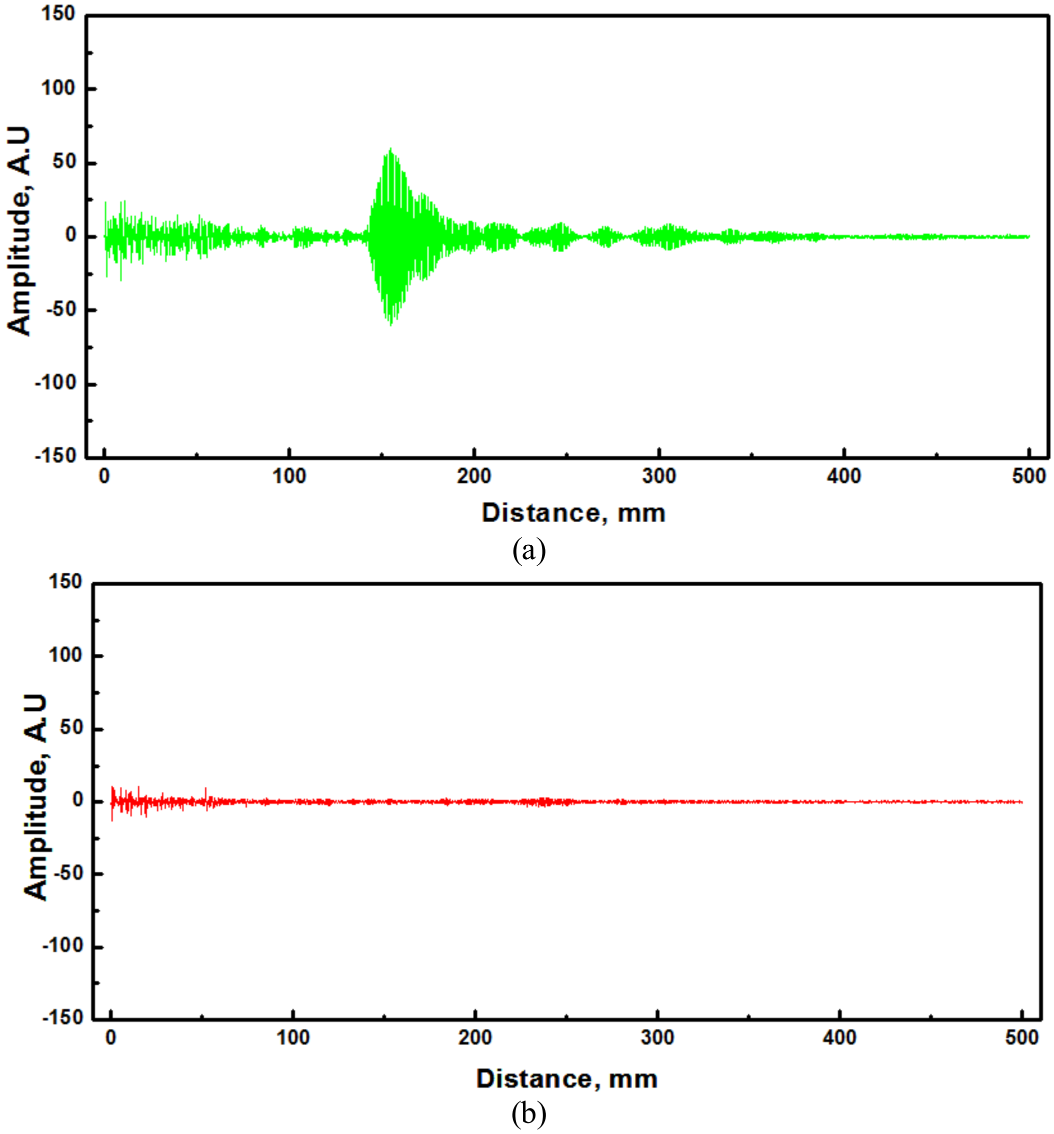

Figure 6.6 Processed signals obtained by subtracting the reference signal (a) with and (b) without plate

6.4 Under-sodium signals obtained from UHAS

Under-sodium signals were obtained from different orientations of UHAS. Figure 6.7 shows one of the orientations used for acquiring the data using the 1 MHz under-sodium ultrasonic transducer. In this orientation, 1st SA (SA_8#1) was protruded by 8 mm from the base plate, then the 2nd SA (SA_24#2) was protruded by 24 mm from the base plate and the 3rd SA (SA_8#2) was protruded by 8 mm from the base plate, respectively. This orientation is represented by ETE. Before inserting the probe and UHAS into sodium, the distance between the probe and different SA heads were measured and noted for identifying the signals from the corresponding SA heads.

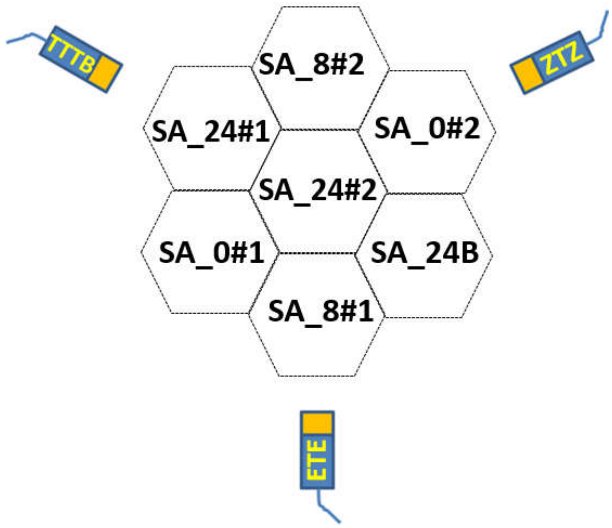

Figure 6.7 Under-sodium scanning of ETE (8-24-8) orientation

Table 6.1 shows the distance of the 3 SA heads in the UHAS from 1 MHz transducer front surface. As in the case of underwater studies, sector scan was performed by an angle of 80° (± 40°) to cover the entire UHAS. Under-sodium scanning of the UHAS was carried out for three different orientations viz., ETE, ZTZ, TTTB.

Table 6.1 Table showing distances of SA heads from the surface of 1 MHz transducer

SA head	**1st SA head**		**2nd SA head**		**3rd SA head**	
	Front	**Back**	**Front**	**Back**	**Front**	**Back**
Distance of the SA heads from transducer (mm)	138	251	272	386	406	520
Corresponding data point	1151	2097	2267	3213	3384	4330
Note: Distance between the base plate of the UHAS and transducer is 118 mm						

Initially, the scanning of UHAS was carried out using the ETE orientations as shown in Fig 6.7. The scanning in the θ-Z mode was carried out by keeping the transducer at a distance of 118 mm from the UHAS base plate. During the scanning the transducer was inclined by an angle of 5° upwards from the horizontal axis to get the glancing angle images. The A-scans were acquired at the θ step of 0.2° in the range of -40° to +40°. The sector scans were acquired at the Z-step size of 2 mm. Figure 6.8 shows the front panel of the LabVIEW program developed for generating the processed images from the B-scan signals obtained in the sodium environment. Images (a) and (b) in Fig. 6.8 show the uncorrected raw B-scan image and processed B-scan image, respectively. Images (c) and (d) show the corresponding A-scan image of uncorrected B-scan image (a) and corrected B-scan image (b), respectively.

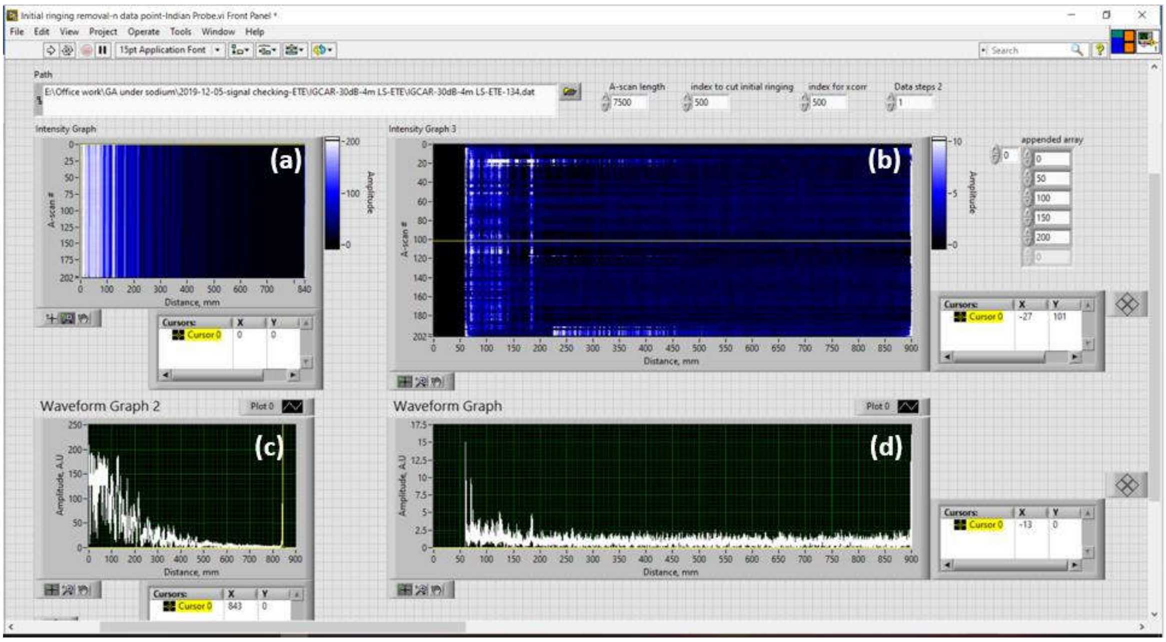

Figure 6.8 Front panel of the LabVIEW program used for processing under-sodium data

Figure 6.9 a shows the B-scan data obtained in under-sodium environment. The y-axis represents number of A-scans in a single B-scan and x-axis represents distance measured in mm. A total of 202 A-scan were obtained in a single B-scan. This B-scan data was obtained at a distance of 25 mm from SA top. In this case, it is expected to get the signals from 1st and

2nd SA heads (i.e., SA_8#1 and SA_24#2). However, from Fig 6.9 a, it can be clearly seen that the diffracted signals are not observed from the SA heads in the UHAS due to inherent noise of 1 MHz transducer signal.

Different processing techniques were performed on the A-scan signals shown in Fig 6.9 a, to extract the diffracted signals from SA head. Initially, a single A-scan signal (out of 202 A-scan signals) from the raw B-scan data was considered as a reference signal. In the raw B-scan data, 50th A-scan signal was considered as the reference signal. Then the entire B-scan data was subtracted from this reference signal. Fig 6.9 b, shows the subtracted B-scan signal. From Fig 6.9 b, it can be observed that the subtraction did not improve the SNR uniformly throughout the B-scan. This is attributed to small variation in A-scan signals time shift due to variation in trigger points in different A-scan signals.

To improve the signal, the initial ringing up to 60 mm was removed and 50th A-scan signal from the original B-scan data was considered as a reference signal and cross-correlation between the reference signal and all individual A-scan signals in the original B-scan data was performed to obtain any time shift in the A-scan signal due to variation in trigger points. Subsequently, the time shifted reference signal was subtracted from individual A-scan signals in the original B-scan data. Fig 6.9 c, shows the processed B-scan image after cross-correlation and subtraction. It can be observed from Fig 6.9 c, that SNR of B-scan data is improved till 120th A-scan. However, the SNR of entire B-scan data was not improved even after cross-correlation and subtraction.

To further improve the signal, 5 A-scan signals at a separation of 50 A-scans (0th, 50th, 100th, 150th and 200th A-scan signals) from the original B-scan data were taken as reference signals and then cross-correlation and time shifting followed by subtraction were performed using these reference A-scan signals for their corresponding neighboring A-scan signals in the original B-scan data. Figure 6.9 d shows the final processed B-scan image of Figure 6.9 a. It can be observed that the cross-correlation and time shifting followed by subtraction in the neighboring A-scan signals improved the SNR uniformly throughout the B-scan data. The inbuilt cross-correlation module present in the LabVIEW software was used for processing the signals.

Figure 6.10 shows the flow chart of the signal processing which was performed on the raw B-scan signals to get the processed signal. All the A-scan signals in the B-scan data obtained at 2 mm step were processed as per the flow chart shown in Fig 6.10. Then the A-scan signals of the processed B-scan signal were observed to identify the diffracted signals from the SA heads in the UHAS setup, if any.

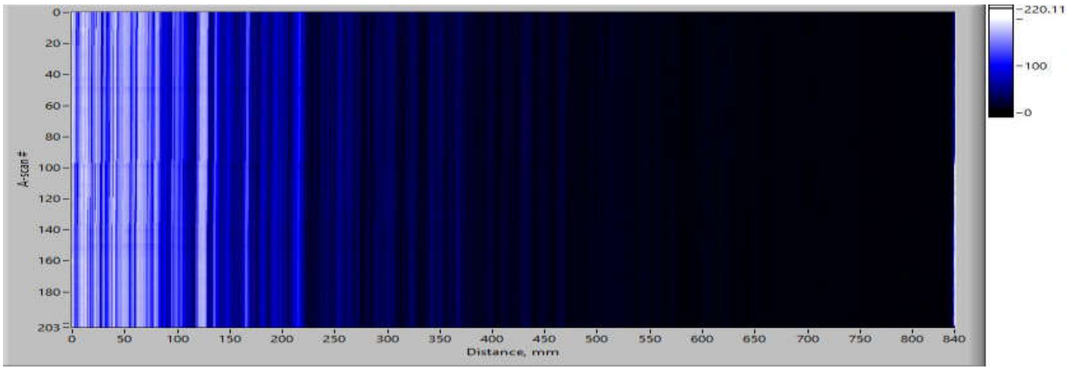

(a)

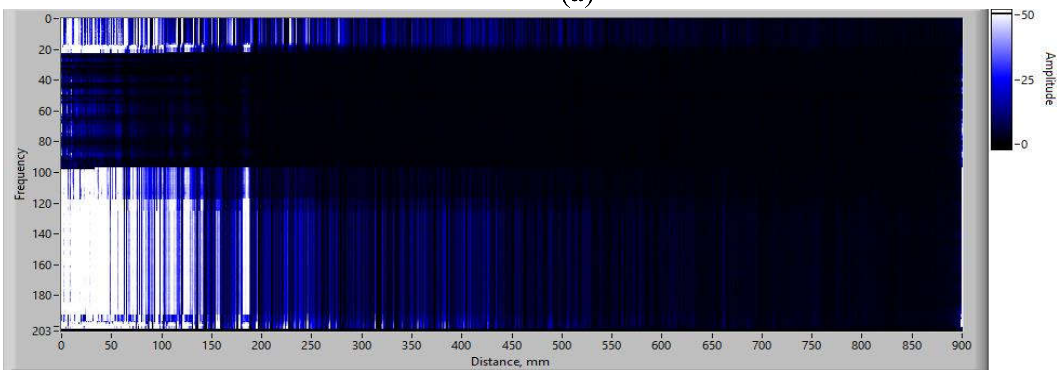

(b)

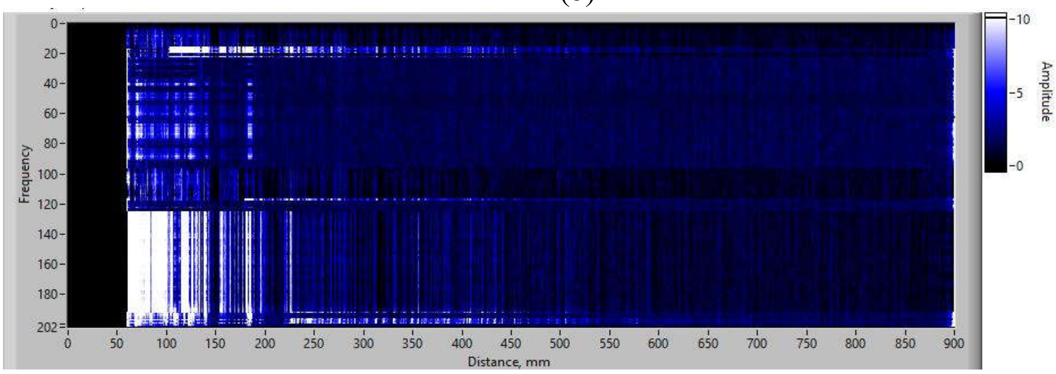

(c)

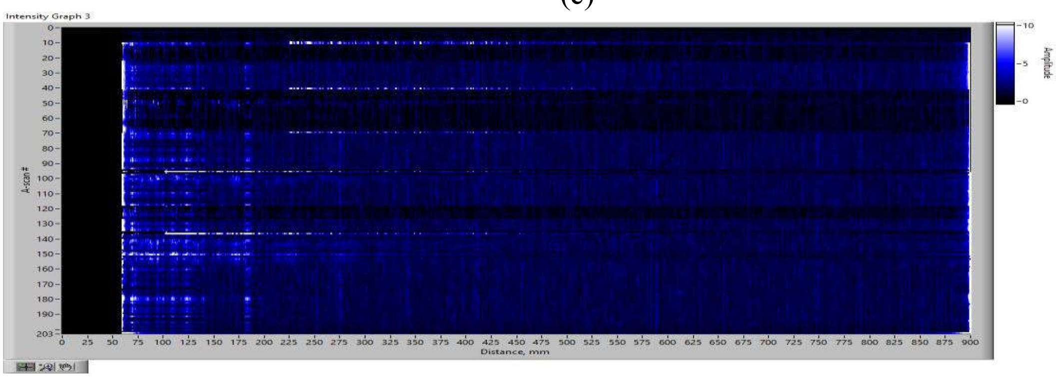

(d)

Figure 6.9 (a) Raw B-scan data, (b) processed B-scan data obtained after subtracting 50th A-scan signal, (c) B-scan data after performing cross-correlation and time shift followed by subtracting 50th A-scan signal and (d) Final processed B-scan signal after performing cross correlation and time shift followed by subtracting 5 different A-scans in the corresponding neighboring A-scans

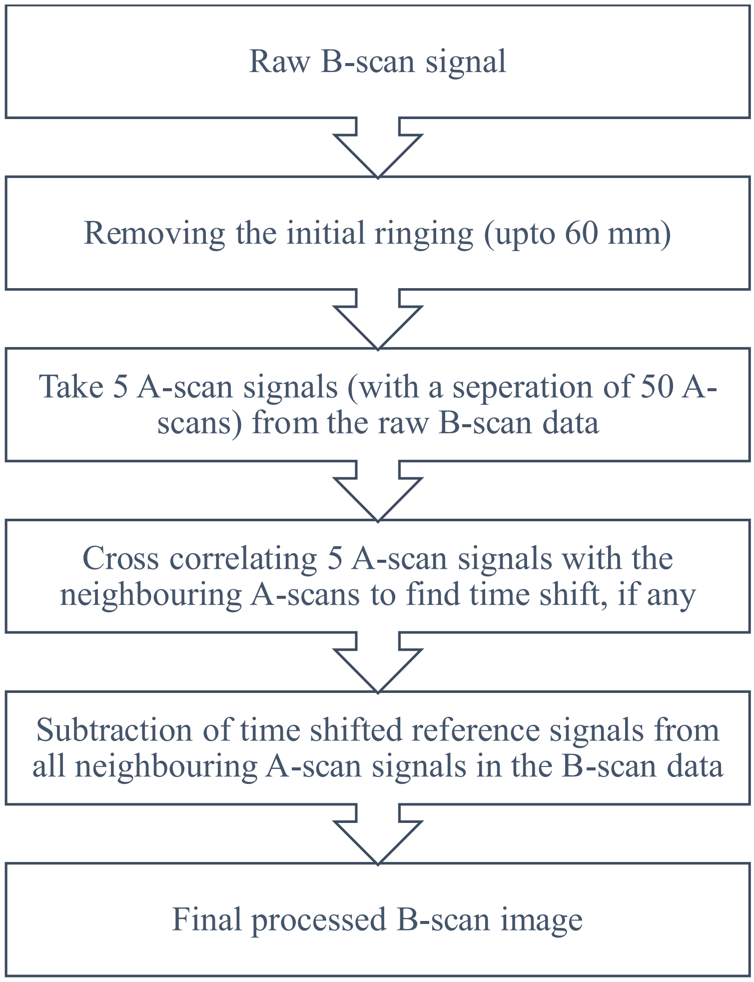

Figure 6.10 Flow chart of signal processing used in the present work

In the B-scan image shown in Fig 6.9, it is expected to observe signals from the 1st SA head (SA_8#1) at a distance of 138 mm. Even after processing the ultrasonic signals, diffracted signals from the SA head (both from ID and OD) could not be resolved. Similarly, the diffracted signals could not be observed in other configurations also. This might be due to the following reasons:

- Inherent low SNR of 1 MHz probe with 10 m long MI cable as compared to the 2 MHz transducer used for underwater studies,
- Larger ringing in sodium environment due to high ultrasonic velocity,
- Very weak diffracted signals from the SA heads and
- Interference from electrical components connected to sodium tank

Improving the signal to noise ratio of ultrasonic signals in the sodium environment by overcoming above limitations is proposed as the scope for future work based on the findings of the thesis.

A point to mention here is that, before tilting the ultrasonic transducer by 5° to demonstrate GAIM in sodium environment, a vertical B-scan of the SA head was performed without giving any tilt (0°) to the ultrasonic transducer to identify the base plate and the SA head face. Figures 6.11 a&b show the photograph and the corresponding B-scan image of the base plate and the SA head face. But, reflection from the SA head or from the base plate could not be observed after tilting the transducer by 5°.

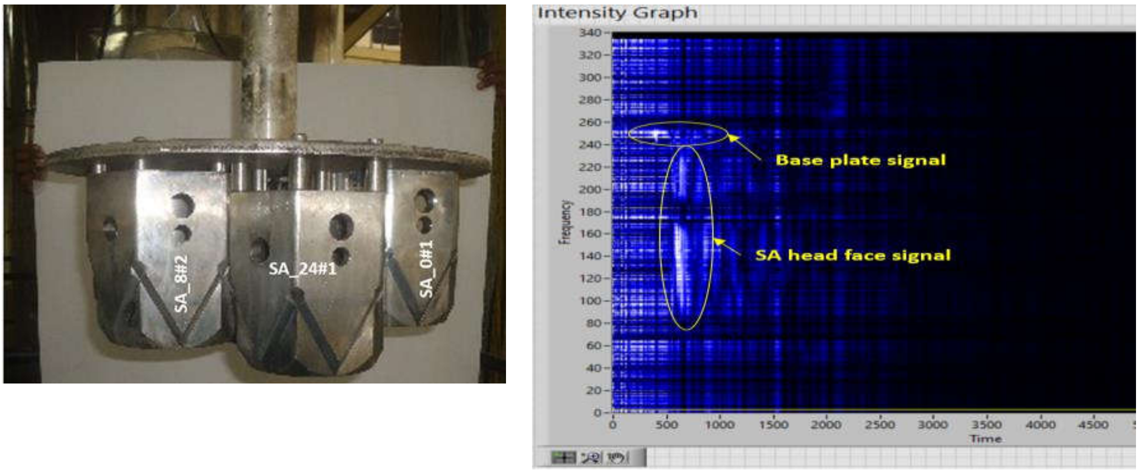

(a) (b)

Figure 6.11 *(a) Photograph and (b) the B-scan image of the base plate and one of the faces of the SA head.*

6.5 Conclusions

In this chapter, application of GAIM in the sodium environment is discussed. Before implementation, under water ultrasonic signals of 1 MHz and 2 MHz transducers were compared. Then, the under-sodium experiments were performed and the suitable signals processing was carried out to extract the reflected and diffracted signals from the reflector plate and SA head, respectively.

- **Comparison of underwater ultrasonic signals of 1 MHz and 2 MHz transducer**

Before carrying out under-sodium experiments, ultrasonic signals of 1 MHz and 2 MHz transducers were compared in water for better understanding of the ultrasonic signals from both transducers. For this, under-water signals of both 1 MHz and 2 MHz transducers were acquired with and without a reflector plate at a distance of 140 mm from the probes. From the ultrasonic signals, it is observed that the initial ringing of both transducers are similar in water. It is observed that the amplitude of the signal from the SS plate for the 1 MHz probe is higher than that for the 2 MHz probe. It is also observed that the divergence of the 2 MHz transducer is less than the 1 MHz transducer.

- **Application of GAIM in sodium environment**

The ultrasonic signal characteristic is decided by the extent of wetting of the ultrasonic transducer in sodium environment. In the present study also, the signal strength has gradually improved after first exposure to 10 days of sodium exposure. The wetting of the ultrasonic transducer improved with time and the initial ringing got reduced. Ultrasonic signals were acquired using 1 MHz without and with a reflector plate (SS) placed at a distance of 140 mm from the probe. From the signals, it was observed that the signal from reflector plate was merged inside the initial ringing. The reflector plate signal was extracted by subtracting a reference A-scan signal from the plate signal.

The under-sodium signals of UHAS from different orientations were acquired using 1 MHz transducer. Signal processing of ultrasonic signals obtained in ETE orientation was performed to identify the diffracted signals from the SA heads of UHAS setup.

Different signal processing techniques as given below were tried to improve the SNR of the B-scan signal and to identify the diffracted signals from the SA heads

* subtraction of the reference signal from the B-scan data (as in the case of reflector plate under-sodium signal),
* cross correlation and time shift followed by subtraction to find the time delay using a single A-scan and
* cross correlation and time shift followed by subtraction to find the time delay using multiple reference signals for different neighboring A-scans.

Even after doing the signal processing, diffracted signals could not be observed/resolved in any of the configurations. This is attribute to, inherent low SNR of 1 MHz probe with 10 m long MI cable, very weak diffracted signal from the SA heads, larger initial ringing due to high ultrasonic velocity, low SNR of 1 MHz probe and EMI from electrical components of sodium tank.

Table of Contents

Thesis Highlights

Name of the Student: G.M.S.K. Chaitanya

Name of CI: Indira Gandhi Centre for Atomic Research **Enrolment No.:** PHYS 02 2012 04 014

Thesis Title: ***Development of glancing angle imaging methodology (GAIM) for detection of protrusion and bowing of PFBR fuel sub-assemblies***

Discipline: Physical Sciences **Sub-Area of Discipline:** Ultrasonic imaging of objects

Date of viva voce: 21/06/2021

Due to high temperature and prolonged irradiation, Fuel Sub-Assemblies (FSAs) in the reactor core undergo protrusion and bowing. Before any fuel handling campaign, it is mandatory to ensure that there is no-protrusion and bowing of any FSA beyond the permissible level. Many robotic arm based scanners were developed for imaging of FSAs and detection of protrusion and bowing. However, due to the rotational constraints of the rotating plugs, on which the scanner is mounted, mapping of the complete core is often not possible. To overcome this limitation, an ultrasonic glancing angle based imaging methodology (GAIM) is developed.

To develop GAIM, 19 nos. of subassembly (SA) heads were arranged in the form of a honeycomb and underwater simulations of protrusion and bowing of SA heads were carried out using a 2 MHz transducer. The experimental parameters such as, vertical height and glancing angle of the transducer have been optimized systematically. The glancing angle images of honeycomb arrangement were obtained from the optimized position of the transducer. Identification of diffracted echo locations from a SA head was carried out using a turn table experiment. A software was developed in LabVIEW for generating the glancing angle images.

Various signatures such as, enhanced echo amplitude and masking of signals corresponding to SAs behind the protruded SA were identified for qualitative estimation of SA protrusion. The sensitivity of GAIM is found to be around 1 mm of protrusion. Quantitative estimation of protrusion has been studied using amplitude and time of flight (TOF) of the diffracted signal at different protrusion heights.

Bowing detection of a SA head was carried using the A-scan signals obtained from 5 collinear SA heads from two different locations separated by an angle of 180°. Various signatures such as, enhanced echo amplitude corresponding to a SA bowed away from the transducer and change in the TOF of the bowed SA head were identified for qualitative estimation of SA bowing. Quantitative estimation of bowing was performed using TOF measurements. The experimentally measured change in TOF of bowed SA head is found to be in good agreement with the theoretically calculated value. Glancing angle images of honeycomb arrangement acquired from two different orientations (clock-wise and counter clock-wise) are superimposed for better visualization of honeycomb arrangement without actually going to the top of each SA head. In addition to this, application of GAIM in sodium environment for protrusion and bowing identification was carried out.

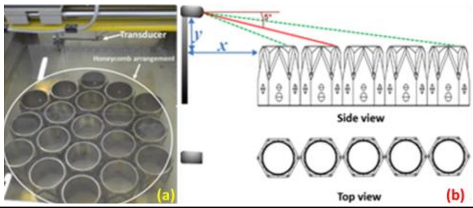

Fig.1 (a) Honeycomb arrangement of SA heads and (b) Schematic of GAIM setup

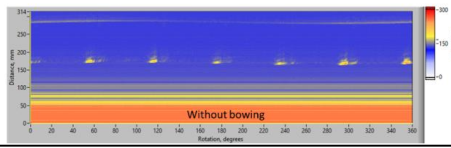

Fig. 2 B-scan image obtained during the 360° rotation of the single SA head

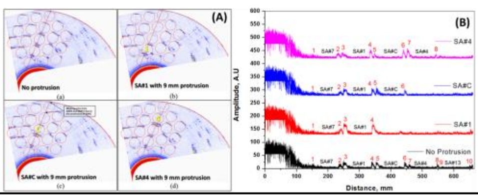

Fig. 3. (A) Glancing angle images of the honeycomb arrangement for qualitative estimation of protrusion and (B) A-scans corresponding to red cursors in Fig. (A)

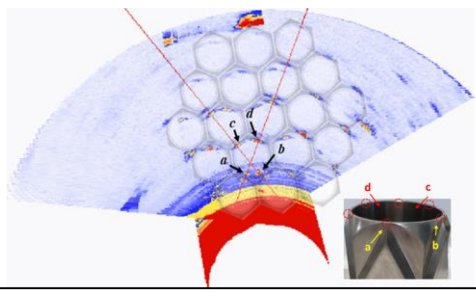

Fig. 4 Superimposition of glancing angle images from clock-wise and counter clock-wise directions